Abstract

4-Dimensional Variational Data Assimilation (4DVAR) assimilates observations

Acknowledgments

Õkæ QË ä@ QÔË@ é<Ë@ é, Õ

(In the name of God, the most bene cent, the most merciful)

I would like to thank my supervisors Prof. Nancy Nichols and Dr. Amos Lawless for all the valuable guidance and support they have given me over the course of the PhD. All the discussions

Declaration

I confirm that this is my own work and the use of all material from other sources has been properly and fully acknowledged.

Adam El-Said

Contents

Chapter 1

Introduction and Motivation

The aim of data assimilation is to provide a statistically optimal estimate of the state of a system given a set of observations and a dynamical model. There are various data assimilation techniques used for a variety of problems in numerical weather prediction (NWP), earth sciences, oceanography, agriculture, ecology and the geo-sciences. The complexity of the data assimilation problem is related to the area of application, since the size and the dynamics of the system or model is dependent on the application.

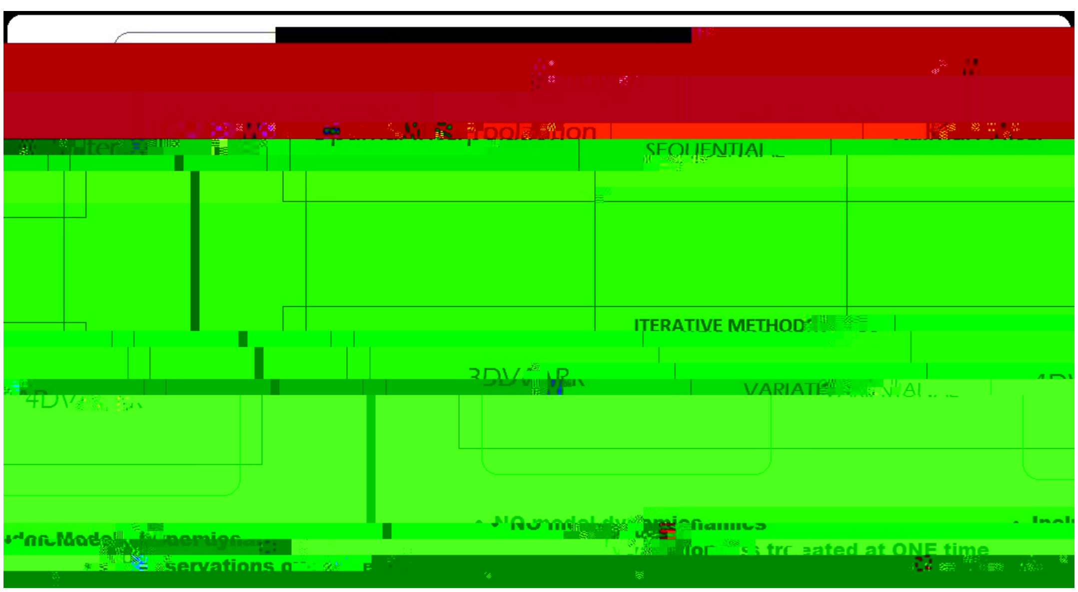

Figure 1.1: Classification of popular data assimilation techniques.

Figure 1.1 is diagrammatic representation of data assimilation techniques and their classification. Each technique has several sub-categories which we deliberately omit. For the remainder of the thesis we abbreviate the optimal interpolation technique as OI, 3-dimensional variational data assimilation as 3DVAR, 4-dimensional variational data assimilation as 4DVAR and the Kalman-filter equations as KF.

The standard 4DVAR approach seeks a statistically optimal fit to the observations, subject to the constraint of the flow, or the model of the physical process for which we are assimilating data. The statistical uncertainties are represented by the 4DVAR objective function, which aims to minimise the mismatch between the model trajectory and the background and observations. The errors in these two quantities are assumed to be independent of each other and possess Gaussian statistics with zero mean. The main assumption of 4DVAR is that the model where it is today, followed by current research involving relevant applications of wc4DVAR. We then state the aims of our research and then give a chapter overview of the thesis.

1.1 Brief Historical Background

In the 1950s there was significant theoretical research progress around the weather forecasting problem, which led to a variety of mathematically similar yet differently formulated ideas, forming the basis of data assimilation. The first marked attempt was by Gilchrist and Cressman, [33], where they use a least-squares method to fit a second degree polynomial presented by their interpretation of a simplified meteorological system. A serially successive correction technique was introduced by Bergthorsen and Döös, [8], where they added statistically weighted increments to a prior estimate. Variational data assimilation was theoretically suggested by Sasaki in the late 1950s in the same era as the OI and KF techniques, [76], [77]. The KF [48] and OI [29] techniques eventually made their way into the weather forecasting arena by the 1960's. The variational techniques at this time were not receiving as much research attention as the OI or KF variants. The strength of variational techniques was not yet realised.

Sasaki formally defined `Variational formalism with weak constraint' as early as 1970, [78]. The weak-constraint variational formulation of the data assimilation problem has received increased attention in the last two decades, [38], [39], [72], [5], [83], [56], [14]. Weak-constraint 4DVAR is most useful when used with observations of a dynamical system or process that perhaps is not yet well-understood.

Notable distinctions and advantages of the variational techniques is the inclusion of model dynamics and feasibility for very large problems such as those in NWP. 4DVAR became feasible for operational NWP centres in 1994, [13], with the introduction of `Incremental 4DVAR', nearly 30 years after itsnearlye3(4D)6a95(neas

Medium-Range Weather Forecasts (ECMWF) in 1997, documented in [74], [64] and [50]. The Met Office then followed with their operational implementation of 4DVAR in 2004, [75].

Operational NWP centres in the last 25 years have largely concentrated their efforts in implementing variational techniques for longer range forecasting due to their computational feasibility. Variational techniques are difficult to implement compared to KF or OI because one of the components required to calculate the gradient is a backward or `adjoint' model. Writing adjoint code is one of the main sources of difficulty and it can take years for scientists to correctly code these for very large NWP models, [75], [74]. The KF technique is infeasible for large problems such as those in NWP because KF requires propagation of background error covariances, which is too computationally expensive. However, there are studies beginning to emerge showing that KF variants may be practicable for large NWP systems. Comparisons between ensemble 4DVAR (4DEnVAR) variants and NWP-applied ensemble KF (EnKF) variants highlight the ease of implementing EnKF over hybrid-4DVAR due to the absence of an adjoint, [59], [22] [60].

The most recent developments surrounding the variational techniques is the implementation of the hybrid 4DVAR technique. These techniques aim to remedy the weakness in sc4DVAR where the background matrix is unable to capture `errors of the day'. At the Met Office, hybrid 4DVAR utilises a variable transformation technique to combine the conventional climatological estimates of the background error covariance matrix with data from the 23-member Met Office ensemble prediction system (MOGREPS). This has been implemented by the Met Office in their global model as of July 2012, [10]. The Met Office are also attempting to develop a hybrid 4DEnVAR technique, which if successful will alleviate the need for linearised and adjoint models. The difference between hybrid 4DVAR and hybrid 4DEnVAR is that 4DEnVAR uses a localised linear combination of non-linear forecasts, whereas hybrid 4DVAR uses the linearised model and its adjoint. A comparison between these two techniques shows that the currently operational hybrid 4DVAR method is still superior to the proposed hybrid 4DEnVAR, [60].

be found in [84]. The operational application is discussed in [56] and [27]. The ECMWF brie y implemented a bias-only corrective version of wc4DVAR, but this has been suspended due to numerical conditioning issues, which is an area we address in this thesis theoretically, [personal communications with Mike Fisher and Yannick Tremolet, 2013], [Poster by Stephen English, ECMWF Research Dept: https://cimss.ssec.wisc.edu/itwg/itsc/itsc19/program/posters/nwp_3_english.pdf].

Another growing area of research that has begun implementing wc4DVAR is earth and soil observation. The main problem in this area is that the current models are not an accurate representation of terrestrial ecosystems. There is also the issue of models not being coupled with each other. So for example in the event of a forest re, abrupt changes in the state would take place in a separate radiative transfer model which will have an e ect on the terrestrial model, however, the terrestrial assimilation window, given the error statistics in the background, observations and the model. The problem is fully 4-dimensional since it seeks temporally evolving

1.4 Thesis Overview

In Chapter 2 we present the variational data assimilation problem. We also discuss the incremental 4DVAR and control variable transform (CVT) techniques which are used to enable operational execution of the variational algorithm. We then introduce the two weak-constraint variational methods and extend the incremental and CVT techniques to wc4DVAR followed by a short discussion of the Hessian structures of the two wc4DVAR formulations. Finally, we review the current literature more closely linked to the wc4DVAR formulations at the focus of the thesis.

In Chapter 3 we introduce the de nition of the condition number used in this thesis as a measure to quantify the sensitivities of the variational problem to changes in its input parameters. We then detail the iterative solvers used to solve the 4DVAR optimisation problem. This is followed by an overview of the particular class of matrix, which are shared by the two covariance structures in the experiments conducted in our research. We then discuss the mathematical techniques and theorems used to obtain the results in the thesis. We then introduce the two models used in our theory and experiments.

In Chapter 4 we detail the practical implementation considerations of both the model error and state estimation wc4DVAR problems. We then detail the experimental design and examine their numerical minimisation characteristics when applied to the 1-dimensional advection equation model.

In Chapter 5 we examine the condition number of the Hessian of the model error objective function. We derive new theoretical bounds on the condition number of the Hessian and derive theoretical insight from the bounds. We explore the sensitivities of the condition number to input data by demonstrating the bounds through numerical experiments, both on the condition number and the iterative solution process. We precondition the problem and derive similar theoretical results and demonstrate in a similar fashion that the overall conditioning of the preconditioned problem is improved as a result.

Chapter 6 is dedicated to examining the condition number of the Hessian of the state estimation objective function. We derive new theoretical bounds on the condition number of the Hessian and derive theoretical insight from the bounds. We examine and highlight certain properties of this Hessian that are uniquely different from the model error formulation Hessian. We demonstrate all our findings through numerical experiments on the condition number and the solution process of the state estimation problem.

In Chapter 7 we implement both weak-constraint formulations on the Lorenz-95 system and show that the sensitivities of both formulations obtained in Chapters 5 and 6 also hold for a non-linear chaotic model.

Chapter 8 concludes our work and discusses avenues for further work.

Chapter 2

Variational Data Assimilation

We introduce the Gauss-Newton 'incremental' and CVT techniques currently used for sc4DVAR. We then introduce the two wc4DVAR formulations. We then extend the theory of the Gauss-Newton and CVT concepts to both formulations and briefly discuss the structures of the two wc4DVAR Hessians. We conclude the chapter with a literature review of applications of wc4DVAR in NWP and current understanding of the conditioning of the wc4DVAR problem.

We begin by detailing the style of notation used in this thesis.

2.1 Notation and Assumptions

Matrices and Vectors

Bold upper-case letters denote partitioned matrices, meaning a matrix of matrices. In this thesis we refer to these partitioned matrices as 4-dimensional (4D) since they possess spatial and temporal information. Matrices with a normal font represent a standard $N \times N$ matrix as opposed to a partitioned 4D $Nn \times Nn$ matrix, for $N, n \in \mathbb{N}$, where N refers to the spatial dimension and n denotes the temporal dimension. Similarly, we represent 4D partitioned vectors with bold lower-case letters and normal vectors of size N are written in normal font.

Operators

This notation also interlinks between operators and matrices. We denote non-linear operators using calligraphic font whereas a non-linear operator which has been differentiated and linearised around a point is denoted with normal font, which can then also be represented as a matrix. This also applies to 4D operators, so a linearised 4D operator for example would be bold. Letters with standard font denote linear or linearised operators,which can be represented in matrix form.

Condition Number

The condition number used throughout this chapter is the 2-norm condition number, composed of the ratio of the largest and smallest eigenvalue of a symmetric positive-definite matrix. We formally introduce the condition number in Chapter 3 Section 3.1.

We now introduce the sc4DVAR problem.

2.2 Strong-Constraint 4DVAR

The aim of data assimilation is to merge the trajectory of a model with observational data from the process being modeled. In sc4DVAR the model is assumed to be perfect meaning each state is described exactly by the model equations. The errors therefore in the strong-constraint problem are the background, a previous forecast, and the observations. The objective is to seek the model initial conditions which minimises the distance between the model trajectory and the background and observations.

space to observation space such that $H_i : \mathbb{R}^N \to \mathbb{R}^p$. Therefore we have

$$H_i(x_i) - y_i = \epsilon_i^o; \quad i = 0; \ldots; n, \tag{2.3}$$

where $\epsilon_i^o \in \mathbb{R}^p$ denotes the observation error at t_i. The errors in the observations are typically assumed to be uncorrelated with all other types of error, and of the form

$$\epsilon_i^o \sim N(0; R_i); \quad i = 0; \ldots; n, \tag{2.4}$$

where $R_i \in \mathbb{R}^{p \times p}$ is the observation error covariance matrix and the mean is equal to zero. The assumption of a normal distribution allows the distributions to be defined by the mean and covariance, which simplifies the problem. The Gaussian assumption in (2.4) is still currently used by leading weather centres' 4DVAR implementations, such as the Met Office and the ECMWF, [74], [75], [13].

Next, we consider model trajectory errors. Initial conditions x_0, produce a model trajectory by utilising the non-linear model described in (2.1), with states at each time $(x_1; \ldots; x_n)$. The initial conditions that produce the previous forecast trajectory, is known as the 'background', denoted as x_0^b. The background is the solution of a previous 4DVAR application, since variational data assimilation is a cyclic process. We therefore have a background trajectory such that

$$x_i^b = M_{i;i-1}(x_{i-1}^b); \quad i = 1; \ldots; n, \tag{2.5}$$

with initial conditions x_0^b producing a trajectory $(x_1^b; \ldots; x_n^b)$. The error associated with the background is such that

$$x_0 - x_0^b = \epsilon_0^b; \tag{2.6}$$

where the error is such that

$$\epsilon_0^b \sim N(0; B_0): \tag{2.7}$$

The background error $\epsilon_0^b \in \mathbb{R}^N$ is assumed to be uncorrelated with all other types of error, have a zero mean and a background error covariance matrix such that $B_0 \in \mathbb{R}^{N \times N}$.

So the aim of the variational problem is to minimise the errors in (2.6) and (2.3) with respect to the states x_i for $i = 0, \ldots, n$, subject to the constraint of the perfect model (2.1).

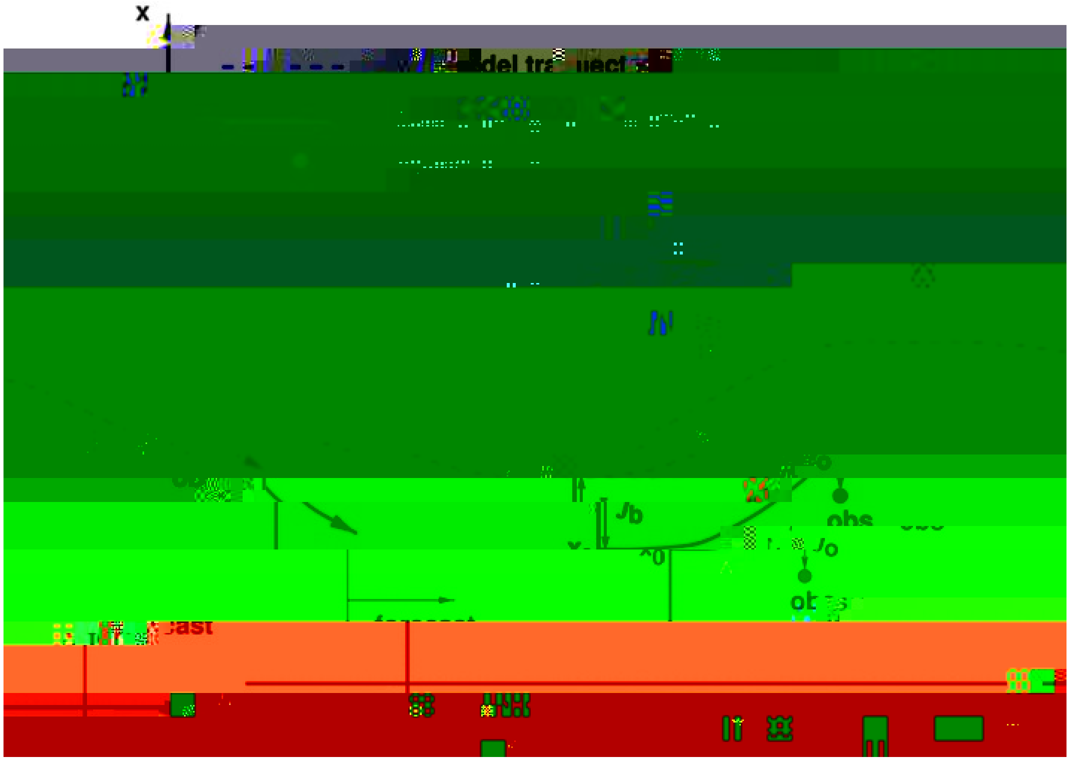

Figure 2.1: Strong-constraint 4DVAR assimilation window with following forecast trajectory. Background estimate (blue dotted line) and solution (red line). (Diagram template courtesy of ECMWF training course presentation by Phillipe Lopez)

Figure 2.1 is a pictorial representation of sc4DVAR. The aim is to find the model trajectory (red line), which minimises the distances between the background (blue dotted line) and the temporally distributed observations (green dots), within the assimilation window. Therefore, sc4DVAR seeks the initial model state x_{0e}

objective function, (2.8), provides the initial conditions for the non-linear model $\mathcal{M}$, which minimises the errors in the background J_b and the observations J_o.

The gradient equation is as follows

$$\nabla J(x_0) = B_0^{-1}(x_0 - x_0^b) + \sum_{i=0}^{n} M_{0;i}^T H_i^T R_i^{-1}(H_i(\mathcal{M}_{i;0}(x_0)) - y_i); \qquad (2.9)$$

where the Jacobian of $\mathcal{M}$ is denoted as M, which is known as the tangent linear or linearised model and M^T is traditionally known as the linearised adjoint model.

The first-order Hessian of (2.8) is

$$S = B_0^{-1} + \sum_{i=0}^{n} M_{0;i}^T H$$

We approximate the non-linear operators in (2.8) to first-order such that

$$
\begin{aligned}
H_i(M_{i;0}(x_0^{(k)})) &= H_i(M_{i;0}(x_0^{(k)} + \delta x_0^{(k)})), \\
&\approx H_i(M_{i;0}(x_0^{(k)})) + (H_i(M_{i;0}(x_0^{(k)})))' \, \delta x_0^{(k)}, \\
&= H_i(M_{i;0}(x_0^{(k)})) + (H_i M_{i;0})_{x_0^{(k)}} \, \delta x_0^{(k)}. \qquad (2.12)
\end{aligned}
$$

Thus an `incremental objective function' can be written in terms of the increment $\delta x_0^{(k)}$,

$$
\begin{aligned}
\min_{\delta x_0^{(k)}} J(\delta x_0^{(k)}) = {} & \frac{1}{2}(\delta x_0^{(k)} - (x_0^b - x_0^{(k)}))^T B_0^{-1} (\delta x_0^{(k)} - (x_0^b - x_0^{(k)})) \\
& + \frac{1}{2} \sum_{i=0}^{n} (H_i M_{i;0} \, \delta x_0^{(k)} - d_i)^T R_i^{-1} (H_i M_{i;0} \, \delta x_0^{(k)} - d_i), \qquad (2.13)
\end{aligned}
$$

where

$$
d_i = y_i - (H_i(M_{i;0}(x_0^{(k)}))). \qquad (2.14)
$$

Solving problem (2.13) is known as the `inner-loop'. The inner-loop objective function (2.13) can be minimised directly using an iterative method, or by solving the gradient equation at the minimum ($\nabla J = 0$),

$$
(B_0^{-1} + \sum_{i=0}^{n} M_{0;i}^T H_i^T R_i^{-1} H_i M_{i;0}) \, \delta x_0^{(k)} = \sum_{i=0}^{n} M_{0;i}^T H_i^T R_i^{-1} d_i + B_0^{-1}(x_0^b - x_0^{(k)}). \qquad (2.15)
$$

We can see that (2.15) is simply the linearised sc4DVAR Hessian applied to δx_0, with the initial input data comprised of the errors in the background and observations on the right-hand side. The incremental 4DVAR Hessian of (2.13) is identical to the first-order Hessian of the non-linear objective function (2.10). Minimising the inner-loop objective function yields a new increment δx_0 to update the current guess for the outer-loop objective function via (2.11).

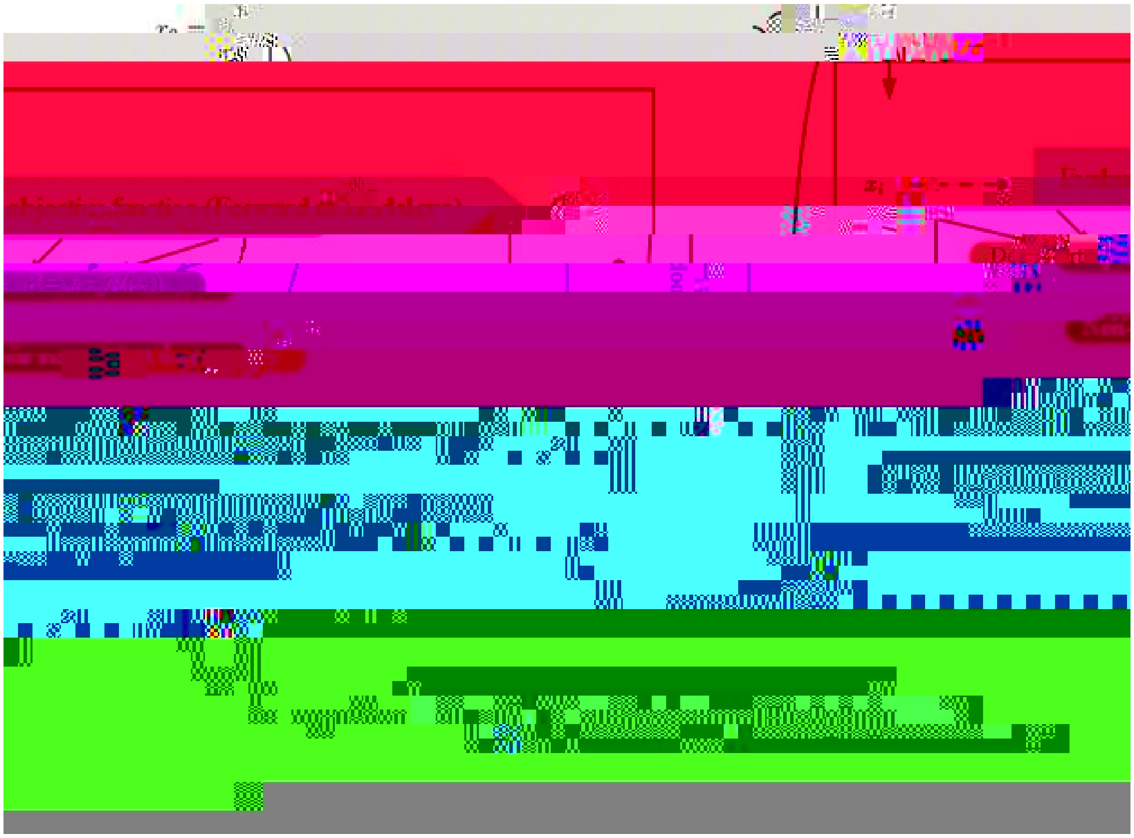

Figure 2.2: Illustration of incremental sc4DVAR. (Diagram template: ECMWF presentation by Sebastien Lafont)

Figure 2.2 illustrates the incremental sc4DVAR algorithm. The initial guess to start the algorithm is $x_0 = x_b$, which is then used to evaluate the non-linear objective function J. Evaluating the 'outer-loop' objective function, J, yields the non-linear model trajectory and 'departures', as seen in Figure 2.2, which allows the linearised inner-loop to begin. The initial guess for the inner-loop objective function is $x_i = 0$, then the iterative minimisation algorithm will solve using the linearised inner-loop objective function J and its gradient ∇J to provide the new x_i increment which is added on to the previous guess x_i. This process is then repeated again until the desired convergence criterion is reached.

The Gauss-Newton approach detailed here is equivalent to solving the equations arising from the gradient equation (2.9), [52]. However, solving the gradient equation is not practicable operationally since it is deemed too computationally expensive, so we do not consider it in this thesis. In operational NWP most of the computational cost is associated with the minimisation of (2.13), [74]. The

ECMWF has the dominant super-computing capability in the NWP community and they perform 50 inner-loop iterations with only 3 outer-loop iterations.

The sc4DVAR problem is known to be ill-conditioned mainly due to the correlations in the background error covariance matrix B_0, [43], [41]. The matrix B_0 is also known to be very large due to the number of variables in the sc4DVAR problem, [4]. We now introduce a technique which is operationally used to deal with the background error covariance matrix.

2.2.2 The Control Variable Transform

The Control Variable Transform (CVT) technique has traditionally been used to deal with the ill-conditioning of the B_0 matrix in variational data assimilation, [58]. More recently the Met O ce has utilised this technique to implement their hybrid 4DVAR and hybrid 4DEnVAR techniques, [60]. A change of variables is introduced which allows for the implicit treatment of B_0, therefore alleviating the need to store an explicit inverse of B_0. The two principal reasons for this transform are; the B_0

and have variance equal to one. Solving (2.17) is equivalent to solving (2.13) as long as (2.18) holds. From (2.18) we require

$$B_0 = UU^T; \tag{2.19}$$

to hold. In practice U does not necessarily have to be square. The challenge is to find U and its adjoint U^T to be an optimum representation of B_0. Obtaining transforms for B_0 is an extensive area of current research, [4], which is not the focus of this thesis. We assume U is the unique symmetric-square root of B_0 in this thesis and thus $U = B_0^{1/2}$.

Therefore (2.17) becomes

$$\hat{J}(z^{(k)}) = \frac{1}{2}\left[z^{(k)} - (z^b - z^{(k)})\right]^T\left[z^{(k)} - (z^b - z^{(k)})\right] \tag{2.20}$$

$$+\frac{1}{2}\sum_{i=0}^{n}(H_i M_{i;0} B_0^{1/2} z^{(k)} - d_i)^T R_i^{-1}(H_i M_{i;0} B_0^{1/2} z^{(k)} - d_i); \tag{2.21}$$

with Hessian

$$\nabla^2 \hat{J}(z) = I + \sum_{i=0}^{n} B_0^{1/2} M_{0;i}^T H_i^T R_i^{-1} H_i M_{i;0} B_0^{1/2}: \tag{2.22}$$

A paper by E.Andersson et al. [1] found the conditioning of (2.22) on a 2-grid point example, with q

In the next section we introduce the two wc4DVAR formulations at the focus of the thesis.

2.3 Weak-Constraint 4DVAR

The weak-constraint problem arises from relaxing the perfect model assumption (2.1) allowing for model error. This implies the model is enforced as a weak-constraint and the control variable has now increased by an order of magnitude as we will see shortly. We revisit (2.1) now and nd

$$x_i \quad M_{i;i\ 1}(x_{i\ 1}) = \quad _i; \tag{2.24}$$

for $i = 1;:::;n$, where $_i$ 2 R^N, represents the model error. We assume the model errors are random with zero mean, Gaussian error statistics and a known covariance such that

$$_i \quad N(0;Q_i); \tag{2.25}$$

for $i = 1;:::;n$, whereQ_i 2 $R^{N \quad N}$ represents the model error covariance matrix. We also assume that model errors are independent of the background and observation errors.

The additional model error now becomes a quantity for consideration and thus is incorporated into the objective function. One way of writing the objective function is in terms of thecoddixids1 andsuchthat errors estimates. This formulation is more common in the literature than the alternative, implemented mainly on non-operational models, [94], [83], [84], [93]. An operational implementation of this formulation was functioning at the ECMWF, [56], until it was taken o ine recently due to numerical conditioning issues.

Another way to consider the problem is in terms of the states x_i such that

min
(
(

Similarly the previous guess for the initial conditions and model errors produces a similar vector to $\mathbf{p}$, denoted as $\mathbf{p}^b \in \mathbb{R}^{N(n+1)}$, where the 'b' superscript denotes the background. We define the 4D model operator, $\mathbf{L} : \mathbb{R}^{N(n+1)} \to \mathbb{R}^{N(n+1)}$ which enables us to map from 'state space' to 'model error space' such that

$$\mathbf{L}(\mathbf{x}) = \mathbf{p}. \tag{2.29}$$

We can think of (2.29) as a 4D representation of (2.24), which links the two vectors $\mathbf{p}$ and $\mathbf{x}$ via (2.29). The operator $\mathbf{L}$ is invertible, since we can determine $\mathbf{x}$ from $\mathbf{p}$ using (2.24).

We now define the following 4D spatial-temporal variables,

$$\mathbf{y} = \begin{pmatrix} \mathbf{y}_0 \\ \mathbf{y}_1 \\ \vdots \\ \mathbf{y}_n \end{pmatrix}, \tag{2.30}$$

$$\mathbf{D} = \begin{pmatrix} \mathbf{B}_0 & & & \\ & \mathbf{Q}_1 & & \\ & & \ddots & \\ & & & \mathbf{Q}_n \end{pmatrix}, \quad \mathbf{R} = \begin{pmatrix} \mathbf{R}_0 & & & \\ & \mathbf{R}_1 & & \\ & & \ddots & \\ & & & \mathbf{R}_n \end{pmatrix}. \tag{2.31}$$

We notice a few subtleties here. We have composed $\mathbf{D} \in \mathbb{R}^{N(n+1) \times N(n+1)}$ such that there are *no temporal correlations* between the initial conditions and model errors. This also applies to the observation error covariance matrix $\mathbf{R} \in \mathbb{R}^{p(n+1) \times p(n+1)}$ which is also assumed to be temporally uncorrelated.

We can now write the wc4DVAR objective function (2.26) in 4D form

$$\min_{\mathbf{p}} \mathcal{J}(\mathbf{p}) = \frac{1}{2}||\mathbf{p} - \mathbf{p}^b||^2_{\mathbf{D}^{-1}} + \frac{1}{2}||\mathcal{H}(\mathbf{L}^{-1}(\mathbf{p})) - \mathbf{y}||^2_{\mathbf{R}^{-1}}, \tag{2.32}$$

where $\mathcal{H}$ is the 4D non-linear observation operator. The alternative formulation, (2.27), is as follows

$$\min_{\mathbf{x}} \mathcal{J}(\mathbf{x}) = \frac{1}{2}||\mathbf{L}(\mathbf{x}) - \mathbf{p}^b||^2_{\mathbf{D}^{-1}} + \frac{1}{2}||\mathcal{H}(\mathbf{x}) - \mathbf{y}||^2_{\mathbf{R}^{-1}}. \tag{2.33}$$

Differentiating (2.32) yields

$$\nabla\mathcal{J}(\mathbf{p}) = \mathbf{D}^{-1}(\mathbf{p} - \mathbf{p}^b) + (\mathbf{H}_{\mathbf{x}}\mathbf{L}_{\mathbf{x}}^{-1})^T\mathbf{R}^{-1}(\mathcal{H}(\mathbf{L}^{-1}(\mathbf{p})) - \mathbf{y}), \tag{2.34}$$

where $\mathbf{H}_{\mathbf{x}}$ and $\mathbf{L}_{\mathbf{x}}^{-1}$ are Jacobians, linearised around the subscripted quantity. Similarly, by differentiating (2.33) we have

$$\nabla\mathcal{J}(\mathbf{x}) = \mathbf{L}_{\mathbf{x}}^T\mathbf{D}^{-1}(\mathbf{L}(\mathbf{x}) - \mathbf{p}^b) + \mathbf{H}_{\mathbf{x}}^T\mathbf{R}^{-1}(\mathcal{H}(\mathbf{x}) - \mathbf{y}). \tag{2.35}$$

The linearisation points in the subscripts of $\mathbf{H}$ and $\mathbf{L}$ are omitted herein since this is not the focus of the thesis. The different gradients (2.34) and (2.35) suggest that the minimisation characteristics of (2.32) and (2.33) will be different.

To be clear on the definition of each term in the gradients above, we write the operators $\mathbf{L}$ and $\mathbf{H}$ in matrix form

$$\mathbf{H} = \begin{pmatrix} \mathbf{H}_0 & & & \\ & \mathbf{H}_1 & & \\ & & \ddots & \\ & & & \mathbf{H}_n \end{pmatrix}; \quad \mathbf{L} = \begin{pmatrix} \mathbf{I} & & & \\ -\mathbf{M}_{1,0} & \mathbf{I} & & \\ & -\mathbf{M}_{2,1} & \ddots & \\ & & \ddots & \\ & & -\mathbf{M}_{n,n-1} & \mathbf{I} \end{pmatrix}. \tag{2.36}$$

The inverse of $\mathbf{L}$ can be obtained from the weak-constraint equation (2.24), thus taking the following form

$$\mathbf{L}^{-1} = \begin{pmatrix} \mathbf{I} & & & & & \\ \mathbf{M}_{1,0} & \mathbf{I} & & & & \\ \mathbf{M}_{2,0} & \mathbf{M}_{2,1} & \mathbf{I} & & & \\ \mathbf{M}_{3,0} & \mathbf{M}_{3,1} & \mathbf{M}_{3,2} & \mathbf{I} & & \\ \vdots & \vdots & \ddots & \ddots & \ddots & \\ \mathbf{M}_{n,0} & \mathbf{M}_{n,1} & \cdots & \cdots & \mathbf{M}_{n,n-1} & \mathbf{I} \end{pmatrix}. \tag{2.37}$$

The linearised forward model of $\mathcal{M}$ is denoted by $\mathbf{M}$, which is embedded in the operator $\mathbf{L}$. The adjoint operators are $\mathbf{L}^T$ and $\mathbf{L}^{-T}$, which have the linearised adjoint model $\mathbf{M}^T$ within them. We notice that $\mathbf{L}^{-1}$ is a lower triangular matrix meaning all its eigenvalues lie on its main diagonal, which all equal 1.

The Hessians of (2.32) and (2.33) are as follows,

$$\mathbf{S}_p = \nabla^2 \mathcal{J}(\mathbf{p}) = \mathbf{D}^{-1} + \mathbf{L}^{-T}\mathbf{H}^T\mathbf{R}^{-1}\mathbf{H}\mathbf{L}^{-1}, \tag{2.38}$$

and

$$\mathbf{S}_x = \nabla^2 \mathcal{J}(\mathbf{x}) = \mathbf{L}^T\mathbf{D}^{-1}\mathbf{L} + \mathbf{H}^T\mathbf{R}^{-1}\mathbf{H}. \tag{2.39}$$

We can already see at this point that the alternate minimimsation problems (2.32) and (2.33) are quite different, leading to different gradients and Hessians. Therefore it is natural to expect differences in their respective minimisation characteristics. Let us now examine the structure of the Hessians of $\mathcal{J}(\mathbf{p})$ and $\mathcal{J}(\mathbf{x})$.

2.3.1 The Weak-Constraint 4DVAR Hessians

The Hessians are important since they provide information on the local curvature of the objective function. The structure of the Hessians give us insights into how each wc4DVAR formulation iteratively achieves its solution, as seen in (2.52) and (2.53).

We now illustrate the structure of the Hessian of $\mathcal{J}(p)$,

$$S_p = \begin{pmatrix} B_0^{-1} & & & \\ & Q_1^{-1} & & \\ & & \ddots & \\ & & & Q_n^{-1} \end{pmatrix} + \begin{pmatrix} \sum_{i=0}^{n} (H_i M_{i,0})^T R_i^{-1} H_i M_{i,0} & \sum_{i=1}^{n} (H_i M_{i,0})^T R_i^{-1} H_i M_{i,1} & \sum_{i=2}^{n} (H_i M_{i,0})^T R_i^{-1} H_i M_{i,2} & \cdots & (H_n M_{n,0})^T R_n^{-1} H_n \\ \sum_{i=1}^{n} (H_i M_{i,1})^T R_i^{-1} H_i M_{i,0} & \sum_{i=1}^{n} (H_i M_{i,1})^T R_i^{-1} H_i M_{i,1} & \sum_{i=2}^{n} (H_i M_{i,1})^T R_i^{-1} H_i M_{i,2} & \cdots & (H_n M_{n,1})^T R_n^{-1} H_n \\ \sum_{i=2}^{n} (H_i M_{i,2})^T R_i^{-1} H_i M_{i,0} & \sum_{i=2}^{n} (H_i M_{i,2})^T R_i^{-1} H_i M_{i,1} & \sum_{i=0}^{n} (H_i M_{i,2})^T R_i^{-1} H_i M_{i,2} & \ddots & \vdots \\ \vdots & \ddots & \ddots & \ddots & (H_n M_{n,n-1})^T R_n^{-1} H_n \\ H_n^T R_n^{-1} H_n M_{n,0} & H_n^T R_n^{-1} H_n M_{n,1} & \cdots & H_n^T R_n^{-1} H_n M_{n,n-1} & H_n^T R_n^{-1} H_n \end{pmatrix}. \tag{2.40}$$

The S_p structure is full block where each block is quite sparse in practice due to the observation operator having much lower dimension than the state.

The Hessian of $\mathcal{J}(x)$ possesses a block tri-diagonal structure,

$$S_x = \begin{pmatrix} B_0^{-1} + M_1^T Q_1^{-1} M_1 & -M_1^T Q_1^{-1} & & & \\ -Q_1^{-1} M_1 & Q_1^{-1} + M_2^T Q_2^{-1} M_2 & -M_2^T Q_2^{-1} & & \\ & \ddots & \ddots & \ddots & \\ & & \ddots & & \\ & & -Q_{n-1}^{-1} M_{n-1} & Q_{n-1}^{-1} + M_n^T Q_n^{-1} M_n & -M_n^T Q_n^{-1} \\ & & & -Q_n^{-1} M_n & Q_n^{-1} \end{pmatrix} + \begin{pmatrix} H_0^T R_0^{-1} H_0 & & & \\ & H_1^T R_1^{-1} H_1 & & \\ & & \ddots & \\ & & & H_n^T R_n^{-1} H_n \end{pmatrix}. \tag{2.41}$$

These Hessians are both symmetric positive-definite matrices implying they possess a unique inverse. It is important to note that the Hessians of the incremental formulations (2.46) and (2.49) are identical to these first-order Hessians provided the linearisation state used to obtain these first-order Hessians is close to the solution of the non-linear objective functions. So our work in this thesis is relevant to both problems. We also notice that the Hessian of sc4DVAR, (2.8), is contained within (2.40), such that S = $S_{p(1;1)}$.

The parallelism of (2.27) over (2.26) can be seen in the Hessian matrices (2.41) and (2.40) respectively. The separate blocks of (2.41) can be calculated much quicker than (2.40) since each block in (2.40) requires sequential model integration. Each single time-step block seen S_x can be allocated to a single processor, and with enough processors to cover each block in S_x, the calculation can be obtained much quicker than S_p. Each block in S_p requires the entire string of model time-step integrations to be completed, which in operational NWP can take a while.

We have discussed the structural differences in the Hessians of (2.32) and (2.33) in this section. We now introduce the Gauss-Newton incremental formulation of the weak-constraint problem.

2.3.2 Incremental Weak-Constraint 4DVAR

In this section we extend the Gauss-Newton incremental 4DVAR approach shown in Section 2.2.1 to the weak-constraint problem.

We derive the incremental formulation by defining an increment in p such that

$$p^{(k+1)} = p^{(k)} + \quad p^{(k)}: \tag{2.42}$$

where the superscripts denote the relevant formulation variable. We substitute (2.43), (2.44) and (2.45) into the non-linear objective function (2.32) giving us the incremental wc4DVAR inner-loop ‘δp’ function

$$\min_{\delta p^{(k)}} J(\delta p^{(k)}) = \frac{1}{2}||\delta p^{(k)} - b^p||^2_{D^{-1}} + \frac{1}{2}||H_x L_x^{-1} \delta p^{(k)} - d^p||^2_{R^{-1}}; \tag{2.46}$$

which is now a quadratic function in $\delta p^{(k)}$. Since all the operators have been linearised as in (2.43), the constraint (2.29) becomes

$$L_{x^{(k)}} \delta x^{(k)} = \delta p^{(k)}. \tag{2.47}$$

Solving the inner loop problem yields a new $\delta p^{(k)}$ increment to update the old $p^{(k)}$ as in (2.42).

We derive the incremental formulation for (2.33) in a similar fashion to (2.46) by approximating $\mathcal{H}$ and $\mathcal{L}$ as in (2.43) and defining increment in x such that

$$x^{(k+1)} = x^{(k)} + \delta x^{(k)}; \tag{2.48}$$

similar to (2.42). We can now write an incremental δx formulation such that

$$\min_{\delta x^{(k)}} J(\delta x^{(k)}) = \frac{1}{2}||L_x \delta x^{(k)} - b^x||^2_{D^{-1}} + \frac{1}{2}||H_x \delta x^{(k)} - d^x||^2_{R^{-1}}; \tag{2.49}$$

where

$$b^x = p^b - \mathcal{L}(x^{(k)}); \tag{2.50}$$

$$d^x = y - \mathcal{H}(x^{(k)}). \tag{2.51}$$

Figure 2.3 illustrates the algorithmic schematic of wc4DVAR incremental formulation (2.46).

Figure 2.3: Illustration of Weak-Constraint Incremental 4DVAR, p formulation. (Diagram

directly have been shown to be equivalent for sc4DVAR, [52], we believe this is also true for wc4DVAR but this has yet to be proven. We see that the left hand side of both equations (2.52), (2.53) are the respective Hessians S_p, S_x, and the right-hand is the initial guess. The emphasis on the gradients and hence the Hessians S_p and S_x can be seen from these gradient equations.

Substituting (2.55) and (2.56) into (2.46) yields the following objective function

$$\min_{z^{(k)}} \hat{J}(\ z^{(k)}) = \frac{1}{2}||\ z^{(k)} - (z^b - z^{(k)})||^2_{U^T D^{-1} U} + \frac{1}{2}||HL^{-1}U\ z^{(k)} - d||^2_{R^{-1}}; \quad (2.57)$$

where ideal U-transform is such that

$$U^T D^{-1} U =$$

In this section we have introduced the method of preconditioning wc4DVAR (2.32) using the CVT technique, which is essential for wc4DVAR to be considered practicable operationally. This naturally extends from concepts used to implement sc4DVAR.

We have introduced the two wc4DVAR formulations at the focus of this thesis and briefly highlighted differences in the minimisation problems that ensue just by viewing the different gradients and Hessians. We have also extended the theory of the incremental and CVT techniques from sc4DVAR to wc4DVAR. We now discuss the literature around the wc4DVAR problem both in its application and any relevant research related to the conditioning of the problem.

2.4 Literature Review

This chapter so far has been dedicated to introducing all the background material relevant to the work in this thesis.

We review the current literature in this section, with the intention of placing the research in this thesis adequately within the current body of research. This section is divided into two parts. We summarise the relevant literature with regards to the application of wc4DVAR, mainly the model error estimation formulation, in the first part. The second part reviews the literature more relevant to the subject of the thesis namely the conditioning of the wc4DVAR problem.

2.4.1 Applications of Weak-Constraint 4DVAR

The sc4DVAR problem has had more time under research focus than wc4DVAR since it became operationally viable in the early 90's, [45], [38], [39], [18]. This can be seen as a necessary stepping stone required to begin to understand the weak-constraint problem, since the sc4DVAR is just a simplification of wc4DVAR, by assuming the model is perfect. There have been numerous suggestions in the literature that wc4DVAR holds an advantage over the sc4DVAR, [84], [16], [17], which we will now discuss. It is important to note that the weak-constraint formulation considered in the majority of the literature refers to the J (p) formulation.

A study by Zupanski [94] examined the application of the both wc4DVAR and sc4DVAR on the regional National Centre for Environmental Prediction (NCEP) model. The author highlights that in the presence of model error, the sc4DVAR method provides a solution with incorrect initial conditions since it attempts to correct errors while enforcing the constraint of a perfect model. However wc4DVAR will average these errors out across the assimilation window yielding state estimates that are more inline with the truth. This means that the solution increment for the initial conditions from wc4DVAR is not as severe as sc4DVAR. She concludes that there is a need for considering wc4DVAR over the sc4DVAR. She also concedes that wc4DVAR is computationally expensive and ill-conditioned, and proposes looking at the lower-dimensional observation-space dual formulation of the problem.

A climate application of wc4DVAR in Korea using satellite data for heavy rainfall simulation was documented in [54]. The authors detail a study where they use both sc4DVAR and wc4DVAR and they clearly show that wc4DVAR provided much improved initial conditions for their model compared to sc4DVAR.

In 2004, Vidard et al. showed that wc4DVAR gives a marked improvement over sc4DVAR when applied to a non-linear one-layer two-dimensional shallow water model, [86]. The model error in this case was a systematic bias, but nevertheless it does serve as a good guide for a more complex setting. The authors conclude that the weak-constraint formulation provides a better solution both over the assimilation window and in the forecast phase.

An article by Lindskog et al. [56] details the implementation of the weak-constraint model error formulation to correct for known biases in the upper stratosphere on the ECMWF operational system. The paper highlights potential issues from a more practical perspective, but this often provides well-informed directions for the requirement of theoretical understanding. They conclude that careful wc4DVAR from a more theoretical perspective was presented by Cullen, [14]. The author compares cycled sc4DVAR to wc4DVAR by simplifying the problem down to a scalar case. He concludes that wc4DVAR must be interpreted as a smoother since it allows the control of error growth throughout the assimilation window. It is shown that where cycled sc4DVAR remains close to the observations, the solution in the scalar case converges to that of a long-window wc4DVAR equivalent. This is true if the regularisation of wc4DVAR, through the Q matrix, is identical to the regularisation of the cycled sc4DVAR method's B matrix at the beginning of each assimilation window cycle.

A. Moore et al. at the University of California discuss their Regional Ocean Modeling System (ROMS) implementation in a lengthy three-part paper, [68], [66] and [67]. The detailed implementation of both the original state-space primal form and lower dimensional observation-space dual form are detailed in [66]. The authors state that wc4DVAR is too large and computationally infeasible when considering the full primal problem. It is suggested that the dual formulation is a sensible step towards an operationally feasible implementation of wc4DVAR. They also discuss methods on error-covariance modeling and suggest preconditioners that have not been fully trialled yet. They conclude that the forecast skill of wc4DVAR is improved over sc4DVAR.

The collective avour of the literature indicates that wc4DVAR is superior to sc4DVAR. The minimisation problem that ensues from the wc4DVAR approach requires further study, since more degrees of freedom and a larger problem needs careful consideration. Some pieces of literature point in the direction of the dual formulation as a remedy for the size of the problem, [12]. However, we are not concerned with dual problem in this thesis.

A few pieces of literature produced by the ECMWF suggest they are actively developing their implementation of wc4DVAR, [27], [83], [84], [26]. Their intention is to tackle the more practical issues since their operational wc4DVAR implementation detailed in [56] has been put o -line (https://cimss.ssec.wisc.edu/itwg/itsc/itsc19/program/posters/nwp_3_english.pdf) due to numerical conditioning issues (conversation with Mike Fisher, ECMWF training course, 2013).

We now review the literature that is more closely related to the conditioning and preconditioning of the wc4DVAR problem.

2.4.2 Conditioning and Preconditioning of Weak-Constraint 4DVAR

At this moment, there are only a few select articles that are directly related to the conditioning or preconditioning of the wc4DVAR problem. They are not related to the study of the condition number, but the areas of research seem to be pointing in the direction of trying to understanding the minimisation process that arises from the wc4DVAR problem.

In [83], the author broadly summarises the variational approaches to the data assimilation problem in the presence of model error. An illustrative example in this paper alludes to the 'Laplacian-like' nature of the first term of $\mathbf{S}_x$ under simplistic assumptions ($\mathbf{M} = \mathbf{I}$ and $\mathbf{B} = \mathbf{Q} = \mathbf{I}$) and using $\mathbf{Q} = \mathrm{diag}\{\mathbf{Q}, \ldots, \mathbf{Q}\} = \mathrm{diag}\{\mathbf{I}, \ldots, \mathbf{I}\}$ to precondition.

$$\mathbf{S}_x^{\mathrm{precond}} = \mathbf{A} + \mathbf{Q}^{1/2}\mathbf{H}^T\mathbf{R}^{-1}\mathbf{H}\mathbf{Q}^{1/2}; \tag{2.61}$$

where

$$\mathbf{A} = \begin{pmatrix} 2\mathbf{I} & -\mathbf{I} & & \\ -\mathbf{I} & 2\mathbf{I} & -\mathbf{I} & \\ & \ddots & \ddots & \ddots \\ & & -\mathbf{I} & 2\mathbf{I} & -\mathbf{I} \\ & & & -\mathbf{I} & \mathbf{I} \end{pmatrix}; \tag{2.62}$$

where the other bold-faced matrices are block-diagonal partitions of their own respective matrices similar to $\mathbf{Q}$. If $\mathbf{M} \neq \mathbf{I}$, then the preconditioner would need to be composed in such a way as to remove the influence of $\mathbf{M}$ from the first part of the Hessian $\mathbf{S}_x^{\mathrm{precond}}$. This leads into the next part of the research efforts by the ECMWF to find a preconditioner which approximates $\mathbf{L}$ well, since $\mathbf{L}$ contains the model $\mathbf{M}$.

An internal ECMWF report, [27], suggests that the Hessian S_x is sensitive to the choice of preconditioner. Fisher et al. introduce an alternative saddle-point formulation of the problem. A disadvantage of the saddle-point system to be solved is that it will be

2.5 Summary

In this chapter we have introduced the strong-constraint and weak-constraint variational data assimilation problems. We introduced concepts such as the Gauss-Newton incremental approach and the CVT technique for both sc4DVAR and wc4DVAR. We also discussed the structures of the weak-constraint Hessians. This was then followed by a review of the current literature detailing the applications and conditioning of the weak-constraint problem.

We now introduce the mathematical framework required to understand and solve the 4DVAR problem and the necessary tools used to obtain the results in this thesis.

Chapter 3

Mathematical Theory

The variational data assimilation problem is statistical in its formulation but obtaining a solution from the non-linear objective function is an optimisation problem. In this chapter we introduce the necessary material and mathematical tools required to understand and solve the wc4DVAR problems. We remind the reader of the model error formulation,

$$\min_{p} \mathcal{J}(p) = \frac{1}{2}||p - p^b||^2_{D^{-1}} + \frac{1}{2}||\mathcal{H}(\mathcal{L}^{-1}(p)) - y||^2_{R^{-1}}; \tag{3.1}$$

and the state estimation formulation,

$$\min_{x} \mathcal{J}(x) = \frac{1}{2}||\mathcal{L}(x) - p^b||^2_{D^{-1}} + \frac{1}{2}||\mathcal{H}(x) - y||^2_{R^{-1}}: \tag{3.2}$$

We begin by introducing the condition number, followed by the numerical optimisation techniques used to solve wc4DVAR problems (3.1), (3.2). We then detail matrix norm properties required to analyse the condition number of the Hessians of (3.1), (3.2). Finally we introduce the models we use in our data assimilation experiments to put into context the sensitivities of the bounds and their effect on the performance of the optimisation problem.

3.1 Condition Number

The condition number measures sensitivities of the solution to perturbations in the input data. The input data for the data assimilation problem in this thesis is governed by the wc4DVAR objective functionals (3.1), (3.2). We examine the effect of perturbing input data on the wc4DVAR problem in this section to show the importance of the condition number, using a similar argument to that used in [34], (pages 302-304).

We assume the wc4DVAR objective functional has a solution, which we denote as x^*. We then perturb the input data by perturbing J and denote the perturbed objective function as $\tilde{J}$. The perturbed objective function has the solution

$$\hat{x} = x^* + h\,\delta x, \tag{3.3}$$

where $h = ||\hat{x} - x^*||$ and $||\delta x|| = 1$. We assume that the perturbation in the objective function is small enough to satisfy the following

$$|\tilde{J}(x^*) - J(x^*)| \leq |J(\hat{x}) - J(x^*)| \leq \epsilon. \tag{3.4}$$

The difference in the perturbed and original objective functions at x^* is assumed to be bounded above by the difference in the original objective functions evaluated at the original solution x^* and the perturbed solution $\hat{x}$. We make this assumption to understand some of the factors influencing solution accuracy. We expand J using the Taylor series

$$J(\hat{x}) = J(x^* + h\,\delta x) = J(x^*) + \frac{1}{2}h^2\,\delta x^T \nabla^2 J(x^*)\,\delta x + O(h^3) + \dots, \tag{3.5}$$

and approximate to second order. Therefore

$$2|J(\hat{x}) - J(x^*)| \approx ||\hat{x} - x^*||^2\,\delta x^T \nabla^2 J(x^*)\,\delta x. \tag{3.6}$$

Using $\frac{1}{|\delta x^T A\,\delta x|} \leq \frac{||A^{-1}||}{|\delta x^T\delta x|}$, we have

$$||\hat{x} - x^*||^2 \leq \frac{2\epsilon}{||\nabla^2 J(x^*)||}, \tag{3.7}$$

where we define the condition number as

$$\kappa = ||(\nabla^2 J)^{-1}||.||\nabla^2 J||. \tag{3.8}$$

We see from the expression (3.7) that the growth of the squared difference of the original and perturbed solutions is proportional to the condition number of the Hessian and the objective function differences. The relationship in (3.7) shows that the condition number of the Hessian is an appropriate measure of the sensitivity of the solution to small perturbations in the input data, and hence the objective function. However, the limitation of this assumption is that the perturbation in the objective function J must be small enough for (3.4) to hold and for the condition number κ seen in (3.7) to be considered a good measure. Another limitation is that the condition number of the Hessian here is linearised at the solution, which is not known in practice.

The specific condition number we use in this thesis is using the 2-norm. Therefore

$$\kappa = \frac{\lambda_{max}(\nabla^2 J)}{\lambda_{min}(\nabla^2 J)}; \tag{3.9}$$

3.2.1

Algorithm 3.1 Linear Conjugate Gradient

Counter $k = 0$.

Initial guess $x^{(0)} = 0$, if initial data does not exist,

Set residual $r^{(0)} = Ax^{(0)} \quad b^{(0)}$,

Set search direction $p^{(0)} =$

3.2.2 Preconditioned Conjugate Gradient

Preconditioned Conjugate Gradient (PCG) is used to speed up the convergence rate of CG by lowering the condition number of the system being solved. The cost of preconditioning must be cheap and reduce the condition number enough to achieve a considerable reduction in iterates. Let P denote the symmetric positive-de nite. The algorithm is as follows

---

Algorithm 3.2 Preconditioned Conjugate Gradient

Counter $k = 0$.

Initial guess $x^{(0)} = 0$, if initial data does not exist,

Set residual $r^{(0)} = Ax^{(0)} \quad b^{(0)}$,

For the rst iteration compute $z^{(0)} = P r^{(0)}$

Set $p^{(0)} = z^{(0)}$,

While $jjr^{(k)}jj > \quad ;$

$$^{(k)} = \frac{(r^{(k)})^T z^{(k)}}{(> \quad ;}$$

(k

3.2.3 The Polak-Ribiere Conjugate Gradient Method

We use the Polak-Ribiere CG (PRCG) method as an alternative to the linear CG method in later chapters to demonstrate links between iteratively solving the full non-linear problem and the iterative treatment of the Gauss-Newton approach to the 4DVAR problem.

Fletcher and Reeves extended the linear CG method to non-linear functions by

In an operational NWP setting there is not enough time or computing power to execute the amount of iterations required to solve the problem completely. Therefore an iterative stopping criterion is required. In the next section we brie y discuss the iterative stopping criterion used in our work.

3.2.4 Iterative Stopping Criterion

The purpose of iterative stopping criteria is to enable the user to stop the iterative solver when certain criterion are met, for example when it reaches a certain

3.3 Matrices

Definition 3.3.4 (See [35], Sec 2.3) The family of matrix p-norms on $\mathbb{R}^{N \times M}$ is such that

$$||C||_p = \sup_{x \neq 0} \frac{||Cx||_p}{||x||_p}, \tag{3.32}$$

for $C \in \mathbb{R}^{N \times M}$ and $x \in \mathbb{R}^M$.

In this thesis we use the 1-norm, 2-norm and ∞-norm. For explicit definitions of these norms please refer to [35], Section 2.3.

We now state some useful norm relations which are used in cases where the norms may be difficult to calculate explicitly.

Theorem 3.3.5 (See [3], Sec A.1) For matrices $A, B \in \mathbb{R}^{N \times N}$ the following

3.3.2 Toeplitz Matrices

We use covariance matrices with a special structure in our research, which fall under a class of matrices known as Toeplitz matrices. So we begin this section by introducing the Toeplitz matrix, which gets its name from the German mathematician Otto Toeplitz. He was the first person to work with Toeplitz operators in 1911, [82]. A Toeplitz matrix is such that

$$T = \begin{pmatrix} t_0 & t_{-1} & t_{-2} & \cdots & \cdots & t_{-(N-1)} \\ t_1 & t_0 & t_{-1} & \ddots & & \vdots \\ t_2 & t_1 & \ddots & \ddots & \ddots & \vdots \\ \vdots & \ddots & \ddots & \ddots & t_{-1} & t_{-2} \\ \vdots & & \ddots & t_1 & t_0 & t_{-1} \\ t_{N-1} & \cdots & \cdots & t_2 & t_1 & t_0 \end{pmatrix}$$

where $T \in \mathbb{R}^{N \times N}$ and the entries

The matrix is composed of cyclic permutations of the first row. A useful property of a circulant matrix is that the eigenvalues and eigenvectors can be written as Fourier transforms of the top row explicitly. The eigenvalues and eigenvectors of circulant matrices are explicitly known.

Theorem 3.3.8 (See [37], Section 3.1) The eigenvalues of C denoted $\lambda_m(C) \in \mathbb{C}$ are such that

Theorem 3.3.10 (See [37]) Circulant matrices have the following eigendecomposition:

$$C = F \;{}_{C} F^{H} \tag{3.39}$$

where ${}_{C}$ = diag(${}_{1}(C); :::; {}_{n}(C))FF$

for $x; y \in R^N$. The expected value of a random field is denoted as $<\cdot>$. A direct consequence of (3.43) is the function is symmetric, $\Gamma(x; y) = \Gamma(y; x)$.

for $i, j = 1, \ldots, N$.

We now discuss the background and model error covariances more specific to the on the real line and on the periodic domain we replace the great circle distance in (3.50) by the chordal distance

$$d = 2a\sin$$

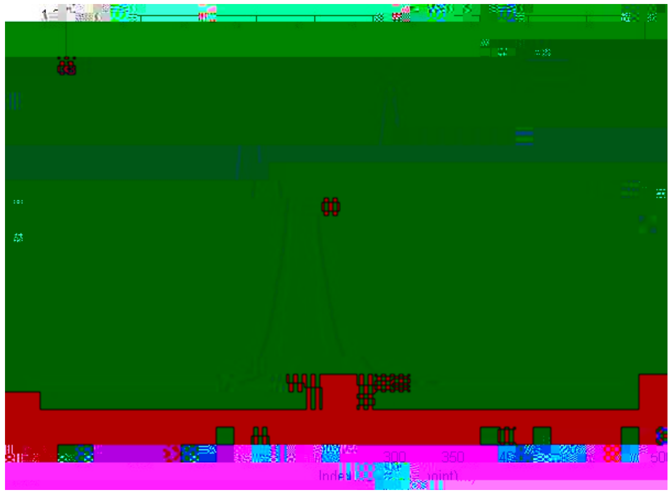

Figure 3.1: 250th row of the Laplacian (red line) and SOAR (blue line) correlation matrices. Model grid points $N = 500$, $L = 0{:}9$ for both Laplacian and SOAR.

The correlation structures of the SOAR and Laplacian covariance matrices are shown in Figure 3.1. The Laplacian covariance matrix has negative correlations whereas the SOAR matrix does not. We also notice that the SOAR correlations have a larger spread across the grid points in comparison to the Laplacian correlation structure.

We now introduce the apparatus we have employed in the thesis to bound the condition number of the Hessian of the wc4DVAR objective functions.

3.4

3.4.1 Eigenvalue Bounds and Mathematical Results

We begin with the following determinant theorem.

Theorem 3.4.1 For any given square matrices $A, B \in R^{N \times N}$ of equal size we have

$$Det(AB) = Det(A)Det(B). \tag{3.55}$$

One of the most useful eigenvalue bounds used on more than one occasion in our work is the following.

Theorem 3.4.2 Courant-Fischer Theorem [See [35], Section 8.1].
For any given symmetric matrices $A, B \in R^{N \times N}$ the k^{th} eigenvalue of the matrix sum $A + B$ satisfies

$$\lambda_k(A) + \lambda_{min}(B) \leq \lambda_k(A + B) \leq \lambda_k(A) + \lambda_{max}(B). \tag{3.56}$$

We also have

Theorem 3.4.3 (See [35], Sec 8.6) Let $E \in R^{N \times M}$ such that $M < N$. Then the non-zero eigenvalues of EE^T and E^TE are equal and EE^T has $N - M$ additional eigenvalues equal to zero.

Another simple yet effective upper bound using norms is as follows:

Theorem 3.4.4 (See [3], Section A.1) For a matrix $A \in R^{N \times N}$ then the following is true:

$$|\lambda_k(A)| \leq \|A\|_p \tag{3.57}$$

for $p \geq 1$.

Finally,

Theorem 3.4.5 (See [11], Section 2.4 (p13-14)) For finite $m, n \in \mathbb{Z}_{>0}$ and $p \in \mathbb{R}$, we have:

$$\sum_{p=-m}^{n} p = \frac{(n+1-m)(n+m)}{2} \tag{3.58}$$

$$\sum_{p=1}^{n} p^2 = \frac{n(n+1)(2n+1)}{6}. \tag{3.59}$$

We now introduce the Rayleigh Quotient.

3.4.2 Rayleigh Quotient

The Rayleigh Quotient is historically named after Baron Rayleigh (John William Strutt), an English physicist who received a Nobel prize in physics in 1904. This function is also known as the 'Rayleigh-Ritz ratio' in engineering, where it was also named after Walther Ritz, a Swiss theoretical physicist. The Rayleigh Quotient is a function which we use for the purpose of eigenvalue estimation in this thesis.

Definition 3.4.6 (See [3], Section 4.4) The Rayleigh quotient of a symmetric matrix $A \in \mathbb{R}^{N \times N}$ is as follows:

$$R_A(x) = \frac{x^H A x}{x^H x} \tag{3.60}$$

for $x \in \mathbb{C}^N$, where x^H is the Hermitian of x.

To find the smallest eigenvalue one would simply substitute the eigenvector that corresponds to the smallest value $R_A(x) = \frac{x^H A x}{x^H x}$

(3.5J/F33 7.9701 Tf 6.5868293793 Td [(A)]miTJ/F15 11.9552 Tf 9.6165 .793 Td [(()]TJ/F32 11.9552 Tf 4.552 0

Theorem 3.4.7 (See [81], Section 5.9) Let $A \in \mathbb{R}^{N \times N}$ be a symmetric matrix. Then the Rayleigh quotient (3.4.6) is bounded such that:

$$\lambda_{min}(A) \le R_A(x) \le \lambda_{max}(A). \tag{3.62}$$

3.4.3 The Block Analogue of Gersgorin's Circle Theorem

Semyon Aranovich Gersgorin introduced his theorem as early as the 1930's, [32], now known as the scalar Gersgorin's circle theorem. He introduced the notion of bounding the eigenvalues of a matrix by the sum of the row and/or column constituents in the following theorem.

Theorem 3.4.8 (See [85]) Let $A \in \mathbb{C}^{N \times N}$. Then all eigenvalues λ of A satisfy

$$|\lambda - a_{i;i}| \le \sum_{j \neq i}^{N} |a_{i;j}|; \tag{3.63}$$

where $a_{i;j}$ denotes the entries of A on the i^{th} row and j^{th} column.

It is a well-known theorem with many applications in linear algebra and numerical

This constitutes all the mathematical apparatus used in the rest of the thesis. We now introduce the models used in our experiments to demonstrate the sensitivities obtained from the theoretical bounds on the condition number of the Hessian.

3.5 Models

In this section we introduce the models used in this thesis to illustrate the theory we have derived.

The first model is a linear advection equation. This is a simplified model describing the transportation of a passive tracer through the atmosphere. In the atmosphere if we consider very small intervals of space and time, the movement of a passive tracer will be approximately linear, similar to that of the advection equation.

The second model is the non-linear chaotic Lorenz 95 system. The variables in this system simulate values of some atmospheric quantity in sectors of a latitude circle. The physics of the model possess useful weather-model-like characteristics such as external forcing, internal dissipation and advective terms. The error growth of this model is also similar to that of full NWP models.

The numerical discretisation of these models presents a set of calculations required to propagate the model from one time step to the next. These are represented in matrix form in the following sections. We now introduce the models used in this thesis.

3.5.1 The Advection Equation

The advection equation is a partial differential equation describing the flow of a scalar quantity, $u(x;t)$, through space, x with respect to time, t:

$$\frac{\partial u}{\partial t} + a\frac{\partial u}{\partial x} = 0 \tag{3.66}$$

where the scalar quantity is moved through a vector eld at a velocity ofa(

For 1 0 the nite di erence system (3.71) is consistent, stable and convergent, [69], Section 5.4.

We have introduced all the necessary properties of the advection model that we use in the thesis. We now discuss the non-linear chaotic Lorenz 95 model.

3.5.2 The Lorenz 95 Model

The Lorenz 95 model was pioneered by Edward Lorenz, making its rst appearance in the article [62], in 1996. This later made its way into published format

To understand the relevance of using the Lorenz 95 system we must understand

leading Lyapunovlet110(will)-7

95 system are similar to that of full weather models, with a doubling time of 2.1 days, making it a suitable model to use for weather prediction purposes.

The Lorenz 95 ODE equations take the form

$$\frac{dX_j}{dt} = \quad X_{j \quad 2} X_{j \quad 1} + X_{j \quad 1} X_{j+1} \quad X_j + F$$;33.62J ET q 27(e9552 Tf 11.761

In the next chapter we discuss the design considerations for the application of both formulations $J(p)$ and $J(x)$ on the 1D advection model. We then compare the performance of both formulations of wc4DVAR when subjected to changes in the data assimilation parameters composing the problem.

4.1.1

[illegible]

and tangent linear arise from linearising $\mathbf{L}$. The input and output of the wc4DVAR operators are '4-dimensional', since they require inputs defined at several temporal points. The wc4DVAR model operator also has linearised inverses $\mathbf{L}^{-1}$ and $\mathbf{L}^{-T}$, which constitute part of the wc4DVAR gradient calculations. So the additional tests required for wc4DVAR are to ensure that the mapping between model states and model errors is correct for non-linear $\mathbf{L}$ and linearised $\mathbf{L}$ operators and their inverses.

We carry out four principal tests in the preceeding sections to ensure the that the wc4DVAR assimilation system is correctly coded. The first test is checking that the numerical mapping of; the $\mathbf{L}$ operator, the linearised $\mathbf{L}$ operator and the linearised adjoint operator $\mathbf{L}^T$ are all correct. The second test ensures that the gradient of the $\mathbf{L}$

(a) $||L x - p|| \approx 0$;

(b) $||L^{-1} p - x|| \approx 0$.

3. Linearised adjoint model operator and inverse;

(a) $||L^{T} x - p|| \approx 0$;

(b) $||L^{-T} p - x|| \approx 0$.

The quantities in tests 1, 2 and 3 must equal exactly zero or be very close to machine precision $O(10^{-15})$. We choose the 2-norm for each test detailed above and ensure it is in the vicinity of machine precision.

Test	Norm of the Difference
1(a)	1.70E-014
1(b)	3.72E-015
2(a)	1.43E-015
2(b)	1.37E-015
3(a)	1.32E-015
3(b)	1.43E-015

Table 4.1: Mapping test results.

Table 4.1 shows that the results are all in the region of machine precision, therefore the numerical mapping tests are all numerically valid.

We now discuss the wc4DVAR equivalent of the tangent linear test.

4.1.3.2 The Linearised Weak-Constraint Model Operator: Correctness Tests

Taylor expansion of our non-linear operator to first-order yields the following approximated identities:

$$\frac{||L(x + \gamma\delta x) - L(x)||}{||L\gamma\delta x||} = 1 + O(\gamma\delta x); \tag{4.3}$$

$$||L(x + \gamma\delta x) - L(x) - L\gamma\delta x|| \approx 0; \tag{4.4}$$

which should hold for small values of $_i$ x. We vary $_i$ such that

$$_i = 10^{1 \quad i}; \tag{4.5}$$

for i = 1; :::; 16. Since the advection model is linear, there should be no higher order terms in the expansions above. The purpose of these tests is to ensure the numerical validity correctness of the gradients of these two operators. We also test the inverse, L in a similar manner.

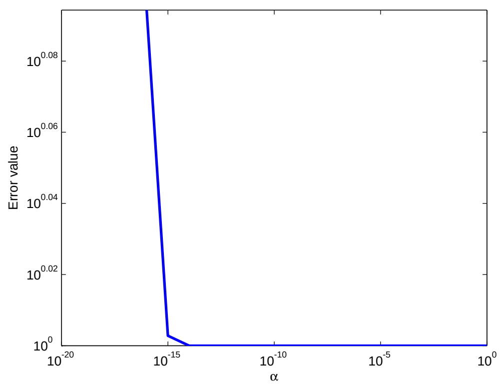

(a) Identity test (4.3).

(b) Identity test (4.4).

Figure 4.1: Correctness test plots for the L operator.

Figure 4.2 shows that the correctness tests also hold for inverse operator, L^{1}.

We now discuss the final test with regards to the L operator. This is required for the calculation of the gradients of $J(p)$ and $J(x)$.

4.1.3.3 The Linearised Weak-Constraint Adjoint Model Operator: Validity Tests

This test is equivalent to the sc4DVAR adjoint test. The aim is to test the validity of the inner products

$$< y; L x > = < L^{T} y; x >; \tag{4.6}$$

$$< y; L^{1} x > = < L^{T} y; x >: \tag{4.7}$$

These tests are done by executing each side of the respective equations numerically and comparing the results. We call the left-hand side of each equation (4.6) and (4.7) the 'forward product' and the right-hand side is called the 'adjoint product'.

	Forward Product	Adjoint Product	Difference
Test (4.6)	-45.484273829763183	-45.484273829763133	4.9738e-014
Test (4.7)	-216.363507105409070	-216.363507105409130	5.6843e-014

The difference of both products is in the range of machine precision, which concludes that the numerical adjoint operator is accurate to machine precision.

This concludes all the tests for the L operator. The L operator is required for both calculating the objective functions (2.32), (2.33) and the gradients of the objective functions (2.34) and (2.35). We now discuss the final test in the assimilation system, which tests the numerical validity of the coded objective function gradient.

4.1.3.4 Objective Function Gradient: Validity Tests

This test is similar to the tests in Section 4.1.3.2, but instead we check the numerical validity of the objective functions (2.32) and (2.33) and their respective gradient calculations (2.34) and (2.35). We verify that

$$\Phi(\alpha) = \frac{J(x + \alpha\delta x) - J(x)}{\alpha\,\delta x^T \nabla J(x)} = 1 + O(\alpha); \qquad (4.8)$$

is accurate for sufficiently small perturbations δx.

The gradient test for the objective function is different to the gradient test in Section 4.1.3.2 because the operators are different. The operator in Section 4.1.3.2 is such that $L : \mathbb{R}^{N(n+1)} \to \mathbb{R}^{N(n+1)}$, which is why norms were used. The weak-constraint objective functions (2.32) and (2.33) are such that $J : \mathbb{R}^{N(n+1)} \to \mathbb{R}$, so no norms are required.

For perturbations that are too large the identity (4.8) will not hold since the higher order terms will increase and the approximation made in (4.8) is to first-order. If the perturbations are too close to machine precision the identity (4.8) will not hold because the denominator of (4.8) will approach zero.

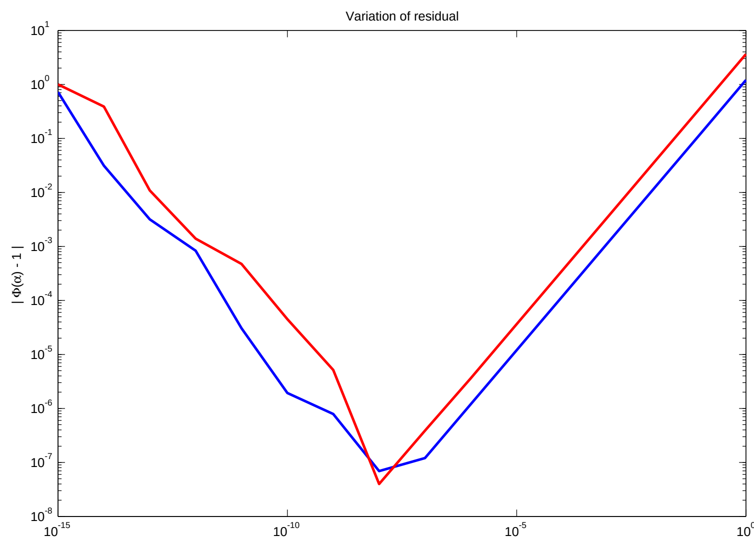

Figure 4.3: Objective function gradient test. The red line shows the gradient test (4.8) for $J(p)$. The blue line shows the gradient test (4.8) for $J(x)$.

Figure 4.3 shows that for sufficiently small perturbations the identity (4.8) holds for both $J(p)$ and $J(x)$.

This concludes all the tests to ensure mathematical and numerical accuracy of both wc4DVAR assimilation systems for solving $J(p)$ and $J(x)$. The second consideration to discuss is the nature of the observations we use to observe the truth.

4.1.4 Observations

The observations y are generated using the truth trajectory plus additive Gaussian noise such that

$$y = y^t + y^e; \tag{4.9}$$

where y^t is the unchanged true state at the appropriate spatio-temporal grid-points, and y^e $N(0; {}^2_o I)$. The observation error variance is stated before each experiment.

We take the observations directly at the grid points with regular intervals in space, where the rst spatial point is always observed. We also observe at regular intervals in time, where the rst temporal point is always observed. We let the temporal observation interval (also referred to in this thesis as an 'assimilation step') be every q model steps. We observe the same grid-points at every assimilation step, thus the observation operator H_i

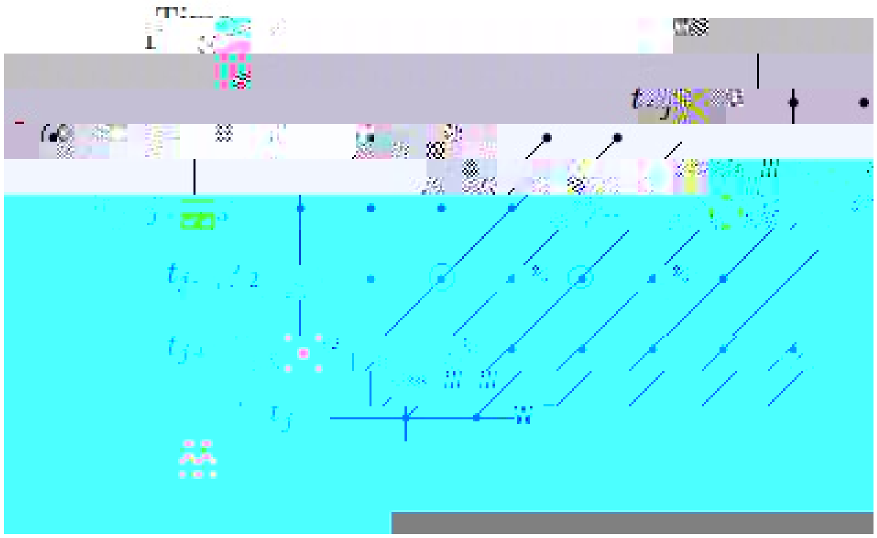

Figure 4.4: Advection Equation characteristic curves. The black lines are the advection equation characteristic lines, and the red circles are observation points.

In Figure 4.4 we see that if we were to observe every other temporal and spatial point, some of the characteristic lines will be missed. Even with a periodic domain, the same characteristic lines will remain unobserved for an inde nite time period. We ensure that the temporal and spatial spacing of the observations is such that none of the characteristic lines are missed.

In this section we have discussed our choice of observation con guration. We now state how our background trajectory is created.

4.1.5 Background Trajectory

The background trajectory, p^b, is created using the truth trajectory plus additive Gaussian noise such that

$$p^b = p^t + p^e; \qquad (4.10)$$

where p^e $_{e}{}_{e}$

4.1.6 Solution Error

The relative solution errors are calculated at each time t_i such that

$$re_i = \frac{||x_i^t - x_i||_2}{||x_i^t||_2}, \tag{4.11}$$

where $x_i \in \mathbb{R}^N$ is the solution vector resulting from the assimilation, which describes the state at time t_i and the superscript denotes ‘truth’. The total relative error is simply the L_2 norm calculation of the vector containing the values of re_i for $i = 1, \ldots, n+1$.

We now state our choice of iterative solver.

4.1.7 Iterative Solver and Stopping Criterion

We use the LCG method detailed in Section 3.2.1 for both (2.32) and (2.33). Both

1. number of observations;
2. length of the assimilation window;
3. correlation length-scales;
4. background, model and observation error variances.

We gauge the performance of the weak-constraint minimisation problems by examining:

1. the relative error within the assimilation window between the truth and the solution. We compare the generated truth to the state estimates obtained using the $J(x)$ formulation. We also compare the generated 'true' model errors to the model error estimates obtained from the $J(p)$ formulation;
2. the number of iterations required to achieve the desired tolerance;
3. the numerical condition number.

The covariances and error variances used to generated the truth are identical to those used in the assimilation experiments. We now present our experimental results.

4.2.1 Experiment 1: Observation Density

The aim of this experiment is to highlight the e ect of number of observations on the solution process of both wc4DVAR formulations. We choose all other parameters in this experiment such that the only possible contribution to any rise in condition number must be the number of observations. So we choose low correlation length-scales, short assimilation windows and error variance ratios which are close to 1.

4.2.1.1 Experiment 1a: Half Spatial Domain Observed

The experiment settings are as follows. We choose the background error, B_0 = ${}^2_b C_{SOAR}$, such that the correlation length-scale $L = 2 \quad x = 0{:}04$ and $_b = 0{:}1$. The model error, $Q_i = \quad {}^2_q C_{LAP}$ is such that the correlation length-scale $L = \quad x = 0{:}02$ and $_q = 0{:}05$. The observation error is such that $R_i = \quad {}^2_o I$, where $_o = 0{:}05$. We take observations every $q = 5$ model time-steps, $n = 10$ in total, with 25 equally spaced observed grid-points out of the $N = 50$ grid-points per assimilation step. The iterative tolerance is set to $= 10 \quad ^4$.

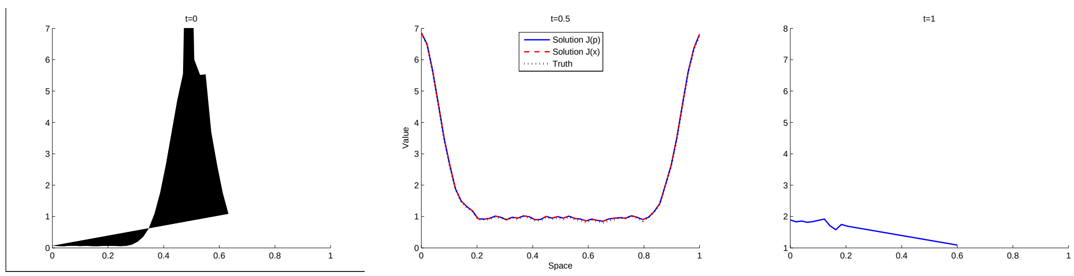

Figure 4.5: Assimilation window time series left to right, $t = 0$, $t = n/2$ and $t = n$. Truth (black-dashed line), wc4DVAR $J(x)$ solution (red line), wc4DVAR $J(p)$ solution (blue line).

In Figure 4.5 we see the time series plot of the truth and the solutions of both wc4DVAR algorithms. We can see that visually the solutions are in close agreement with the truth.

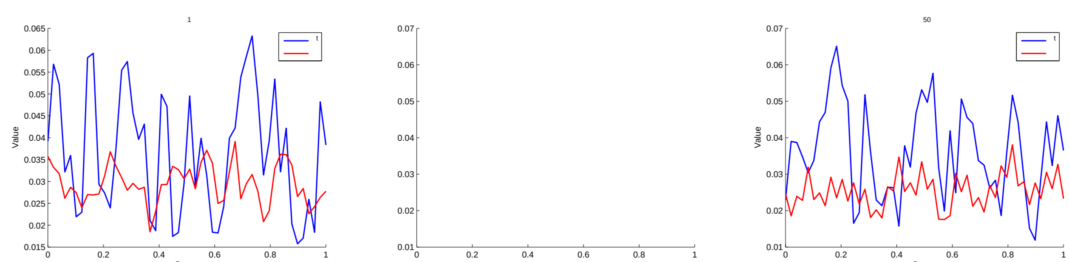

Figure 4.6: Model error time series left to right, $t = 0$, $t = n/2$ and $t = n$. Estimated model error (red line) using wc4DVAR $J(p)$. True model error (blue line).

In Figure 4.6 we see the time series plot of the true model error vs the estimated model error at the end of the minimisation using $J(p)$. The variance of the

4.2.1.2 Experiment 1b: Sparse Spatial Observations

The experiment settings are identical to those in Experiment 1a, except that there

$t = 0$ and $t = n=2$ with a noticeable under-estimation of the variance. We also see evidence of poor model error estimation at the final time step in Figure 4.9. The final time step estimated model error mean is incorrect, however the variance has been well estimated.

Matrix	Condition Number	No. of iterations
S_p	278	43
S_x	1663	412
D	837	-

Table 4.3: Numerical condition numbers and iteration count of respective objective function minimisations.

Table 4.3 shows that minimisation of $J(x)$ takes 10 times more iterations than $J(p)$, as well as an increase in Hessian condition number. These condition numbers are still not particularly indicative of any serious ill-conditioning. We believe the condition number of D is not the main contributor of ill-conditioning in this experiment since it remains the same as Experiment 1a, while the only change we have introduced is a decrease in the number of observations. The observations are associated with the second term of both Hessians S_p and S_x, where D is the first term.

We also see that the condition numbers of S_p and S_x have both roughly doubled, compared to Experiment 1a, while the condition number of S_x remains approximately 3 times higher than the numerical condition number of S_p. It is possible that the $J(x)$ formulation is sensitive to the decrease in spatial observations, due to the increase in condition number and iterations exhibited in this experiment.

Figure 4.10: Assimilation relative error calculations. Errors in wc4DVAR $J(x)$ solution (red line), wc4DVAR $J(p)$ solution (blue line).

In Figure 4.10 we see that the errors look the same throughout the assimilation window, with total relative errors of 0.356 for $J(x)$ and 0.357 for $J(p)$. We also see that the errors are distributed at the beginning and mostly the end of the assimilation window, showing that both solutions failed to correctly specify the initial conditions and the model errors at the end of the assimilation window.

4.2.1.3 Summary

The number of observations a ects the assimilation problem in that there is less information to t. In this experiment we see two pieces of evidence, which show the sensitivities of $J(x)$ to the number of observations: the increase in numerical condition number and the number of iterations required for convergence. The errors in the solution remain the same as they should, since we solve both

4.2.2 Experiment 2: Error Variance Ratios

The aim of this experiment is to highlight the e ect of changing the error variances (^2_b, ^2_q, ^2_o) on the minimisation of J (p) and J (x). We choose all other parameters to ensure that any change in condition number or iterations comes solely from the error variances. The iterative tolerance is changed to = 10^{10} to ensure high solution accuracy. The iterative solver will reach the solution before the tolerance is reached, but we are ensuring that each algorithm yields its respective optimal solution. The iterations after reaching the solution are not important and the algorithm that reaches its solution in the least number of iterations will still take

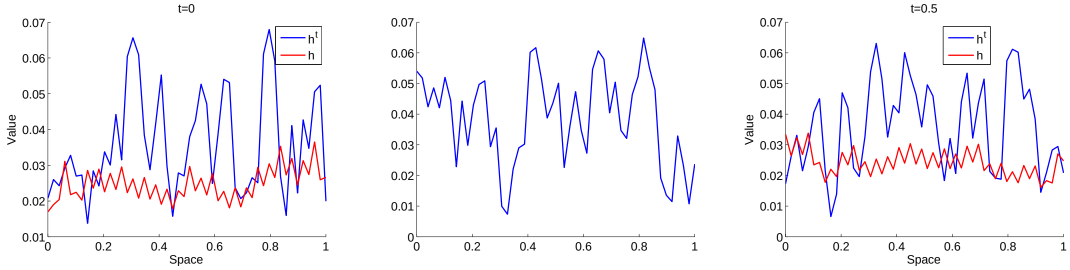

Figure 4.12:

Ratio	Value
$_b = \ _q$	200
$_b = \ _o$	200
$_q = \ _o$	1

Table 4.5: Assimilation error variance ratios.

The $_b = \ _q$ ratio in Table 4.5 explains the large condition number of D since this ratio increases the difference between the largest and smallest eigenvalue of the matrix D

4.2.2.2 Experiment 2a (ii): Small Background Error Variance

In this experiment we use the same parameters as the previous experiment except we change the background standard deviation from $_b = 10$ to $_b = 2{:}5 \quad 10^{4}$ so that it is now 200 times smaller than $_q$, as opposed to being 200 times bigger as in Experiment 2a (i). We only show results related to the performance of the minimisation of both J (p) and J (x).

Matrix	Numerical Condition No.	No. of iterations
S_p	$8{:}53 \quad 10^{6}$	635
S_x	$1{:}00 \quad 10^{8}$	1756
D	$8{:}53 \quad 10^{6}$	-

Table 4.6: Numerical condition numbers and iteration count of respective objective function minimisations.

In Table 4.6 we see that the minimisation of J (x) requires just under 3 times as many iterations as J (p) to achieve the same gradient tolerance respective to each objective function. The numerical condition number of S_x is $O(10^2)$ higher than S_p. This complements the higher number of iterations seen for J (x) over J (p). We also see that the numerical condition number of S_p is of the same order of magnitude as D.

Ratio	Value
$_b = _q$	$5 \quad 10^{3}$
$_b = _o$	$5 \quad 10^{3}$
$_q = _o$	1

Table 4.7: Assimilation error variance ratios.

The small $_b = _q$ is the reason for the large condition number of D. The large condition numbers of S_p and S_x follow the large condition number of D in this experiment, with S_x exhibiting more sensitivity.

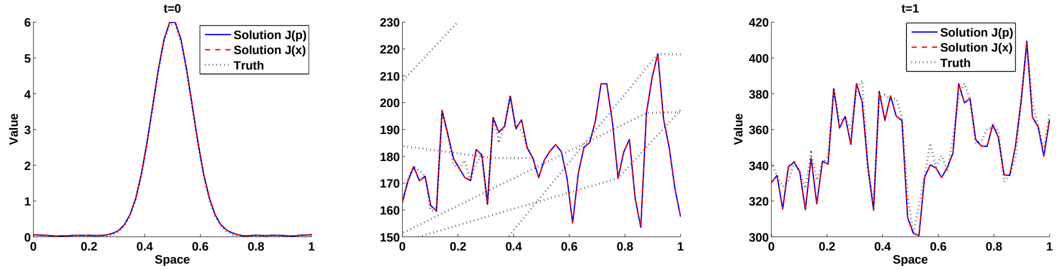

Figure 4.15: Assimilation window time series left to right, t = 0, t = n=2 and t = n. Truth (black-dashed line), wc4DVAR J (x) solution (red line), wc4DVAR J (p) solution (blue line).

Figure 4.15 shows that the solutions are of similar quality. The problem is more demanding since the variance of the model errors are much larger now. Even with the power of wc4DVAR to closely match the trajectory inside the assimilation window, both solutions are noticeably missing the truth because the true model errors are considerably large.

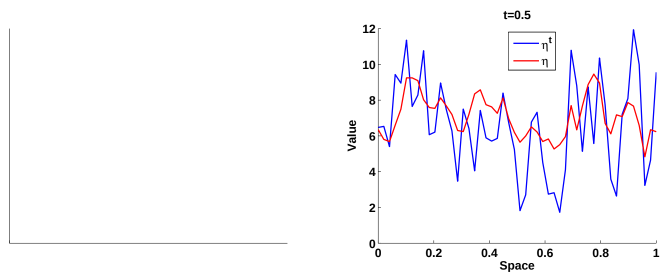

Figure 4.16: Model error time series left to right, t = 0, t = n=2 and t = n. Estimated model error (red line) using wc4DVAR J (p). True model error (blue line).

In Figure 4.16 we see the variance of the estimated model error is again not quite as large as the true model error. On the nal time step the variance of the true model error is more than twice as large as the range of the estimated model error.

Matrix	Numerical Condition No.	No. of iterations
S_p	1:09 10^7	341
S_x	1:88 10^7	972
D	2:13 10^6	-

Table 4.8: Numerical condition numbers and iteration count of respective objective function minimisations.

Table 4.8 shows the numerical condition number of S_x to be nearly double that of

S_p. Similarly, the minimisation of $J(x)$ requires more than double the number of iterations compared to$J(p)$.

Ratio	Value
$_b = {}_q$	10^q

We now reduce the model error variance and examine its effect on the minimisation of both wc4DVAR problems.

4.2.2.4 Experiment 2b (ii): Small Model Error Variance

In this experiment we use the same parameters as the previous experiment except we change the model standard devation from $\sigma_q = 10$ to $\sigma_q = 5 \times 10^{-4}$. We now discuss the effect this has on the assimilation.

Matrix	Numerical Condition No.	No. of iterations
S_p	7.85×10^{3}	182
S_x	1.57×10^{6}	2693
D	1.41×10^{6}	-

Table 4.10: Numerical condition numbers and iteration count of respective objective function minimisations.

Table 4.10 shows the minimisation of $J(x)$ requiring over 15 times as many iterations as $J(p)$. The numerical condition number of S_x and D are 3 orders of magnitude higher than S_p, which complements the difference in the number of iterations. We also see that the numerical condition number of S_x is of the same order of magnitude as D.

Ratio	Value
σ_b/σ_q	200
σ_b/σ_o	2
σ_q/σ_o	0.01

Table 4.11: Assimilation error variance ratios.

The high σ_b/σ_q value is the reason for the high condition number of D, since they increase the distance between the extrema eigenvalues of D.

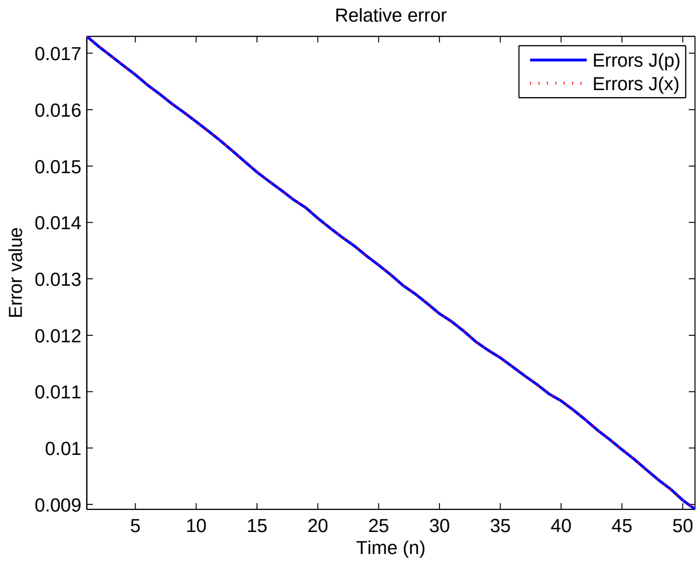

Figure 4.18: Assimilation relative error calculations. Errors in wc4DVAR J (x) solution (red line), wc4DVAR J (p) solution (blue line).

In Figure 4.18 we see that the errors are identical again with total relative error values for both formulations at 0095, while the distribution of errors is linear and di ers from the previous experiment, Figure 4.17. The bulk of the errors are in the beginning of the assimilation window, which linearly decrease until nal time. The errors are largest at the beginning of the window because the size of the background error variance $_b$ is large relative to $_q$.

We now examine the e ects of the observation error variance.

4.2.2.5 Experiment 2c (i): Large Observation Error Variance

The experiment settings identical to the previous experiment with the exception of, the background standard deviation, $_b$ = 0:1, model standard deviation, $_q$ = 0:05 and increased observation standard deviation$_o$ = 10, thus yielding the following error variance ratios:

Ratio	Value
$_b = _q$	2
$_b = _o$	0.01
$_q = _o$	5 10 ^{3}

Table 4.12: Assimilation error variance ratios.

We now present the time series plots of the solution with the truth

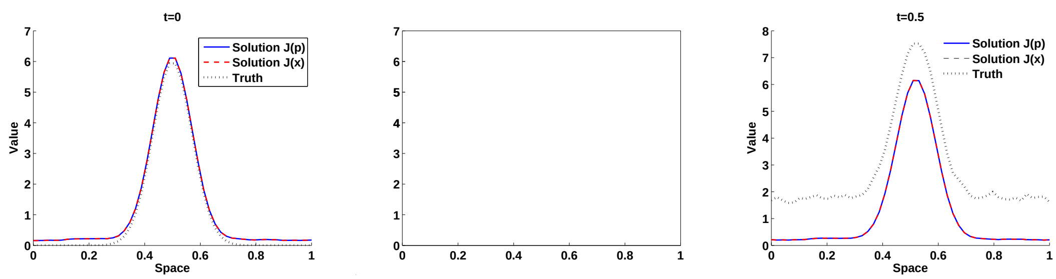

Figure 4.19: Assimilation window time series left to right, t = 0, t = n=2 and t = n. Truth (black-dashed line), wc4DVAR J (x) solution (red line), wc4DVAR J (p) solution (blue line).

Figure 4.19 shows that both solutions are showing visually noticeable shortfalls at this scale, even with the truth and assimilation error settings being identical. This is mainly due to the $_q$ parameter being too restrictive and not allowing for

Matrix	Numerical Condition No.	No. of iterations

4.2.2.6 Experiment 2c (ii): Small Observation Error Variance

In this experiment we use the same parameters except we change the observation standard devation from $_o = 10$ to $_o = 5 \quad 10^{4}$, yielding the following error variance ratios

Ratio

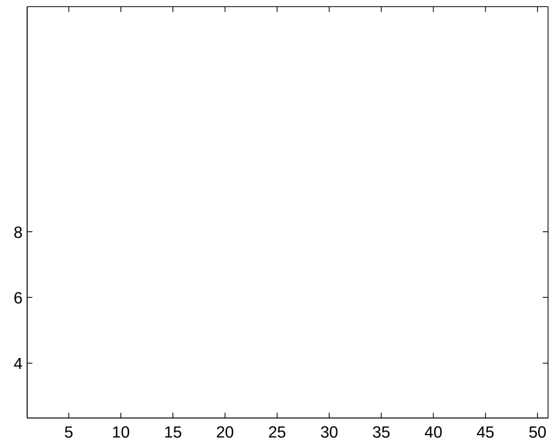
8
6
4
5
10
15
20
25
30
35
40
45
50

The experiments we have considered with model errors show that even with model errors larger than the background error, both algorithms can still solve the problem relatively well, as seen in Figure 4.18. However this comes at the cost of increased condition numbers and iterations for both $J(x)$ and $J(p)$, where $J(x)$ exhibits the most sensitivity in terms of iterations to convergence. When the model error is small the problem becomes less demanding in general, and both algorithms solve to much improved accuracy as seen from Figure 4.18. But it is clearly evident that $J(x)$ is far more sensitive to changes in $_q$

the e ect of a longer assimilation window.

In previous experiments in this chapter we had an assimilation window which allowed the advection model to propagate the Gaussian curve far enough through the domain so it passes by its original percevied position, we denote this as one period. In the following experiment we lengthen the assimilation window to allow for the Gaussian curve to pass its original starting position 5 times. We reduce the spatial resolution so that the Hessian matrix remains a reasonable size for an notice the Gaussian curve has moved upwards and deformed considerably over time, since the assimilation window is now much longer and the model has more time to evolve the initial state. We can also see that some ner details of the Gaussian curve structure have been missed by both solutions.

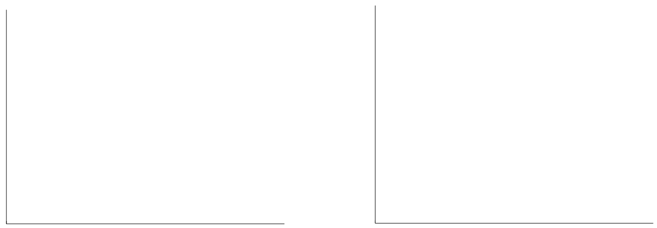

Figure 4.24: Model error time series left to right, $t = 0$, $t = n=2$ and $t = n$. Estimated model error (red line) using wc4DVAR $J(p)$. True model error (blue line).

Figure 4.24 agrees with Figure 4.23 in that the $J(p)$ formulation has mimicked the truth. The estimated model errors have a much improved error variance than in previous experiments. It is likely that the longer assimilation window has improved the estimates of the model error.

Matrix	Numerical Condition No.	No. of iterations
S_p	$6:13 \quad 10^4$	71
S_x	$1:66 \quad 10^3$	42
D	878	-

Table 4.16: Numerical condition numbers and iteration count of respective objective function minimisations.

Table 4.16 shows that $J(p)$ requires nearly twice as many iterations as $J(x)$ to converge on an equivalent solution. The condition number of S_p is an order of magnitude higher than S_x. This is not proportional to the increase in iterations, but we see a simultaneous increase in condition number and iteration count of $J(p)$ over $J(x)$, further reinforcing the possibility of $J(p)$ being more sensitive to assimilation window length than $J(x)$.

Figure 4.25: Assimilation relative error calculations. Errors in wc4DVAR $J(x)$ solution (red line), wc4DVAR $J(p)$ solution (blue line).

Figure 4.25 shows that the errors in $J(p)$ are slightly higher, with a total relative error of 0.196, whereas $J(x)$ has a total relative error of 0.153. The relative errors are low with the exception of the beginning of the assimilation window.

Summary

This experiment shows that the length of the assimilation window, while it affects both algorithms, has a more profound effect on the minimisation of $J(p)$, through an increased Hessian condition number and iterations. The $J(x)$ formulation performs better in this experiment in terms of condition number, number of iterations and relative solution error, with a fully observed domain.

4.3 Conclusions

In this chapter we detailed the design of the weak-constraint variational system along with the tests to ensure its numerical validity. We then explained our reasoning behind the choice of observation configuration and model setup to carry out the experiments. The experiments were carried out on a simple 1-dimensional linear system using correlated background and model error covariances and regular observation spacing to enable us to study the e ects of di erent parameter settings on the minimisation process. The experiment results showed the following:

1. The $J(x)$ formulation is more sensitive to lower observation density than $J(p)$. The $J(x)$ formulation takes longer to converge onto an identical quality solution to $J(p)$ with the same settings. The Hessian condition number of $J(x)$ is also higher than that of $J(p)$. This is shown in Experiments 1a and 1b.

2. The $J(x)$ formulation is more sensitive than $J(p)$ to the balance of model errors with background errors. This can be seen from ndings in Experiments 2a and 2b.

   (a) Experiment 2a shows that $J(x)$ is sensitive to changes in the background error, more so when the background error is small. This is seen in the number of iterations only.

   (b) Experiment 2b shows the increased sensitivity of $J(x)$ over $J(p)$ for small model error variances $_q$. This is seen in the condition number and the number of iterations required for convergence.

   (c) Experiment 2c shows that a large observation error variance dramatically increases the number of iterations required by $J(x)$ to converge. The condition number is also very large, of order 5 times larger than the condition number of S_p. We see that for a small observation error variance, the $J(x)$ formulation takes less iterations to converge than $J(p)$ for the rst time, albeit not by a signi cant amount.

3. The $J(p)$ formulation is more sensitive than $J(x)$ to assimilation window length where the spatial domain is fully observed, shown in Experiment 3.

4. Another more general conclusion about wc4DVAR is that the variance of the estimated model errors provided by the solutions of both $J(p$

of the model error variance by both algorithms was noticeably improved in Experiment 3, with a longer assimilation window.

The aim is to gain a deeper theoretical understanding into the behaviour of both the minimisation problems presented by $J(p)$ and $J(x)$. In the next chapter we bound the condition number of the Hessian of $J(p)$ and analyse it more rigorously.

solution process of the sc4DVAR. The proof of this result is contained in Appendix A.

In this chapter we present new theoretical bounds on the condition number of

0 B_0 1

$S_p =$ @

The insight gained from the bounds are demonstrated through numerical experiments on the condition number. We also further demonstrate the condition number sensitivities obtained from the bounds by examining their effect on the convergence rate of the model error estimation an preconditioned model error estimation minimisation problems.

We now present the theoretical bounds.

5.1 Theoretical Results: Bounding the Condition Number of S_p

The following result bounds the spectral condition number of S_p.

Theorem 5.1.1 Let $B_0 \in R^{N \times N}$ and Q

and

$$_{max}(D^{\ 1}) + {}_{min}(L^{\ T}H^{T}R^{\ 1}HL^{\ 1}) \qquad {}_{max}(S_p)$$

$$_{max}(D^{\ 1}) + {}_{max}(L^{\ T}H^{T}R^{\ 1}HL^{\ 1}): \quad (5.5)$$

We then take the upper bound of $_{max}(S_p)$ and lower bound of $_{min}(S_p)$ giving us the following upper bound on the condition number,

$$(S_p) \qquad \frac{{}_{max}(D^{\ 1}) + {}_{max}(L^{\ T}H^{T}R^{\ 1}HL^{\ 1})}{{}_{min}(D^{\ 1}) + {}_{min}(L^{\ T}H^{T}R^{\ 1}HL^{\ 1})}: \quad (5.6)$$

Similarly for the lower bound we take the lower bound of $_{max}(S_p)$ and upper bound of $_{min}(S_p)$, which yields the following lower bound on the condition number,

$$(S_p) \qquad {}_{max}(D^{\ 1}) + {}_{min}(L^{\ T}H^{T}R$$

the time invariant model error covariance matrix, for $i = 1, \ldots, n$, where C_Q is a symmetric, positive-definite circulant correlation matrix and $\sigma_q^2 > 0$ is the model error variance. Assume $q < N$ observations are taken with the same error variance $\sigma_o^2 > 0$ at each time interval such that $R_i = R = \sigma_o^2 I_q$ for $i = 0, \ldots, n$, where I_q is a $q \times q$ identity matrix. Assume that observations of the parameter are made at the same grid points at each time interval such that $H_i^T H_i = H^T H \in \mathbb{R}^{N \times N}$, so $H^T H$ is a diagonal matrix with unit entries at observed points and zeros otherwise. Finally, we assume that $M_{i,i-1} = M \in \mathbb{R}^{N \times N}$ for $i = 1, \ldots, n$ is a circulant matrix, and $M_{i,i} = I_N$. The following bounds are satisfied by the condition number of S_p:

$$\left(\frac{1 + \frac{q}{N}\frac{\min\{\sigma_b^2\lambda_{\min}(C_B);\ \sigma_q^2\lambda_{\min}(C_Q)\}}{\sigma_o^2}\ \lambda_{\min}}{1 + \frac{q}{N}\frac{\max\{\sigma_b^2\lambda_{\max}(C_B);\ \sigma_q^2\lambda_{\max}(C_Q)\}}{\sigma_o^2}\ \lambda_{\max}}\right)\kappa(D) \leq \kappa(S_p) \leq$$

With this in mind we choose a vector, $V_k \in R^{N(n+1)}$ such that

$$V_k = \begin{pmatrix} v_k \\ v_k \\ \vdots \\ v_k \end{pmatrix}; \qquad (5.12)$$

where $v_k \in R^N$ is an arbitrary eigenvector of a circulant matrix. We apply the Rayleigh quotient using (5.12) to obtain the lower bound of S_p. We begin by considering the second term of S_p

$$\frac{1}{{}^{2}_{o}} \frac{V_k^H [L^{\ T} H^T H L^{\ 1}] V_k}{V_k^H V_k}; \qquad (5.13)$$

while deliberately omitting D for now.

The denominator of (5.13) yields

$$V_k^H V_k = n + 1; \qquad (5.14)$$

since the eigenvectors of a circulant matrix are orthogonal, Theorem 3.37. The computation in (5.13) requires v_k and v_k^H to multiply every matrix block inside $L^{\ T} H^T H L^{\ 1}$. Each block multiplication yields the following:

$$v_k^H (M^j)^T = v_k^H \ {}^j(M); \qquad (5.15)$$

$$(M^j) v_k = \ {}^j(M) v_k; \qquad (5.16)$$

where ${}^j(M)$ is some eigenvalue of M and ${}^j(M)$ is the corresponding complex conjugate eigenvalue of M. We write $(M) =$ for convenience.

Substituting (5.14), (5.15) and (5.16) into (5.13), we obtain the following series:

$$\frac{1}{n+1}\left[\sum_{i=0}^{n}\sum_{j=0}^{n\ i}(\ )^j(\ )^j v_k^H H^T H v_k + \sum_{i=1}^{n}\sum_{j=0}^{n\ i}(\ )(\ )^j(\ )^j v_k^H H^T H v_k \right.$$
$$\left. + \sum_{i=1}^{n}\sum_{j=0}^{n\ i}(\ )(\ )^j(\ )^j v_k^H H^T H v_k + \ \ + \ \ + (\ )^n v_k^H H^T H v_k + (\ )^n v_k^H H^T H v_k \right]; \qquad (5.17)$$

where the first term in the geometric series (5.17) comes from the main diagonal of (5.13). The second term of (5.17) is from the upper off-diagonal block entries of (5.13) and the third term is from the lower off-diagonal block entries. This pattern continues until the final term in the bottom right hand corner of (5.13), which coincides with the final term in (5.17).

We consider the Rayleigh quotient as in (5.13) but for the vector $v_{max=min}$, since the Rayleigh quotient of D yields the respective extreme eigenvalues for $v_{max=min}$.

which bounds the largest eigenvalue. Similarly for the smallest eigenvalue,

$$_{min}\,(S_p) \qquad \frac{V_{min}^H\, S_p V_{min}}{V_{min}^H\, V_{min}} \qquad _{min}\,(D\;\;^1) + \frac{q}{N}\,\frac{1}{\;^2_o}\;\;_{max} \tag{5.27}$$

where $_{max=min}$ is as computed in (5.24) and (5.25)

$$_l = 8 \quad \mathrm{P}^n_{k=0}\; j\;\;_l j^{2k} \qquad\qquad \text{if} \;\;_l(D) = \;_l($$

As the ratio σ_b/σ_q approaches zero, or diverges away from 1, the condition number of D and hence the condition number of S_p will grow. This means if the model error variance were to be too small, or too large, in comparison to the background error variance, the condition number of S_p will be large. This argument also applies to the background error variance. Secondly, as the correlation length-scales in the background and the model error covariance matrices grows, the condition number of D and hence the condition number of S_p will also grow. The upper bound in Theorem 5.1.2 also shows that as the observation accuracy (decreasing σ_o) increases, then the upper bound will increase. The lower bound will also increase as σ_o decreases, provided $\lambda_{min} << \lambda_{max}$ is true. So both bounds suggest that the condition number of S_p may grow as σ_o decreases.

We now use the 1D advection equation as described in Section 3.5.1 to derive more specific bounds to investigate $\kappa(S_p)$ further.

5.1.1 The 1D Advection Equation

Theorem 5.1.3 In addition to the assumptions in Theorem 5.1.2, let M be matrix (3.71), which is the advection equation discretised using the upwind scheme. Then for Courant number $\mu \in [-1, 0]$ we have the following bounds on $\kappa(S_p)$:

$$\kappa(D)\left(\frac{1+\frac{q}{N}\frac{\min\{\sigma_b^2\lambda_{min}(C_B);\,\sigma_q^2\lambda_{min}(C_Q)\}}{\sigma_o^2}\lambda^{adv}_{min}}{1+\frac{q}{N}\frac{\max\{\sigma_b^2\lambda_{max}(C_B);\,\sigma_q^2\lambda_{max}(C_Q)\}}{\sigma_o^2}\lambda^{adv}_{max}}\right) \leq \kappa(S_p)$$

$$\leq \kappa(D)\left(1+\frac{\min\left(\sigma_b^2\lambda_{min}(C_B);\,\sigma_q^2\lambda_{min}(C_Q)\right)}{\sigma_o^2}(n+1)^2\right); \quad (5.32)$$

where

$$\lambda^{adv}_{min} = \begin{cases} \frac{1}{n}\sum_{i=1}^{n-1}\left[2-\frac{1-(1+2\mu)^{(i+1)}}{1-(1+2\mu)}\right]\left[1-\frac{1-|1+2\mu|^{2(n+1-i)}}{1-|1+2\mu|^2}\right] & \text{if } \lambda_{min}(D)=\lambda_{min}(Q) \\ \frac{1-|1+2\mu|^{2(n+1)}}{1-|1+2\mu|^2} & \text{if } \lambda_{min}(D)=\lambda_{min}(B_0) \end{cases}$$

(5.33)

and

$$\lambda^{adv}_{max} = \begin{cases} \frac{n^2}{3}+\frac{3}{2}n-\frac{5}{6}-\frac{1}{n} & \text{if } \lambda_{max}(D)=\lambda_{max}(Q) \\ (n+1) & \text{if } \lambda_{max}(D)=\lambda_{max}(B_0) \end{cases}: \quad (5.34)$$

Proof: We require results on the minimum and maximum eigenvalues of M to obtain bounds for (S_p). We use similar methodology as in [41], where the author obtained the extreme eigenvalues of a matrix similar to (3.71). Since M is circulant with entries as shown in (3.71), by Theorem 3.3.8 the eigenvalues take the following form,

$$_m = 1 + \quad e^{\frac{2 \ im}{N}} \tag{5.35}$$

for $m = 0; :::; N \quad 1$ where $i = \sqrt{\quad 1}$. We also have

$$j \ _m j^2 = (\ _m)(\ _m) = (1 + \quad)^2 \quad 2 \ (1 + \quad) \cos(\frac{2 \ m}{N}) + \quad ^2 : \tag{5.36}$$

Let $f(m) = j \ _m j^2$ be a continuous function of $m \ 2 \ [0; N)$. We can nd the minimum and maximum of this function by di erentiation:

$$f^0(m) = 2 \ (1 + \quad)(\frac{2}{N}) \sin(\frac{2 \ m}{N}); \tag{5.37}$$

$$f^{00}(m) = 2 \ (1 + \quad)(\frac{2}{N})^2 \cos(\frac{2 \ m}{N}): \tag{5.38}$$

Now we see that $f^0(m) = 0$ implies the extrema occur at $m = 0; \frac{N}{2}$. It follows that $f^{00}(0) < 0$ and $f^{00}(\frac{N}{2}) > 0$ for all permissible values of $\ 2 \ (\quad 1; 0)$. Therefore, for N even, it is trivial to see that

$$_{max}(M) =$$

Computing (5.49) we find:

$$
\begin{aligned}
{}^{adv}_{max} &= \frac{1}{n}\left(\sum_{i=1}^{n-1} 2i(n+1-i) + \sum_{i=1}^{n-1}(n+1-i)\right) \\
&= \frac{1}{n}\left(2\left[\sum_{i=1}^{n-1} i(n+1) - i^2\right] + (n+1)(n-1) - \sum_{i=1}^{n-1} i\right) \\
&= \frac{1}{n}\left(2\left[\frac{(n+1)(n-1)(n)}{2} - \frac{(n-1)(n)(2n-1)}{6}\right] + (n+1)(n-1) - \frac{(n-1)(n)}{2}\right) \\
&= \frac{n-1}{n}\left((n+1)(n) - \frac{n(2n-1)}{3} + (\frac{n}{2}+1)\right) \\
&= \frac{n-1}{n}(\frac{n}{6}(2n+11)+1) \\
&= \frac{n^2}{3} + \frac{3}{2}n - \frac{5}{6} - \frac{1}{n}. \qquad (5.50)
\end{aligned}
$$

Therefore,

$$
{}^{adv}_{max} = \begin{cases} \frac{n^2}{3} + \frac{3}{2}n - \frac{5}{6} - \frac{1}{n} & \text{if } {}_{max}(D) = {}_{max}(Q) \\ (n+1) & \text{if } {}_{max}(D) = {}_{max}(B_0) \end{cases}. \qquad (5.51)
$$

It remains to find ${}^{adv}_{min}$. For the case ${}_{min}(D) =$

by using the definition of the 2-norm and norm relationship in Theorem 3.3.6.

We now briefly discuss the 2-norm of the observation operator $H \in \mathbb{R}^{p(n+1) \times N(n+1)}$. The main assumption states that there are fewer observations than state space, so from Definition 3.3.4, we have

$$\|H\|_2 = \sup_{x \neq 0} \left(\frac{|x_1|^2 + |x_3|^2 + \dots + |x_{q(n+1)}|^2}{|x_1|^2 + |x_2|^2 + \dots + |x_{N(n+1)}|^2} \right); \tag{5.56}$$

where $x \in \mathbb{R}^{N(n+1)}$, such that

$$x = \begin{pmatrix} x_1 \\ x_2 \\ \vdots \\ x_{N(n+1)} \end{pmatrix}. \tag{5.57}$$

It is obvious that the numerator can never exceed the denominator because $q < N$. To illustrate this, let us assume every other point in the state is observed, therefore it is obvious that

$$\frac{|x_1|^2 + |x_3|^2 + \dots + |x_{q(n+1)}|^2}{|x_1|^2 + |x_2|^2 + \dots + |x_{N(n+1)}|^2} \leq 1. \tag{5.58}$$

We have assumed a particular instance, which adheres to the original assumption of $q < N$. In general, the number of observations being less than the state means the denominator in (5.58) can never exceed the numerator. Therefore the supremum of (5.58) is

$$\|H\|_2 = 1. \tag{5.59}$$

To calculate $\|L^{-1}\|_2$ we use the inequality

$$\|L^{-1}\|_2 \leq \sqrt{\|L^{-1}\|_1 \|L^{-1}\|_\infty}; \tag{5.60}$$

while also noting that the infinity-norm and 1-norm of L^{-1} are equal, which can be seen by quick inspection of L^{-1}, (2.37). The matrix L^{-1} can be written as a power series such that,

$$L^{-1} = I + M + M^2 + \dots + M^n; \tag{5.61}$$

$$L^{-1} = \begin{pmatrix} I & & & \\ & I & & \\ & & \ddots & \\ & & & I \end{pmatrix} + \begin{pmatrix} 0 & & & & \\ M_1 & 0 & & & \\ & M_2 & 0 & & \\ & & \ddots & \ddots & \\ & & & M_n & 0 \end{pmatrix} + \begin{pmatrix} 0 & & & & & \\ 0 & 0 & & & & \\ M_2 M_1 & 0 & 0 & & & \\ & M_3 M_2 & 0 & 0 & & \\ & & \ddots & \ddots & \ddots & \\ & & & M_n M_{n-1} & 0 & 0 \end{pmatrix} +$$

$$\dots + \begin{pmatrix} 0 & 0 & 0 & 0 & 0 \\ 0 & 0 & 0 & 0 & 0 \\ 0 & 0 & 0 & 0 & 0 \\ 0 & 0 & 0 & 0 & 0 \\ M_n \dots M_1 & 0 & 0 & 0 & 0 \end{pmatrix}. \tag{5.62}$$

The ECMWF write the L^{1} operator as a Neumann series to approximate L, [27]. The authors hope to approximate L to precondition the state estimation formulation (2.33). We write it as a series here with the intent of approximating it

L,L,,L,,L,L,L,L,,L,L1,,L,L,LL,,,

information. We can see that the assimilation window length, n, has a quadratic influence from the $^{adv}_{max}$ expression in (5.34). The upper bound of Theorem 5.1.3 shows the quadratic influence of the assimilation window length n. Both the upper and lower bounds suggest that the assimilation window length will have an influence on the condition number of S_p.

This concludes the derivation of our bounds on S_p. We now briefly compare the bounds on the condition number of S_p to the bounds on the condition number of the sc4DVAR Hessian, before demonstrating the bounds numerically.

5.1.2 Comparison to Strong-Constraint 4DVAR

The bounds in Theorem 5.1.2 bear some similarities to the bounds derived on the condition number of the Hessians of the sc4DVAR and 3DVAR problems as shown in [41] (Theorem 6.1.2 and Theorem 7.1.2). The influence of the condition number of B_0 on the condition number of the sc4DVAR Hessian is similar to the influence of the condition number of D on the condition number of S_p. The B_0 matrix was influenced only by the condition number of the background error covariance matrix C_B, whereas D is influenced by C_B, C_Q and the ratio of σ_b/σ_q. We further illustrate this by taking a simplified scenario as an example.

Assume the background and model errors are uncorrelated in space such that

$$D = \begin{pmatrix} \sigma_b^2 I & & & & \\ & \sigma_q^2 I & & & \\ & & \sigma_q^2 I & & \\ & & & \ddots & \\ & & & & \sigma_q^2 I \end{pmatrix}. \qquad (5.66)$$

We also assume that the background error variance is larger than the model error variance, $\sigma_b > \sigma_q$. The background error variance is representative of the errors in the previous assimilation window in its entirety, which normally consists of several model time steps. The model error variance represents the errors in one model time step. It is intuitive to believe the error variance in one time step is less than multiple model time steps. Allowing for more model time steps between error corrections implies that the model error variance will grow such that $_q$! $_b$.

The condition number of D becomes

$$(D) = \frac{b}{q}^{2} : \qquad (5.67)$$

We now brie y analyse the wc4DVAR bounds from Theorem 5.1.2 in light of these additional arguments. We have

$$\frac{\frac{b}{q}^{2} + \frac{q}{N}\frac{b}{o}^{2}{}_{min}}{1 + \frac{q}{N}\frac{b}{o}^{2}{}_{max}} \quad (S_p) \quad \frac{b}{q}^{2} + \frac{b}{o}^{2}{}_{max}(L^{T}H^{T}HL^{1}); \qquad (5.68)$$

which can be compared directly to the sc4DVAR bounds in [41] (Theorem 7.1.2), with the same assumptions:

$$\frac{1 + \frac{q}{N}\frac{b}{o}^{2}{}_{min}}{1 + \frac{q}{N}\frac{b}{o}^{2}{}_{max}} \quad (S) \quad 1 + \frac{b}{o}^{2}{}_{max}(\hat{H}^{T}\hat{H}); \qquad (5.69)$$

where S is the sc4DVAR rst order Hessian and is the sc4DVAR equivalent to , (5.21). We see the added dimension of the background and model error variance covariance matrix represented by the ratio $\frac{b}{q}$ playing a signi cant role in the conditioning of S_p. We also see the contribution of the maximum eigenvalue of the terms $L^{T}H^{T}HL^{1}$ and $\hat{H}^{T}\hat{H}$, which is linked to the length of the assimilation window and observation operator.

We showed in Theorem (5.1.3) that $_{max}(L^{T}H^{T}HL^{1})$ can be approximated to $(n+1)^2$, where the author in [41] showed that $_{max}(\hat{H}^{T}\hat{H})$ for sc4DVAR reduces to $(n+1)$. So the e ect of the assimilation window on the bounds from sc4DVAR to wc4DVAR is greater by an order of magnitude.

In this section we have demonstrated the inherent similarities between the condition numbers of S_p and S. In the next section we demonstrate the sensitivities shown by the bounds in the Theorems on the condition number of S_p.

5.1.3 Numerical Results

We now demonstrate the bounds through numerical experiments. We also highlight sensitivities of the condition number of S_p with respect to assimilation parameters, which have been revealed by the theorems in Section 5.1.

We let M be the linear advection model as in (3.71), with a one-dimensional domain of size $N = 500$ grid points and spatial intervals of $x = 0.1$. We use temporal intervals of $t = 0.1$ and wave speed $a = 0.3$. We let n

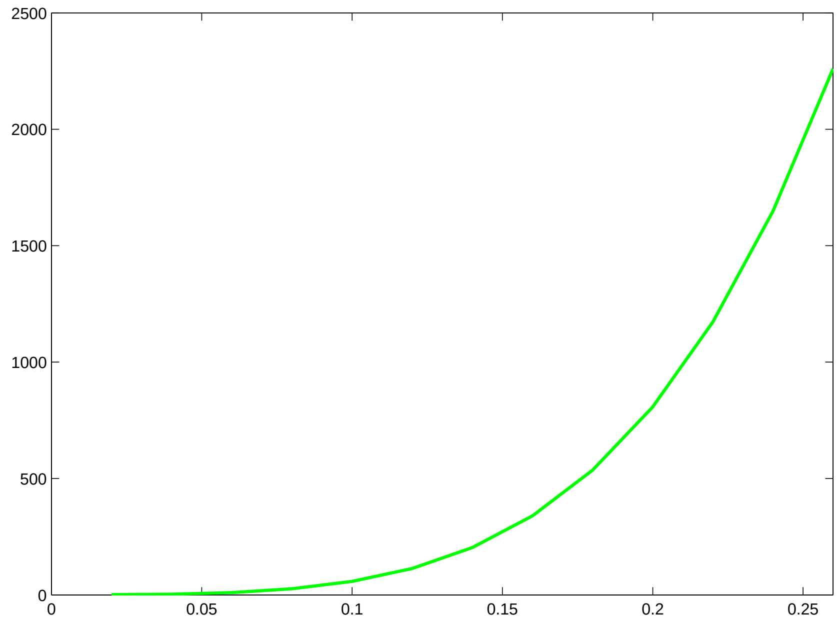

Figure 5.1: (S_p) (blue line), (D) (green line) and theoretical bounds (red-dotted line) as a function of $L(C_B)$. Model error correlation length-scale $L(C_Q) =$ x=5.

Figure 5.1 shows the bounds from Theorem 5.1.2 with the condition numbers of S_p and D. We see the dependence of (S_p) on (D), which rises as a result of the e77 as a8d

Figure 5.2: (S_p) (blue-surface) and bounds (red-mesh surface) as a function of $L(C_B)$ and $L(C_Q)$.

In Figure 5.2 we show that the increasing the model error correlation length-scale does not a ect the condition number as much as the increase in length-scale in the B matrix. This is due to the Laplacian covariance matrix being better conditioned than the SOAR covariance matrix in general, [41], Chapter 5. We see evidence of this in this experiment: with correlation length-scales of $L(C_B) = L(C_Q) = 2.5\ x$, the condition numbers of the SOAR and Laplacian matrices are $(C_{SOAR}) = 1973$ and $(C_{LAP}) = 359$.

Figures 5.1 and 5.2 demonstrate the following:

1. The sensitivity of the condition number of the Hessian S_p to the condition number of the background and model error covariance matrix DC_L

the correlation length-scales in the covariance matrices C_B and C_Q, which in uences the condition number of S_p.

3. The bounds accurately and closely estimate the true condition number when varying the correlation length-scales of C_B and C_Q in these experiments.

We now demonstrate the bounds and Hessian condition number sensitivities to the error variance ratios.

5.1.3.2 Experiment 2: Error Variance Ratios

Figure 5.3: (S_p) (blue line) and theoretical bounds (red-dotted line) as a function of ratio $_b = _q$. L(

the condition number of D increasing as the ratio of $_b = \ _q$ tends to 0 and increases from 1. b,-4/89twh

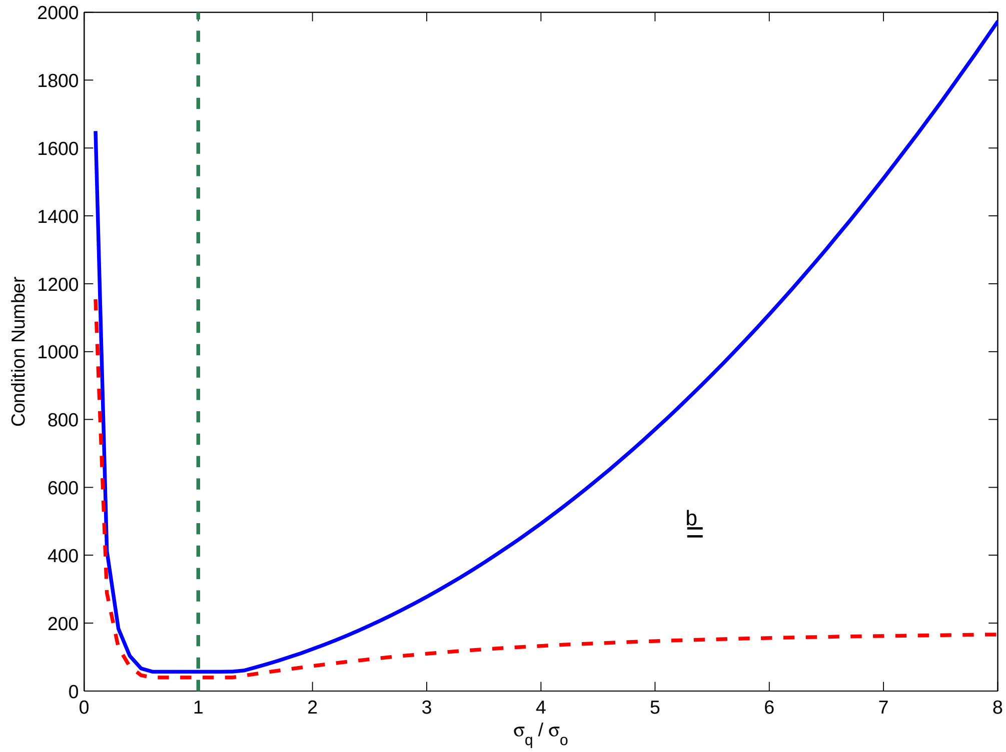

b= as the of =

bsholi7(wn34/ b=

ɑ 33 ɑ 33

Figure 5.4: (S_p) (blue line) and theoretical bounds (red-dotted line) as a function of ratio $_q = \ _o$. $L(C_B) = L(C_Q) = 1 \quad x$. Green dotted line at the point $_q$

S_p increases.

2. As the ratio $\max = \min \ {}^{2}_{b} \ {}_{\min}(C_B); \ {}^{2}_{q} \ {}_{\min}(C_Q) \ = {}^{2}_{o} \rightarrow \ 0;1$ the condition number of S_p increases.

3. The bounds estimate the true condition number well when varying the background and model ${}_{b}= {}_{q}$ error variance ratios in these experiments. The upper bound is also tight for the model and observation error variance ratio whereas the lower bound is a poor estimate of the ${}_{q}= {}_{o}$ ratio.

We now demonstrate the bounds and Hessian condition number sensitivities to the length of the assimilation window.

5.1.3.3 Experiment 3: Assimilation Window Length

We now examine the e ects of assimilation window length on the condition number of S_p.

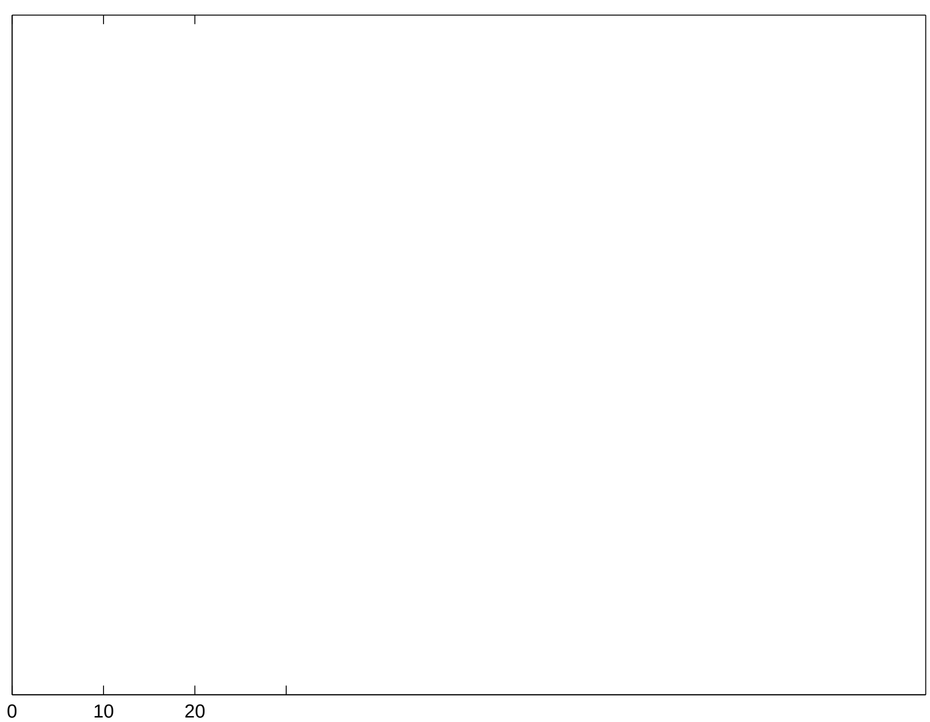

Figure 5.5: (S

Figure 5.5 demonstrates the bounds in Theorem 5.1.3. The upper bound has the term $(n + 1)^2$, which shows that the bound is quadratically influenced by the assimilation window length. We see that the actual condition number of S_p does increase quadratically as the assimilation window length increases, for example doubling the window from 50 to 100 sees approximately 4 times the increase in the condition number of S_p from 500 to 2000. The upper bound has similar behaviour which can be seen from the shape of the graph but it is not exactly quadratic, doubling the window from 50 to 100 increases the upper bound from 1000 to 3500. The lower bound is uninformative.

5.1.4 Summary

We have obtained new general bounds on the condition number of the wc4DVAR $J(p)$ formulation. We then developed the bounds by making simple assumptions length-scales of the background and model error covariance matrices since these have a direct influence on $\kappa(\mathbf{D})$ and hence $\kappa(\mathbf{S}_p)$. We have also shown for the advection equation in Theorem 5.1.3, that the assimilation window length, n, influences the condition number of $\mathbf{S}_p$.

We now examine the preconditioned problem.

5.2 Theoretical Results: Bounding the Condition Number of $\hat{\mathbf{S}}_p$

We recall the preconditioned $\mathbf{S}_p$ Hessian as in Chapter 4, Section 2.3.3 equation (2.60),

$$\hat{\mathbf{S}}_p = \mathbf{I} + \mathbf{D}^{1/2}\mathbf{L}^{-T}\mathbf{H}^T\mathbf{R}^{-1}\mathbf{H}\mathbf{L}^{-1}\mathbf{D}^{1/2}. \tag{5.70}$$

The following result bounds the condition number of $\hat{\mathbf{S}}_p$,

Theorem 5.2.1 Let $\mathbf{B}_0 \in \mathbb{R}^{N \times N}$ and $\mathbf{Q}_i \in \mathbb{R}^{N \times N}$ for $i = 1, \ldots, n$ be our background and static model error covariance matrices respectively. We assume q observations are taken such that $q < N$ with covariance $\mathbf{R}_i \in \mathbb{R}^{q \times q}$ thus $\mathbf{R} \in \mathbb{R}^{q(n+1) \times q(n+1)}$. Let $\mathbf{H}_i = \mathbf{H} \in \mathbb{R}^{q \times N}$ for $i = 0, \ldots, n$, be the time invariant observation operator. Finally, let $\mathbf{M}_{i,i-1} = \mathbf{M} \in \mathbb{R}^{N \times N}$ for $i = 1, \ldots, n$, represent the time invariant model equations. Then the following bounds are satisfied by the condition number of the Hessian $\hat{\mathbf{S}}_p$:

$$1 + \frac{1}{q(n+1)} \sum_{i,j=1}^{q(n+1)} \left(\mathbf{R}^{-1/2}\mathbf{H}\mathbf{L}^{-1}\mathbf{D}\mathbf{L}^{-T}\mathbf{H}^T\mathbf{R}^{-1/2}\right)_{i,j} \leq \kappa(\hat{\mathbf{S}}_p)$$
$$\leq 1 + \frac{\lambda_{max}(\mathbf{D})}{\lambda_{min}(\mathbf{R})}\lambda_{max}(\mathbf{L}^{-T}\mathbf{L}^{-1}) \tag{5.71}$$

where $\mathbf{R}^{-1/2}$ is the symmetric square root of $\mathbf{R}^{-1}$.

Proof: Let $\mathbf{E} = \mathbf{R}^{-1/2}\mathbf{H}\mathbf{L}^{-1}\mathbf{D}^{1/2}$. We remember that since $\mathbf{H}$ is not full rank,

${}_{\min}(E^T E) = 0$. Therefore

$$(\hat{S}_p) = \frac{{}_{\max}(\hat{S}_p)}{{}_{\min}(\hat{S}_p)} = \frac{1 + {}_{\max}(E^T E)}{1 + {}_{\min}(E^T E)} = 1 + {}_{\max}(E^T E) = {}_{\max}(\hat{S}_p); \qquad (5.72)$$

meaning the condition number of $\hat{S}_p$

the condition number by applying the Rayleigh quotient to $\tilde{S}_p$ using a unit vector $y \in \mathbb{R}^{q(n+1)}$, such that,

$$y = \frac{1}{\sqrt{q(n+1)}}(1; 1; \ldots; 1): \tag{5.79}$$

The Rayleigh Quotient is bounded by Theorem 3.4.7, so it follows that

$$\kappa(\hat{S}_p) = \lambda_{max}(\tilde{S}) \geq R_{\tilde{S}_p}(y); \tag{5.80}$$

where $R_{\tilde{S}_p}(y)$ denotes the Rayleigh Quotient of $\tilde{S}_p$ using the vector y. Therefore

$$\kappa(\hat{S}_p) \geq R_{\tilde{S}_p}(y) = y^T \tilde{S}_p y; \tag{5.81}$$

$$= 1 + \frac{1}{q(n+1)} \sum_{i;j=1}^{q(n+1)} R^{1=}$$

$H_i H_i^T = I_q$ and $M_{i,i-1} \in \mathbb{R}^{N \times N}$ denote the observation and model operators respectively and $M_{i,i} = I_N$. We then have the following bounds on the condition number of $\hat{S}_p$:

$$1 + \frac{1}{q(n+1)}\left(\frac{\sigma_b^2}{\sigma_o^2}\sum_{i,j=1}^{q(n+1)} (H\tilde{C}_B H^T)_{i,j} + \frac{\sigma_q^2}{\sigma_o^2}\sum_{i,j=1}^{q(n+1)} (H\tilde{C}_Q H^T)_{i,j}\right) \le \kappa(\hat{S}_p)$$
$$\le 1 + \frac{\max\left(\sigma_b^2\lambda_{\max}(C_B),\ \sigma_q^2\lambda_{\max}(C_Q)\right)}{\sigma_o^2}\left(\sum_{k=0}^{n}\|M\|_1^k\right)\left(\sum_{k=0}^{n}\|M\|_\infty^k\right) \tag{5.83}$$

where

$$\tilde{C}_B = \begin{pmatrix} C_B & C_B M_{1,0}^T & \cdots & C_B M_{n,0}^T \\ M_{1,0}C_B & M_{1,0}C_B M_{1,0}^T & \cdots & M_{1,0}C_B M_{n,0}^T \\ & & M_2 C_B M_2^T & \\ \vdots & \vdots & \ddots & \vdots \\ M_{n,0}C_B & M_{n,0}C_B M_{1,0}^T & \cdots & M_{n,0}C_B M_{n,0}^T \end{pmatrix}; \tag{5.84}$$

$$\tilde{C}_Q = \begin{pmatrix} 0 & 0 & \cdots & 0 \\ 0 & C_Q & \cdots & C_Q M_{n-1,0}^T \\ \vdots & & M_{1,0}C_Q M_{1,0}^T + C_Q & \end{pmatrix}$$

For the upper bound we know

$$_{max}(D) = \max \quad {}^{2}_{b} \; {}_{max}(C_B); \; {}^{2}_{q} \; {}_{max}(C_Q) \quad ; \tag{5.88}$$

and

$$_{min}(R) =$$

3. If the size of the entries in both the background and model error evolved covariance matrices are large and positive, this will also increase the lower bound.

4. Longer assimilation windows will increase the summation terms in the upper bound. This increase will be more noticeable if the one and in nity norms of M are larger than one.

We now derive bounds in the case where the model is a circulant matrix to obtain more informative bounds.

where $V_{max} \in R^{N(n+1)}$ is a vector of eigenvectors which correspond to the largest eigenvalues of B and Q such that

$$V_{max} = \begin{pmatrix} {}_{max} \\ {}_{max} \\ \vdots \\ {}_{max} \end{pmatrix}; \tag{5.97}$$

where ${}_{max}$ and ${}_{max}$ refer to the eigenvector corresponding to the largest eigenvalue of B and Q respectively. We now compute

$$V_{max}^T [\frac{1}{{}^2_o} D^{-1/2} L^{-T} H^T H L^{-1} D^{-1/2}] V_{max}; \tag{5.98}$$

in segments. We refer to the blocks of $D^{-1/2} L^{-T} H^T H L^{-1} D^{-1/2}$ as $A_{i;j}$, where i refers to the block row and j refers to the block column. We recall the structure of $L^{-T} H^T H L^{-1}$,

$$\begin{pmatrix} \sum_{i=0}^{n} (HM^i)^T HM^i & \sum_{i=0}^{n-1} (HM^{i+1})^T HM^i & \sum_{i=0}^{n-2} (HM^{i+2})^T HM^i & \cdots & (HM^n)^T \end{pmatrix}$$

on either side of the observation and model operator matrices. We collate the terms emerging from the computation of (5.98) by computing the first block row and first block column together while omitting $A_{1;1}$ computed in (5.101). The first block row and column computation is as follows

$$v^T_{max}[Q^{1/2}\sum_{i=0}^{n-1}(HM^i)^T HM^{i+1}B^{1/2}]v_{max} = \lambda_k \frac{q}{N}\sqrt{\lambda_{max}(B)\lambda_{max}(Q)}\sum_{i=0}^{n-1}|\lambda_k|^{2i}; \quad (5.104)$$

$$v^T_{max}[B^{1/2}\sum_{i=0}^{n-1}(HM^{i+1})^T HM^{i}Q^{1/2}]v_{max} = \lambda_k \frac{q}{N}\sqrt{\lambda_{max}(B)\lambda_{max}(Q)}\sum_{i=0}^{n-1}|\lambda_k|^{2i}; \quad (5.105)$$

where (5.104) refers to block $A_{1;2}$ and (5.105) refers to block $A_{2;1}$. To represent the emerging summation arising from the first row and column blocks, $n \lambda_{max}\sqrt{N}$

We write the summation that encompasses the main block diagonal, $\sum_{i,j=2}^{n+1} A_{i,j}$ for i=j while excluding the first block, as

$$\frac{q}{N}\sigma_q^2\lambda_{max}(C_Q)\sum_{i=1}^{n}\sum_{j=0}^{i}|\lambda_k|^{2j}. \qquad (5.110)$$

For the remaining blocks, we examine the sub and super diagonals that sequentially emanate from the main diagonal, which exclude the first block row and column since they have been computed above,

$$\begin{pmatrix} A_{1,1} & A_{1,2} & A_{1,3} & \cdots & A_{1,n+1} \\ A_{2,1} & A_{2,2} & A_{3,2} & \cdots & A_{2,n+1} \\ A_{3,1} & A_{3,2} & A_{3,3} & \cdots & A_{3,n+1} \\ \vdots & \ddots & \ddots & \ddots & \vdots \\ A_{n+1,1} & \cdots & \cdots & \cdots & A_{n+1,n+1} \end{pmatrix}.$$

A geometric progression in M and M^T manifests itself, which when computing the Rayleigh quotient presents a geometric progression in the eigenvalues of M, similar to that in Section 5.1 equation (5.17). This can be seen in the first terms of the super and sub diagonals (5.108), (5.109) respectively. Summing together the sums that arise from the super and sub-diagonals emanating from the main the computation (5.98) is equal to $(n+1)$, we have

$$
\begin{aligned}
&R_{\hat{S}_p}(V_{max}) = \\
&\frac{q}{N(n+1)}\frac{1}{\sigma_o^2}\left(\sigma_b^2\lambda_{max}(C_B)\gamma_k + \sigma_q^2\lambda_{max}(C_Q)\omega_k + \sigma_b\sigma_q\sqrt{\lambda_{max}(C_B)\lambda_{max}(C_Q)}\,\psi_k\right);
\end{aligned}
\tag{5.113}
$$

which by the bounds of the Rayleigh quotient, Theorem 3.4.7 gives,

$$
\begin{aligned}
R_{\hat{S}_p}(V_{max}) \geq 1 + \frac{q}{N(n+1)}\frac{1}{\sigma_o^2}(&\sigma_b^2\lambda_{max}(C_B)\gamma_{min} + \sigma_q^2\lambda_{max}(C_Q)\omega_{min} \\
&+ \sigma_b\sigma_q\sqrt{\lambda_{max}(C_B)\lambda_{max}(C_Q)}\,\psi_{min});
\end{aligned}
\tag{5.114}
$$

establishing the lower bound.

For the upper bound we recognise that for a circulant matrix $C \in \mathbb{R}^{N\times N}$ as in Definition (3.3.7), the following is always true:

$$
||C||_1 = ||C||_\infty. \tag{5.115}
$$

The upper bound in Theorem (5.2.2) becomes

$$
\kappa(\hat{S}_p) \leq 1 + \frac{\max\left\{\sigma_b^2\lambda_{max}(C_B);\ \sigma_q^2\lambda_{max}(C_Q)\right\}}{\sigma_o^2}\left(\sum_{k=0}^{n}||M||_\infty^k\right)^2; \tag{5.116}
$$

which completes the proof, as required.

In both the upper and lower bounds the contribution of the eigenvalues and norm of M are influential. Thus the effect of the assimilation window length still exists in both bounds, and the lower bound has a further dependency on the eigenvalues of M. The lower bound operators γ, ω and ψ all depend on the assimilation window length and the size of the smallest eigenvalue of M, all multiplied by either the largest eigenvalue of the background or model error covariance matrices. The upper bound is much clearer in that it quadratically depends on the infinity-norm of M. Therefore the only definitive message we can deduce here is that bounds suggest that the assimilation window length will increase the condition number. The bounds also suggest that the condition number of D no longer affects $\kappa(S_p)$. We instead have the ratio $\frac{\max\{\sigma_b^2\lambda_{max}(C_B);\ \sigma_q^2\lambda_{max}(C_Q)\}}{\sigma_o^2}$ now influencing both bounds.

In a bid to extract more meaningful information we now deduce bounds using the 1D advection model.

Theorem 5.2.4 In addition to the assumptions in Theorem 5.2.2, we assume the model operator $M_{i;i-1} \in \mathbb{R}^{N \times N}$ represents the matrix presented by the discretisation of the advection equation using the upwind scheme, (3.71) with $M_{i;i} = I$. Then for Courant number $\in (-1;0)$ the following bounds on the condition number of $\hat{S}_p$ therefore hold:

$$1 + \frac{q}{N(n+1)} \frac{1}{{}^2_o} \left({}^2_b \max(C_B) \, {}^{adv}_{min} + {}^2_q \max(C_Q) \right) {}^{adv}_{min} + {}_b \, {}_q \sqrt{\max(C_B) \max(C_Q)} \, {}^{adv}_{min}$$

$$(\hat{S}_p) \quad 1 + \frac{\max\left({}^2_b \max(C_B); \; {}^2_q \max(C_Q) \right)}{{}^2_o} (n+1)^2 \qquad (5.117)$$

where

$$ {}^{adv}_{min} = \frac{1 \;\; j \;\; 1 + 2 \;\; j^{2(n+1)}}{1 \;\; j \;\; 1 + 2 \;\; j^2}; \qquad (5.118)$$

$$ {}^{adv}_{min} = \sum^{n}$$

i9738 Tf 5.89.962 0 Td [( )]TJ.240422 11.50

We substitute $_{\min}(M) = 1 + 2$, into the lower bound expression presented in Theorem 5.2.3 and compute the values of $_{\min}$, $_{\min}$ and $!_{\min}$:

$$^{adv}_{\min} = \sum_{i=0}^{n} |1+2\ |^{2i} = \frac{1 - |1+2\ |^{2(n+1)}}{1 - |1+2\ |^{2}} ; \tag{5.125}$$

and

$$^{adv}_{\min} = \sum_{i=1}^{n} \sum_{j=0}^{n-i} |1+2\ |^{2j} : (2(1+2\ )^{i}) = \sum_{i=1}^{n} (2(1+2\ )^{i}) : \frac{1 - |1+2\ |^{2(n-i+1)}}{1 - |1+2\ |^{2}} ; \tag{5.126}$$

and

$$!^{adv}_{\min} = \sum_{l=1}^{2} \sum_{i=k}^{n} \sum_{j=0}^{n-i} |1+2\ |^{2j} : (2\mathrm{Re}(1+2\ )^{(l-1)i} - 1); \tag{5.127}$$

$$= \sum_{i=1}^{n} \sum_{j=0}^{n-i} |1+2\ |^{2j} + \sum_{i=2}^{n} \sum_{j=0}^{n-i} |1+2\ |^{2j} : (2(1+2\ )^{i} - 1);$$

5.2.1 Numerical Results

The parameter settings for the experiments in this section are identical to the

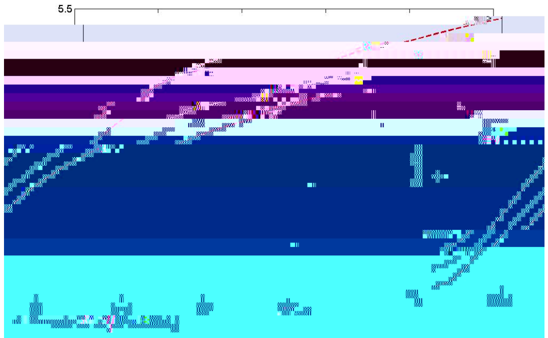

(a) $L(C_Q)$ = x=2, while $L(C_B)$ varies.

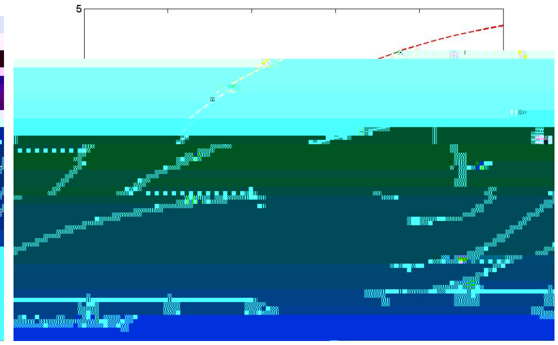

(b) $L(C_B)$ = x=2, while $L(C_Q)$ varies.

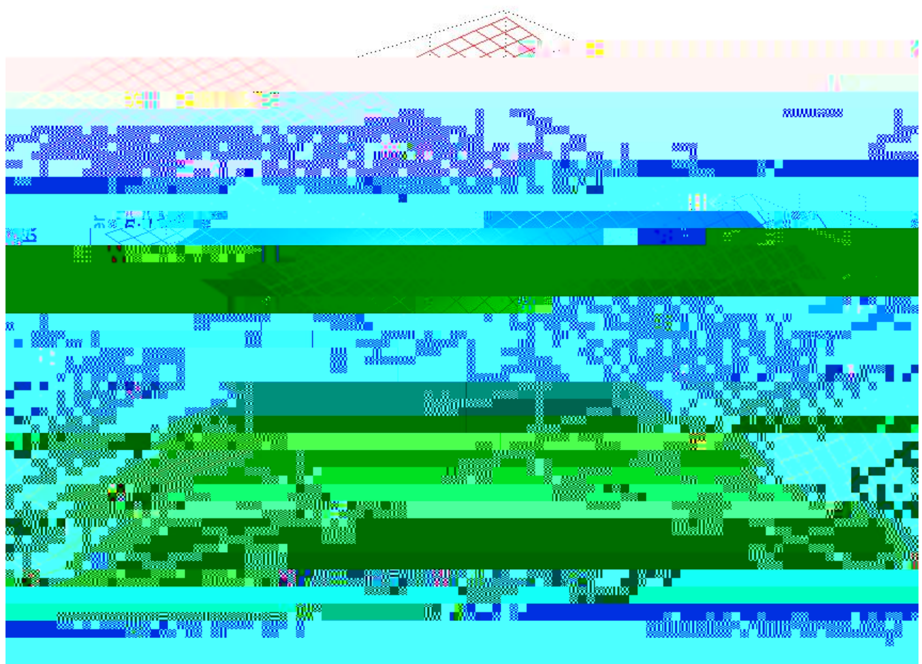

(c) $L(C_B)$ and $L(C_Q)$ varying.

Figure 5.6: Graph (a) and (b) $L(\hat{S}_p)$ (black line) and theoretical bounds (red dotted lines)

Figure 5.1. We also see that the bounds for$(\hat{S}_p)$ are a good estimate of the condition number.

5.2.1.2 Experiment 2: Assimilation Window Length and Observation Density

We now examine the e ects of varying observation density and assimilation window length on the condition number of$\hat{S}_p$.

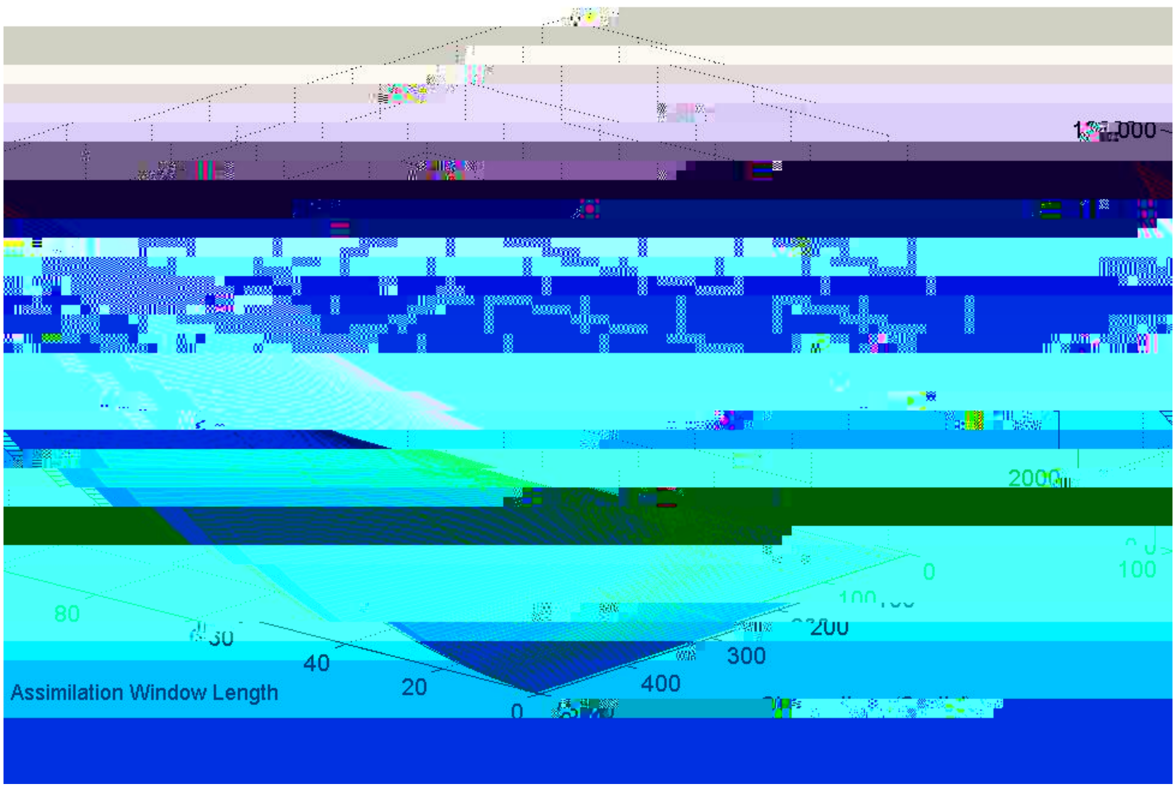

(a)

Figure 5.7: $(\hat{S}_p)$ (blue surface) and theoretical bounds (red-mesh surfaces) with assimilation window length, n, and number of spatial observations,q.

Figure 5.7 shows that the condition number of $\hat{S}_p$ grows as the assimilation window length increases and as the number of spatial observations at every assimilation step is increased. This is not dissimilar from the unpreconditioned problem as shown in Section 5.1.3, Figure 5.5. The bounds in Theorem 5.2.3, show a dependence on the assimilation window length, the upper bound shows a potential quadratic influence on the assimilation window length, which becomes much clearer in the upper bound of Theorem 5.2.4. Examining Figure 5.7 further, we see a quadratic increase of the actual condition number of $(\hat{S}_p)$ for example with 500 observed points at $n = 50$, $(\hat{S}_p) = 2026$, and at $n = 100$ $(\hat{S}_p) = 8056$.

In this section we have demonstrated the bounds derived in Section 5.2 of the preconditioned Hessian $\hat{S}_p$.

5.2.2 Summary

We have shown through numerical experiments that the original exhibited sensitivity of the unconditioned Hessian S_p to D has been greatly reduced. The absence of (D) can be seen in Theorems 5.2.1, 5.2.2 and 5.2.3 when compared to the bounds derived for the unconditioned Hessian in Section 5.1. The numerical experiments in Figure 5.6 compared to Figure 5.1 also confirm the alleviation of the sensitivity of (S_p) to (D), since the rise in correlation length-scale increases (D) (shown in Figure 5.1).

The preconditioner chosen in this thesis does not address any ill-conditioning which could arise from the second term of S_p. We see that S_p and $\hat{S}_p$ both exhibit sensitivities to the length of the assimilation window and the spatial observation density through the theory (Theorems 5.2.2 and 5.1.2) and in Figures 5.7 and Figure 5.5 in Section 5.1.3. This is an inherent trait of S_p as well as the preconditioned Hessian $\hat{S}_p$.

We also notice in the experiments that the lower bound is usually poorer than the upper bound. The Rayleigh quotient was used to obtain the lower bound, while the Courant Fischer theorem (Theorem 3.4.2) was used to obtain the upper bound. Although the Rayleigh quotient yields expressions that have aided in our analysis, it has proven to be a poorer estimator than the Courant Fisher theorem.

We now show results of the effect of the condition number sensitivities found in this chapter on the minimisation of $J(p)$ and its preconditioned counter-part.

5.3 Convergence Results: Model Error Formulation vs Preconditioned Model Error formulation

We begin by designing numerical experiments for both the unpreconditioned problem $J(p)$ and the preconditioned problem $\hat{J}(z)$. We perform data assimilation experiments which focus on the minimisation problems $J(p)$ and $\hat{J}(z)$, rather than experiments on the Hessian themselves. We now discuss the experimental design for our experiments.

5.3.1 Experimental Design

of = 10^{10} throughout this section. The solution relative errors is calculated in the same way as shown in Chapter 4 Section 4.1.6.

5.3.2 Experimental Results 1: Correlation Length-Scales

We now examine the effect of varying correlation length-scales of the background the solution accuracies are not e ected since we are solving to the same solution accuracy.

We can conclude that as the condition number of D increases, the condition numbers of S_p and $\hat{S}_p$ and the number of iterations to minimise $J(p)$ and $\hat{J}(\ z)$ also increase respectively. The preconditioned Hessian condition number increases at a much reduced rate and the number of iterations of the preconditioned problem barely increase at all.

5.3.3 Experimental Results 2: Assimilation Window Length

We now show the e ect of the length of the assimilation window on the minimisation problem. From our results on the condition number both theoretically and numerically, we know that the length of the assimilation window increases the condition number of S_p and $\hat{S}_p$. We also expect that this will increase the number of iterations required for convergence.

The experiment parameters are identical to the previous experiment with L

We see from Table 5.2 that as the assimilation window length increases so do the number of iterations to minimise $J(p)$ and $\hat{J}(z)$. We also see that the numerical condition numbers of both S_p and $\hat{S}_p$ increase. The rate of increases in the condition numbers of S_p and $\hat{S}_p$ di er in that S_p increases much more rapidly, numerical experiments using the 1D advection equation. Through the bounds, we demonstrated the following sensitivities both theoretically and numerically:

1. Error variance ratios.
2. Correlation length-scales.
3. Assimilation window length.

More05(twhve)1lJi7i etically

1.

problem $\hat{J}(z)$ is no longer sensitive to the increase in correlation length-scale of the matrices inside D, and hence the condition number of D. The convergence rate is much improved for the preconditioned problem $\hat{J}(z)$ over the original problem $J(p)$. We also showed that the condition number of the preconditioned problem is still sensitive to the length of the assimilation window and spatial observation density, which in turn was shown to affect the number of iterations required to converge.

This concludes the analysis of the Hessian condition number and convergence rates of the wc4DVAR $J(p)$ formulation and its preconditioned counter-part complement. It is important to realise that these results are illustrative examples of the behaviour we expected to see from the theory we have derived. We now consider the alternative formulation $J(x)$, (2.33).

Chapter 6

Conditioning of the State Formulation: $J(x)$

The previous chapter was dedicated to the conditioning of the Hessian S_p. We bounded the condition number of S_p and uncovered the parameters exhibiting the largest sensitivities with respect to the Hessian condition number. We found the Hessian S_p to be sensitive to the D matrix, containing the background and model error correlations. We then preconditioned the Hessian using the symmetric square root of D which improved the condition number sensitivity characteristics with respect to the condition number of D. We then demonstrated the sensitivities obtained from the bounds through numerical experiments on the condition number. We further demonstrated the e ect of some of these sensitivities on the number of iterations required for convergence.

In this chapter we bound the condition number of

$$S_x = \begin{pmatrix} B_0^{-1}+M_1^TQ_1^{-1}M_1 & -M_1^TQ_1^{-1} & & & \\ -Q_1^{-1}M_1 & Q_1^{-1}+M_2^TQ_2^{-1}M_2 & -M_2^TQ_2^{-1} & & \\ & \ddots & \ddots & \ddots & \\ & & \ddots & & \\ & & -Q_{n-1}^{-1}M_{n-1} & Q_{n-1}^{-1}+M_n^TQ_n^{-1}M_n & -M_n^TQ_n^{-1} \\ & & & -Q_n^{-1}M_n & Q_n^{-1} \end{pmatrix} + \begin{pmatrix} H_0^TR_0^{-1}H_0 & & & \\ & H_1^TR_1^{-1}H_1 & & \\ & & \ddots & \\ & & & H_n^TR_n^{-1}H_n \end{pmatrix}. \tag{6.1}$$

Through bounding the condition number of S_x we uncover the paramete sensitivities and demonstrate these through numerical experiments on condition number. We then show that these sensitivities can also effec minimisation of $J(x)$ by examining their effect on the number of iterations requ for convergence and solution accuracy.

We begin by deriving new bounds on the condition number of S_x.

6.1 Theoretical Results: Bounding t Condition Number of S_x

The following theorem27(accura)1(-375(326(theorem27(9701 Tf Tf 199.203 -2.3

Proof: We begin by bounding $_{min}(S_x)$ and $_{max}(S_x)$ using Theorem 3.4.2, yielding

$$_{min}(L^T D \;\; ^1 L) + \;\; _{min}(H^T R \;\; ^1 H) \qquad _{min}(S_x)$$
$$_{min}(L^T D \;\; ^1 L) + \;\; _{max}(H^T R \;\; ^1 H \;\; ^1); \tag{6.3}$$

and

$$_{max}(L^T D \;\; ^1 L) + \;\; _{min}(H^T R \;\; ^1 H) \qquad H$$

which shows the influence of $\kappa(L^T D^{-1} L)$, instead of just $\kappa(D)$ when compared to Theorem 5.1.1. We also see that as $\lambda_{max}(H^T R^{-1} H) \to 0$ both bounds tend to the condition number of $L^T D^{-1} L$. Therefore the bounds in Theorem 5.1.1 show that the condition number of S_x

where $2\ [\ _{min}(S_x);\ \ _{max}(S_x)]$ and $S_{x(i;j)}$ refers to the block matrix on the i^{th} block row and j^{th} block column. The left hand side of (6.10) for S_x yields

$$jj(S_{x(i;i)} \quad I\ )\ ^{1}jj_2{}^{1} = q\ \overline{\qquad\qquad\qquad\qquad\qquad\qquad}$$

We know the eigenvalues of S_x will lie on the positive real line since it is positive definite. Using (6.16) and recalling that S_x is block tri-diagonal, we have the following Geršgorin circles:

$$|\lambda^{(1;1)}_{1;\ldots;N}| \leq \|S_{x(1;2)}\|_2; \tag{6.18}$$

$$|\lambda^{(2;2)}_{1;\ldots;N}| \leq \|S_{x(2;1)}\|_2 + \|S_{x(2;3)}\|_2; \tag{6.19}$$

$$\vdots$$

$$|\lambda^{(n;n)}_{1;\ldots;N}| \leq \|S_{x(n;n-1)}\|_2 + \|S_{x(n;n+1)}\|_2; \tag{6.20}$$

$$|\lambda^{(n+1;n+1)}_{1;\ldots;N}| \leq \|S_{x(n+1;n)}\|_2; \tag{6.21}$$

all or some of which could contain a certain number of eigenvalues of S_x.

eigendecomposition structure as in Theorem 3.3.10,

$$
\begin{aligned}
\|S_{x(1,2)}\|_2 = \|-M^T Q^{-1}\|_2 &= |\sigma_q^{-2}| \cdot \|M^T C_Q^{-1}\|_2, \\
&= \sigma_q^{-2}\|F \Lambda_M^H C_Q^{-1} F^H\|_2, \\
&= \sigma_q^{-2}\sqrt{\lambda_{max}\left((F \Lambda_M^H C_Q^{-1} F^H)^H (F \Lambda_M^H C_Q^{-1} F^H)\right)}, \\
&= \sigma_q^{-2}\sqrt{|\lambda_{max}(C_Q^{-1})|^2 |\lambda_{max}(\Lambda_M)|^2}, \\
&= \sigma_q^{-2}|\lambda_{max}(C_Q^{-1})||\lambda_{max}(\Lambda_M)|, \qquad (6.25)
\end{aligned}
$$

where Λ_M denotes the diagonal matrix containing the eigenvalues of M. We observe that the blocks $S_{x(1,1)}$ and $S_{x(n+1,n+1)}$ will yield the same term on the right-hand side of the block Gersgorin theorem. The blocks $S_{x(i,i)}$ for $i = 2, \ldots, n$ will yield a term that is exactly twice as large.

The eigenvalue $\lambda_{max}(S_x)$ is bounded above by the edge of the Gersgorin circle furthest from the origin on the positive real line. So the quantity we are interested in for the upper bound is

$$
\lambda_{max}(S_x) \leq \max \begin{cases} \|(S_{x(i,i)} - \lambda I)^{-1}\|_2^{-1} + \sum_{j \neq i}^{n} \|S_{x(i,j)}\|_2 \\ \|(S_{x(i,i)} - \lambda I)^{-1}\|_2^{-1} + \sum^{n} \ldots \end{cases}
$$

and

$$\sum_{i=2}^{n} y_i^H \left(Q^{-1} + M^T Q^{-1} M + H^T R^{-1} H \right) y_i$$

$$= (n-1)\left(\lambda_{max}(Q^{-1}) + \mu_b(M^T Q^{-1} M) + \sigma_o^{-2}\sqrt{\frac{q}{N}} \right); \qquad (6.37)$$

and finally

$$y_{n+1}^H \left(Q^{-1} + H^T R^{-1} H \right) y_{n+1} = \lambda_{max}(Q^{-1}) + \sigma_o^{-2}\sqrt{\frac{q}{N}}; \qquad (6.38)$$

where $\mu_a, \mu_b \in \mathbb{R}$ are some arbitrary eigenvalues of $M^T Q^{-1} M$. Therefore,

$$f_1 = \lambda_{max}(B^{-1}) + \mu_a(M^T Q^{-1} M) + \lambda_{max}(Q^{-1}) + 2\sigma_o^{-2}\sqrt{\frac{q}{N}}$$

$$+ (n-1)\left(\lambda_{max}(Q^{-1}) + \mu_b(M^T Q^{-1} M) + \sigma_o^{-2}\sqrt{\frac{q}{N}} \right): \qquad (6.39)$$

We now compute f_2. Notice that due to our choice of $\hat{y}$, the first constituent of y, namely y_1 is the only vector that is different to the other y_i for $i = 2, \ldots, n+1$, so the first term in the sum f_2 is

$$y_2^H(-Q^{-1}M)y_1 = 0; \qquad (6.40)$$

since we chose the vectors in y to be orthonormal. The remaining constituent vectors of y are all identical, and will therefore yield non-zero terms,

$$f_2 = \sum_{i=2}^{n} y_{i+1}^H(-Q^{-1}M)y_i = \sum_{i=2}^{n} -\lambda_{max}(Q^{-1})\mu_c(M)\, y_{i+1}^H y_i;$$

$$= -(n-1)(\lambda_{max}(Q^{-1})\mu_c(M)); \qquad (6.41)$$

where $\mu_c(M) \in \mathbb{C}$ is some arbitrary eigenvalue of M and $\lambda_{max}(Q^{-1}) = \lambda_{max}(Q^{-1})$ since Q is a symmetric positive-definite matrix. Similarly for f_3, we have

$$f_3 = \sum_{i=2}^{n} y_{i+1}^H(-M^T Q^{-1})y_i = -(n-1)(\lambda_{max}(Q^{-1})\mu_c(M)); \qquad (6.42)$$

which when combined with f_2 gives us

$$f_2 + f_3 = -2(n-1)\lambda_{max}(Q^{-1})\mathrm{Re}(\mu_c(M)); \qquad (6.43)$$

where $\mathrm{Re}(\mu_c(M))$ denotes the real part of $\mu_c(M) \in \mathbb{C}$. Combining f_1, f_2 and f_3, we have the following expression for the Rayleigh quotient (6.33),

$$R_{S_x}(\hat{y}) = \frac{1}{n+1}\Big[(n-1)\lambda_{max}(Q^{-1})(1-2$$ Td [(max)]TJ/F15 11.9512 Tf 9.2719 .9701 Td [5.7 M & 1.508 .97d [(2 11.9552 Tf 18.97 0 Td

To obtain a bound on $_{max}(S_x)$ we recall the bounds of the Rayleigh quotient from Theorem 3.4.7,

$$
\begin{aligned}
{}_{max}(S_x) \quad & \frac{1}{n+1}\;(n \quad 1) \quad {}_{max}(Q^{\;1})(1 \quad 2\mathrm{Re}(\;{}_{c}(M))) + \quad {}_{b}(M^{T}Q^{\;1}M) + \quad {}_{o}^{2}\frac{q}{N} \\
& + \quad {}_{max}(Q^{\;1}) + \quad {}_{max}(B^{\;1}) + \quad {}_{a}(M^{T}Q^{\;1}M) + 2\;{}_{o}^{2}\frac{q}{N}^{i} \;; \\
& \frac{1}{{}_{o}^{2}}\frac{q}{N} + \frac{1}{{}_{q}^{2}}\frac{1}{n+1}\; n \quad {}_{max}(C_Q^{\;1}) + \quad {}_{min}(M^{T}C_Q^{\;1}M) \quad 2\;{}_{max}(C_Q^{\;1})\mathrm{Re}(\;{}_{min}(M)) \\
& + 2\;{}_{max}(C_Q^{\;1})\mathrm{Re}(\;{}_{min}(M)) + \frac{{}_{q}^{2}}{{}_{b}^{2}}\;{}_{max}(C_B^{\;1}) \;: \qquad (6.45)
\end{aligned}
$$

We also do a similar calculation for $_{min}(S_x)$ by choosing y in a similar fashion to (6.32). So y_i 2 R^N for each $i = 1;:::;n+1$ is chosen such that y_1 is the orthonormal eigenvector corresponding to $_{min}(B^{\;1})$ and y_i for $i = 2;:::;n+1$ is the orthonormal eigenvector corresponding to $_{min}(Q^{\;1})$. This gives us

$$
\begin{aligned}
{}_{min}(S_x) \quad & \frac{1}{{}_{o}^{2}}\frac{q}{N} + \frac{1}{{}_{q}^{2}}\frac{1}{n+1}\; n \quad {}_{min}(C_Q^{\;1}) + \quad {}_{max}(M^{T}C_Q^{\;1}M) \quad 2\;{}_{min}(C_Q^{\;1})\mathrm{Re}(\;{}_{max}(M)) \\
& + 2\;{}_{min}(C_Q^{\;1})\mathrm{Re}(\;{}_{max}(M)) + \frac{{}_{q}^{2}}{{}_{b}^{2}}\;{}_{min}(C_B^{\;1}) \;: \qquad (6.46)
\end{aligned}
$$

Combining the bounds on the lowest and largest eigenvalues of S_x, we divide (6.45) by (6.46) to obtain the lower bound on the spectral condition number of S_x

$$
(S_x) \quad \frac{\frac{{}_{q}^{2}}{{}_{o}^{2}}\frac{q(n+1)}{N} + n \quad {}_{max}(C_Q^{\;1}) + \;{}_{min}(M^{T}C_Q^{\;1}M) \;\; 2\;{}_{max}(C_Q^{\;1})\mathrm{Re}(\;{}_{min}(M)) \;\; +2\;{}_{max}(C_Q^{\;1})\mathrm{Re}(\;{}_{min}(M)) + \frac{{}_{q}^{2}}{{}_{b}^{2}}\;{}_{max}(C_B^{\;1})}{\frac{{}_{q}^{2}}{{}_{o}^{2}}\frac{q(n+1)}{N} + n \quad {}_{min}(C_Q^{\;1}) + \;{}_{max}(M^{T}C_Q^{\;1}M) \;\; 2\;{}_{min}(C_Q^{\;1})\mathrm{Re}(\;{}_{max}(M)) \;\; +2\;{}_{min}(C_Q^{\;1})\mathrm{Re}(\;{}_{max}(M)) + \frac{{}_{q}^{2}}{{}_{b}^{2}}\;{}_{min}(C_B^{\;1})}\;; \qquad (6.47)
$$

which completes the proof.

The bounds obtained here are quite complex and require analysis before any de nitive conclusions can be drawn about the nature of the sensitivities of the condition number of S_x. We now analyse the S_x matrix and condition number bounds further and discuss interpretations of the bounds.

6.2 Discussion

We begin by highlighting some simple points by inspecting S_x under simpli ed assumptions. We make simplistic assumptions in addition to the assumptions made in Theorem 6.1.2: $M = I_N$, $B = \sigma_b^2 I_N$, $Q = \sigma_q^2 I_N$, $R = \sigma_o^2 I_N$ and $HH^T = I_q$, thus

$$S_x = \frac{1}{\sigma_q^2}\begin{pmatrix} ((\frac{\sigma_q}{\sigma_b})^2+1)I & -I & & & \\ -I & 2I & -I & & \\ & \ddots & \ddots & \ddots & \\ & & -I & 2I & -I \\ & & & -I & I \end{pmatrix} + \frac{1}{\sigma_o^2}\begin{pmatrix} H^TH & & & & \\ & H^TH & & & \\ & & \ddots & & \\ & & & H^TH & \\ & & & & H^TH \end{pmatrix}. \quad (6.48)$$

Examining (6.48) we can clearly see the parameters governing both the first and second term of the Hessian. The first term depends on the ratio of σ_b/σ_q, arising from D. This is different from S_p since the first term of S_p is D^{-1} and the bounds

The lower bound in Theorem 6.1.2 shows that σ_o^2 is tied to the ratios σ_q/σ_o and σ_b/σ_o. We also see that changes in $\frac{\sigma_q^2}{\sigma_o^2}$ will not affect the overall size of the lower bound, since it is present in both the numerator and denominator of the lower bound with identical coefficients. Whereas if $\frac{\sigma_q^2}{\sigma_b^2}$ changes then the bound could increase if C_B is ill-conditioned, which is highly likely in an operational NWP context.

We now turn our attention to the upper bound of Theorem 6.1.2, where we have used a novel approach in an attempt to uncover the condition number sensitivities of S_x. We see three separate things here:

1. the model error variance σ_q^2;
2. the largest eigenvalue of the main diagonal blocks of S_x;
3. the denominator of the upper bound, the minimum eigenvalue of $L^T D^{-1} L$.

We see that as $\sigma_q \to \infty$ the upper bound will increase since $\lambda_{max}(S_{x(i,i)})$ will increase. We also see that as $\sigma_q \to 0$, the upper bound will increase because of the term $2\sigma_q^{-2}\lambda_{max}(C_Q^{-1})\lambda_{max}(M)$. Therefore the upper bound shows that the condition number of S_x will

We now examine the eigenvalue spectrum of $L^T D^{-1} L$ to understand the impact of $\lambda_{min}(L^T D^{-1} L)$ on the upper-bound. Note that

$$L^T D^{-1} L = \begin{pmatrix} B_0 + M_{0;1}^T Q_1 M_{1;0} & -M_{0;1}^T Q_1 & & & \\ -Q_1 M_{1;0} & Q_1 + M_{1;2}^T Q_2 M_{2;1} & -M_{1;0}^T Q_1 & & \\ & -Q_2 M_{2;1} & Q_2 + M_{2;3}^T Q_3 M_{3;2} & \ddots & \\ & & \ddots & \ddots & -M_{n-1;n}^T Q_n \\ & & & -Q_n M_{n;n-1} & Q_n \end{pmatrix}. \tag{6.51}$$

In addition to the assumptions at the beginning of this section, we assume $\sigma_o = 1$ and let $\sigma_b > \sigma_q$ since it is intuitive that the variance of the errors in the previous forecast will be larger than the variance of the model errors in a single time step. Therefore,

$$L^T D^{-1} L = \sigma_q^{-2} \begin{pmatrix} ((\frac{\sigma_q}{\sigma_b})^2 + 1) I & -I & & \\ -I & 2I & -I & \\ & \ddots & \ddots & \ddots \\ & & -I & 2I & -I \end{pmatrix}$$

L

C 0

where v 2 R^n is an eigenvector such that

$$v = \begin{pmatrix} v_1 \\ v_2 \\ \vdots \\ v_{n+1} \end{pmatrix} ; \tag{6.56}$$

with corresponding eigenvalue . We can rewrite the eigenvalue equation as a recurrence relation

$$v_{k\quad 1} + 2v_k \quad v_{k+1} = \; v_k ; \tag{6.57}$$

where

$$v_0 = 0 ; \tag{6.58}$$

$$v_{n+2} = v_{n+1} : \tag{6.59}$$

We introduce the appropriate auxiliary equation

$$x^2 \quad (2 \qquad)x + 1 = 0 ; \tag{6.60}$$

Using boundary condition (6.59) on (6.66) yields

$$(x_1^{n+1} \quad x_2^{n+1})A = (\,x_1^{n+2} \quad x_2^{n+2})A; \tag{6.67}$$

which, with some manipulation becomes,

$$(1 \quad x_1)x_1^{n+1} = x_2^{n+1}(1 \quad x_2); \tag{6.68}$$

we then substitute (6.63) into the right hand side of (6.68) obtaining,

$$(1 \quad x_1)x_1^{n+1} = x_2^{n+1}(1 \quad {}^{1}$$

Since the squared sine function is bounded between 0 and 1, the eigenvalues $_k(P)$ are bounded between 0 and 4 as the assimilation window length, n, grows. The extreme eigenvalues tend to their limits (0 and 4) at a rate of $=4n^2$. The possibility of a 0 eigenvalue as the assimilation window grows implies that $(P) ! 1$ as n grows. The analysis in this simplified scenario shows that a major source of ill-conditioning of S_x can arise from the smallest eigenvalue of the $L^T D^{-1} L$ term as the assimilation window length, n, grows.

We now make the link between the sensitivity of $_{min}(L^T D^{-1} L)$ and the previous analysis in (6.49). If the number of observations were to equal the number of states, the dependence of the condition number of S_x on $(L^T D^{-1} L)$ term will no longer be an issue. This is because the second term of S_x, $H^T R^{-1} H$, will be full rank and the condition number of S_x will not be vulnerable to the minimum eigenvalue of $L^T D^{-1} L$, since the lowest eigenvalue of S_x will be bounded by $_o^{-2}$. This also implies that if there were a full set of observations, long assimilation windows will not affect the conditioning of S_x, since the minimum eigenvalue of $L^T D^{-1} L$ is no longer an issue.

We now demonstrate the bounds and verify sensitivities of the condition number of S_x discussed here.

6.3 Numerical Results

The aim of this section is to numerically demonstrate the sensitivities of the condition number of S_x. We organise this section as follows.

In the first part of this section we demonstrate the uses of the Gersgorin circle theorem both in scalar and block forms for estimating the condition number of S_x, since this was used to obtain the upper bound in Theorem 6.1.2.

The second part is solely dedicated to the demonstration of the bounds on the condition number of S_x, and the sensitivities obtained from the theoretical analysis in the previous sections. We demonstrate the following sensitivities of the condition number of S_x, which were obtained from the theory in this chapter:

1. the model error variance ${}_q^2$;
2. correlation length-scales;
3. the length of the assimilation window with the number of spatial observations per assimilation step.

6.3.2 Experiment 1: Gersgorin's Circles

We note that we could not utilise either of the Geršgorin circle theorems for the lower bound, since S_x is positive definite, and the lower bounds shown in Figures 6.1 and 6.2 are negative. The condition number is relatively high due to the high correlation length-scale for the model error covariance matrix. This does not hinder the Geršgorin theorem from estimating the whereabouts of the eigenvalues. We can see from Figures 6.1 and 6.2 that the block Geršgorin circle theorem is at least as good as the Geršgorin circle theorem and that it gives a far better indication as to the whereabouts of the eigenvalues of S_x in this particular case. The same is also observed in [23], where the authors showed the block analogue of Geršgorin's theorem to be at least as good as the scalar Geršgorin circle theorem in general.

We also observe $\lambda_{max}(S_x) = 1.956 \times 10^6$ and that the upper bound estimated by the block Geršgorin circle theorem is 1.976×10^6 compared with the upper bound scalar Geršgorin estimate of 2.218×10^6. We conclude that both bounds are good and the block Geršgorin circle theorem provides a tighter upper bound in this particular situation.

We now demonstrate the effects of the model error variance σ_q^2 on the condition number of S_x

6.3.3 Experiment 2: Model Error Variance

The experiment parameters remain as stated in Section 6.3.1 with the exception of the following. The model error covariance matrix correlation length-scale is reduced to $L(C_Q) = \Delta x = 0.01$ and the observation standard deviation $\sigma_o = 0.5$. We also reduce the number of equally spaced spatial grid-points observed to 10 out of the $N = 50$ grid-points per assimilation step. These settings are arbitrarily chosen to ensure that the only source of ill-conditioning will be from σ_q.

(a) $_q$ varying.

(b) $_q = \ _o$ ratio.

(c) $_b = \ _q$ ratio.

Figure 6.3: Log-scale graphs of (S_x) (black line) with bounds from Theorem 6.1.1 (green dotted lines) and Theorem 6.1.2 (red dotted lines) as a function of $_q$ (a), $_q = \ _o$ (b) and $_b = \ _q$ (c).

As the parameter $_q$ varies, so do the ratios $_b = \ _q$ and $_q = \ _o$, prompting us to study the behaviour of the condition number of S_x with respect to these ratios as well as $_q$. Figure 6.3 demonstrates that the upper bounds of both Theorems 6.1.1 and 6.1.2 resemble the behaviour of the condition number of S_x, whereas the

S_x. We see a minimum condition number value for $_b = {}_q = \;\; {}_q = {}_o = 2$ or $\;\; {}_q = 0{:}5$, but the condition number of S_x continues to rise as $_q\,! \;\; 0; 1$. This confirms the sensitivity of the condition number of S_x to the model error variance, which we obtained from the bounds in Theorem 6.1.1.

We have demonstrated the bounds and confirmed the sensitivity of S_x to $\;\; {}_q$.

6.3.4 Experiment 3: Correlation Length-Scales

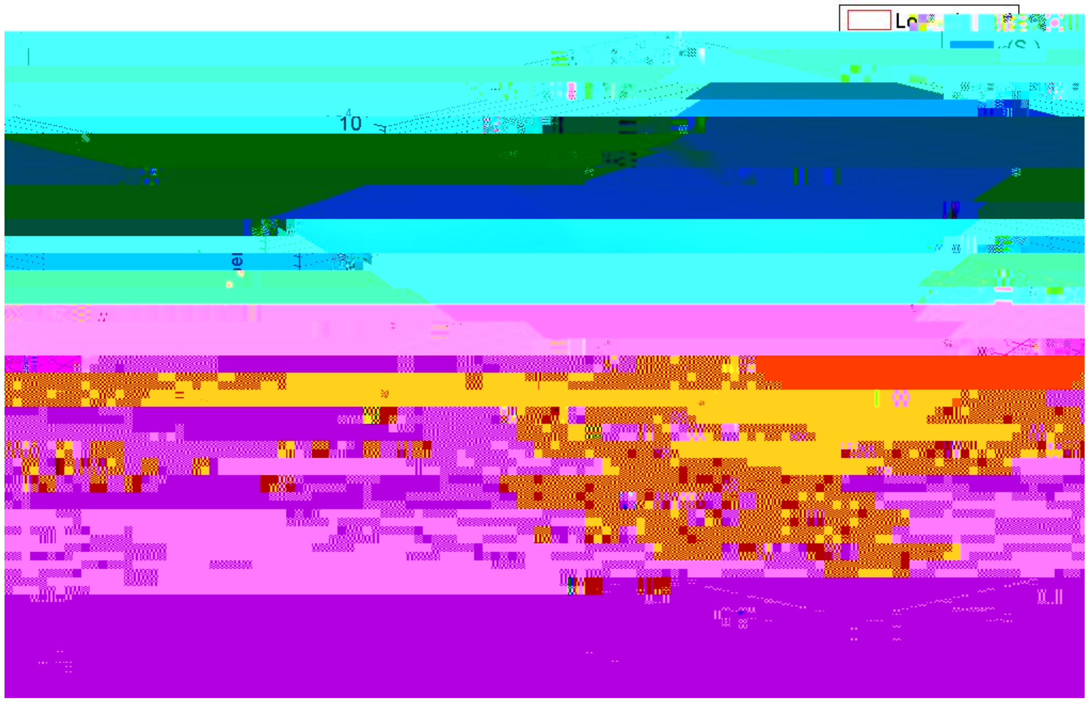

Figure 6.5: Log-scale surface plot of (S_x) (blue surface) and lower bound (red mesh). Horizontal axes are the background error correlation length-scale $L(C_B)$ and model error correlation length-scale $L(C_Q)$. Vertical axis measures condition number on a log scale.

Figures 6.4 and 6.5 demonstrate the sensitivity of the condition number of S_x to correlation length-scales in the background and model error covariance matrices. We see the upper bound is a good estimate of the condition number of S_x in Figure 6.4, while the lower bound is uninformative. However, Figure 6.5 shows that the behaviour of the lower bound is similar to the behaviour of the condition number of S_x on a log-scale.

Comparing this to the behaviour shown in the previous chapter [Section 5.1.3, Figure 5.2], the condition number of S_x is far more sensitive than (S_p) to changes in the correlation length-scales of C_B and C_Q and hence (D), rising to a condition number range of 5000 7000 for L the maximum

condition number of

We have demonstrated the sensitivity of the condition number of $\mathbf{S}_x$ to correlation length-scales in the background and model error covariance matrices, along with the bounds. We now investigate the sensitivity of the condition number of $\mathbf{S}_x$ to observation density and assimilation window length.

6.3.5

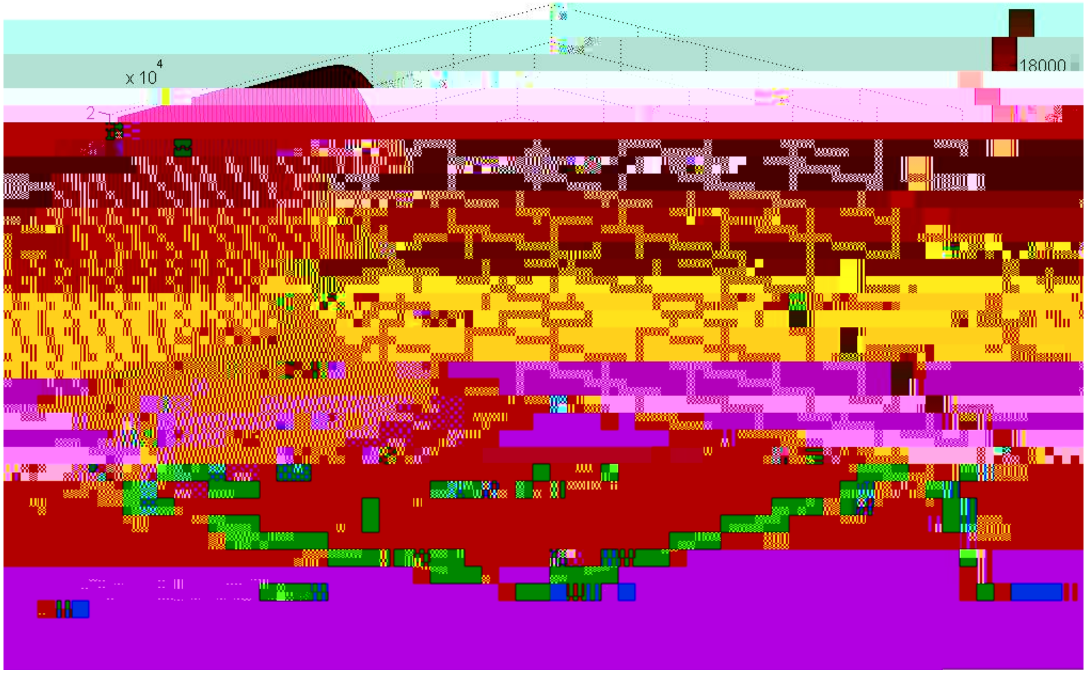

Figure 6.6: Surface plot of (S_x). Vertical axis measures condition number. The non-vertical axes measure spatial observation density q and assimilation window length, n.

Figure 6.6 demonstrates the sensitivity of the condition number of S_x to increasing assimilation window length as the number of spatial observations per assimilation step decreases below $q = N=5$. Interestingly, we see that the rise in assimilation window length has no effect on the condition number of S_x if there are a good number of spatial observations, more than $q = N=2$. This confirms our findings in the discussion in Section 6.2, that as the term $H^T R^{-1} H$ approaches full rank, the condition number of S_x becomes less dependent on the condition number of $L^T D^{-1} L$.

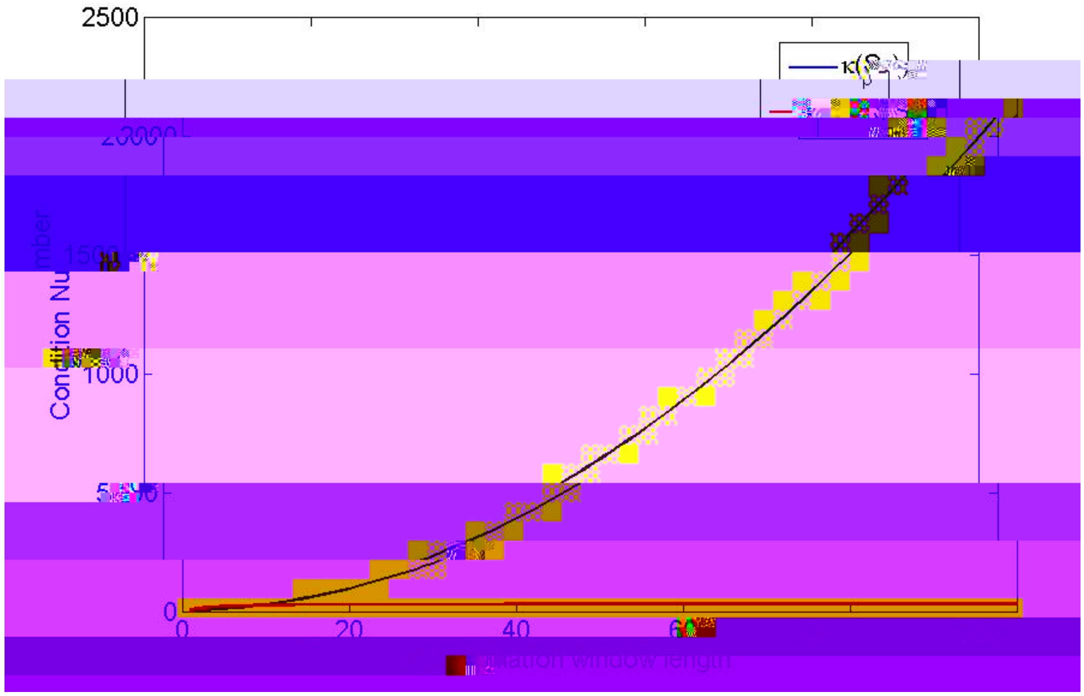
2500
2000
1500
1000
500
0
0
20
40
Condition Number

6.4 Convergence Results

$_q$	$_q = _o$	$_b = _q$	No. of iterations	Condition number	Solution relative error
0.11	0.11	9.09	220	4824	0.29
0.21	0.21	4.76	139	1351	0.30
0.31	0.31	3.23	115	641	0.29
0.41	0.41	2.44	98	385	0.28
1.81	1.81	0.55	101	367	0.23
2.81	2.81	0.36	126	882	0.25
3.81	3.81	0.26	151	1619	0.25
5.81	5.81	0.17	183	3762	0.29
7.81	7.81	0.13	208	6796	0.28

Table 6.1: Standard deviation ratios, number of iterations to convergence and the solution relative error of J (x), and the condition number of S_x. Standard deviations $_b = \ _o = 1$.

We see here that when $_q$ tends to zero or increases from 2, the condition number of S_x, the number of iterations to convergence and the solution relative error all increase. The other ratios involving $_q$ are the underlying reason for the changes seen in the minimisation characteristics in Table (6.1). As the ratios move away from 2, the condition number of S_x, number of iterations and relative solution error all increase.

6.4.2 Experiment 2: Correlation Length-Scales

We now investigate to the sensitivity of the minimisation problem to correlation length-scales. We preserve the settings from the previous experiment, Section 6.4.1 and we vary the correlation length-scales of C_B and C_Q, remembering that (C_{LAP}) is less sensitive than (C_{SOAR}) to identical changes in the correlation length-scales.

$L(C_B)$	No. of iterations	Condition number
0.01	86	134
0.05	608	43,637
0.10	978	492,394
0.15	1301	2,203,292
0.20	1687	6,537,759

$L(C_Q)$	No. of iterations	Condition number
0.01	86	134
0.05	361	65,670
0.10	491	560,326
0.15	572	1,924,374
0.20	596	4,563,487

Table 6.2: Tables of convergence and condition number values with varying correlation length-scales. Table on the left $L(C_B) = \quad x$, while $L(C_Q)$ varies. Similarly the right table $L(C_Q) = \quad x$, while $L(C_B)$ varies.

Table 6.2 shows the effects of correlation length-scale on the minimisation problem presented by $J(x)$. Both tables confirm the sensitivity of the condition number of S_x to the correlation length-scales of C_B and C_Q, also shown in Section 6.3.4 Experiment 3. We have also shown the adverse affect this has on the number of iterates.

We now examine the effect of observation density and assimilation window length.

6.4.3 Experiment 3: Assimilation Window Length and Observation Density

In this experiment we examine the sensitivity of the minimisation problem presented by $J(x)$ to the length of the assimilation window and the observation density simultaneously. We will discuss three tables in this section; number of iterates, solution accuracy and condition numbers.

We aim to show that increasing assimilation window length renders S_x ill-conditioned, as discussed in Section 6.2 for low observation densities. We also show that as we increase the number of spatial observations per assimilation step the condition number of S_x becomes less effected by the rise in assimilation window length. This due to the second term of the Hessian $\mathbf{H}^T R^{-1} H$ approaching full rank as the observation density increases.

Assimilation window length	No. of spatial observations: 50	25	10	5	2	1
1	19	24	32	38	48	50
11	20	26	49	83	165	193
21	19	26	51	93	215	271
31	19	25	51	97	230	349
41	18	25	50	97	230	420
51	18	24	49	98	241	460
61	17	24	49	98	240	429
71	17	24	49	97	241	459
81	17	23	49	96	239	460
91	16	23	49	94	241	465

Table 6.3: No. of iterations

Assimilation window length	No. of spatial observations: 50	25	10	5	2	1
1	0.26	0.27	0.30	0.30	0.27	0.35
11	0.09	0.09	0.12	0.22	0.51	0.58
21	0.05	0.05	0.06	0.11	0.40	0.64
31	0.04	0.04	0.04	0.07	0.26	0.57
41	0.03	0.03	0.03	0.05	0.17	0.48
51	0.02	0.02	0.02	0.03	0.12	0.37
61	0.02	0.02	0.02	0.03	0.09	0.28
71	0.02	0.02	0.02	0.02	0.08	0.24
81	0.01	0.01	0.02	0.02	0.07	0.19
91	0.01	0.01	0.01	0.02	0.05	0.16

experiments using the 1D advection equation. Through the bounds, we showed the sensitivities of the condition number of S_x to the following:

1. the model error variance σ_q^2;
2. correlation length-scales in the background and model error covariance matrices;
3. assimilation window length and observation density.

More specifically we showed

1. The condition number of $L^T D^{-1} L$ heavily influences the condition number of S_x, shown in Theorem 6.1.1. We highlight this sensitivity further through the condition number of the background and model error covariance matrix, D, which is sensitive to correlation length-scales and the σ_b/σ_q ratio. The theory suggests that S_x is potentially more vulnerable to the condition number of D than S_p. This was shown theoretically in Section 6.2 and also demonstrated numerically in Section 6.3.4, Experiment 3.

2. The sensitivity of the condition number of S_x to assimilation window length. This is different to S_p, which sees an increase in its condition number (as shown in Chapter 5) as the observation density increases and as the assimilation window increases.

   (a) The minimum eigenvalue of the first term of the S_x Hessian has the potential to converge to 0 as the assimilation window grows. The upper bound in Theorem 6.1.2 shows that as the assimilation window increases, $\lambda_{min}(L^T D^{-1} L)$ decreases and therefore increasing $\kappa(S_x)$. We showed this through examination of the first term of S_x when reduced to the P matrix (as discussed in Section 6.2).

   (b) As the observation density decreases the condition number of S_x grows at a faster rate as the length of the assimilation window increases.

becomes immune to increasing assimilation window length (as discussed in Section 6.2).

(c) Decreasing observation accuracy (increasing σ_o) reduces the contribution of the second term of S_x and puts greater emphasis on the first term of S_x, which is sensitive to assimilation window length and the condition number of D. This is shown through the analysis of the bounds in Theorem 6.1.1 in the discussion in Section 6.2, equation (6.49).

These sensitivities were shown through theoretical analysis of the bounds and numerical demonstrations of the theory on the condition number of S_x. We showed further that these sensitivities also reflect in the minimisation characteristics,

Chapter 7

Weak-Constraint 4DVAR: Lorenz95 Model

In this chapter, we show an example where it is possible for the theory established in the previous chapters to provide valuable insight for applications in a wider context. We explore the application of the wc4DVAR algorithms discussed in this thesis on the non-linear chaotic model known as Lorenz 95, described in Chapter 3, Section 3.5.2. This model possesses error growth characteristics similar to that of weather prediction models. It is also one of the models used by the ECMWF

7.1 Lorenz 95 Model Example

The purpose of this chapter is to put the theory in the previous chapters into wider context. We do this by testing if the parameters, which were found to be responsible for ill-conditioning in the theory on linear models, also have the same effect the solution process of wc4DVAR when applied to a non-linear model. The specific sensitivities we investigate are:

1. the observation density and assimilation window length;
2. the correlation length-scales in the background and model error covariance matrices.

The theory showed that as the observation density and assimilation window length increase, the condition number of S_p and hence the number of iterations for the model error formulation also increase. The theory also showed that as the number of observations decreases and the assimilation window length increases the condition number of S_x and the number of iterations of the state formulation to converge, also increase. We also found a particular special case where if the state domain was fully observed, the increase in assimilation window length no longer affected the condition number of S_x or the number of iterations required for convergence. We also saw that as the correlation length-scales grow S_p and S_x become more ill-conditioned, where S_x showed potential of being more sensitive to this than S_p.

Both wc4DVAR algorithms implemented on the Lorenz 95 model have been tested and verified in the same manner as for the implementation of the wc4DVAR

7.1.1 Experimental Design

The model parameters used for the Lorenz 95 are explained in Chapter 3, Section 3.5.2, but we restate the parameter settings here for clarity. The variables are treated as points on a latitude circle, therefore the spacing between each of the $N = 40$ variables is $x = 1/N = 0.025$. Throughout this chapter we use a time-step of $t = 0.025$, which is equivalent to 3 hours. We use the Polak-Ribiere non-linear conjugate gradient technique as described in Chapter 3, Section 3.2.3, to minimise the objective functions. The iterative minimisation stopping criterion used is described in Chapter 3, Section 3.2.4, where we set the tolerance to 10^{3} for all experiments unless otherwise stated. The solution errors and relative errors are all calculated as in previous chapters, as shown in Chapter 4, Section 4.1.6. The model parameters chosen here remain unchanged throughout our experiments.

The assimilation parameters are as follows. The background covariance matrix is such that $B = {}^{2}_{b}C_{SOAR}$ with $_{b} = 0.1$ and $L(C_B) = 0.005 = x/5$. The model error covariance matrix is such that $Q = {}^{2}_{q}C_{LAP}$ with $_{q} = 0.05$ and $L(C_Q) = 0.005 = x/5$. The observation error covariance matrix is $R = {}^{2}_{o}I$ with $_{o} = 0.05$. It is important to note that for all our experiments, the data assimilation parameters used to generate the truth are identical to the assimilation parameters.

We use the Polak-Ribiere code used is as described in Secion 3.2.3, written by C.E. Rasmussen, to minimise the objective functionals. The Polak-Ribiere code is written such that it requires the code for the procedure which evaluates $J(p)$ and $J(x)$ and their respective gradients.

We now present our experimental results.

7.1.2 Experiment 1 (i): Assimilation Window Length and Observation Density

In this section we examine the sensitivity of the model error and state formulations to the length of the assimilation window and the observation density simultaneously. We now present the number of iterations needed for both formulations to achieve the minimisation tolerance.

No. of spatial observations

the increasing length of the assimilation window. The results in Table 7.2 agree with ndings in Chapter 6, Section 6.3.5, Experiment 4. We can also see the special case in Table 7.2, where the state is fully observed (rst column, where observations $q = 40$), agreeing with Chapter 6, Section 6.3.5, Experiment 4.

Comparing the number of iterations of the two formulations, we see that the model error formulation generally performs better than the state formulation, unless the state is half ($q = 20$) or fully ($q = 40$) observed. The assimilation runs in Tables 7.1 and 7.2 show that with enough observations, the state formulation out-performs the model error formulation and has the unique property of not being a ected by the assimilation window length with a fully observed state. This agrees with ndings in Chapter 6.

	No. of spatial observations							
	40	20	10	8	5	4	2	1
1	0.004	0.008	0.008	0.009	0.008	0.009	0.008	0.008
6	0.005	0.009	0.011	0.009	0.011	0.011	0.012	0.012
12	0.006	0.013	0.019	0.021	0.022	0.028	0.028	0.029
18	0.006	0.013	0.028	0.037	0.041	0.046	0.061	0.052
24	0.007	0.015	0.032	0.032	0.049	0.051	0.065	0.081
30	0.007	0.022	0.033	0.040	0.099	0.090	0.082	0.106
36	0.007	0.020	0.048	0.034	0.415	0.066	0.172	0.110
42								

the Taylor series of the non-linear objective functionals. Therefore the condition number alone may not be responsible for the increase in iterations and solution relative error.

In Table 7.4 we see a clear trend of increased relative errors in the solution with the increase of assimilation window length. We also see that as the observation density decreases, the relative errors in the solution increase, which is consistent with the increase in iterations shown in Table 7.2. The increase of relative errors with assimilation window length is evident for all numbers of observations except when the state is fully observed, $N = 40$. We also see many cases of divergence of the solution, where the solution relative error of the state formulation is 1. This emphasises the sensitivity of the state formulation to observation density, where if there are not enough observations, the solution relative error can be $O(10^2)$ larger than errors in the model error formulation solution.

Tables 7.3 and 7.4 show that the accuracy of the model error formulation is clearly superior to the state formulation. The increased non-linearity of $J(x)$ over $J(p)$ could be the reason for the di erence in solution relative errors. In Table 7.4 for $n = 48$ and q 10, we see an example where the state formulation solution has diverged. This may be due to the increase in non-linearity of the state formulation objective function or the inadequacy of the stopping criterion.

We now examine the condition numbers.

	No. of spatial observations							
	40	20	10	8	5	4	2	1
1	1.49E+05	5.44E+07	4.96E+07	4.36E+07	3.56E+07	4.45E+07	1.26E+07	2.73E+07
6	1.07E+16	2.47E+19n6 of m .-327(m .-3272)-4902(15/-3272)-427(2.22727a.456d02(15/-007)a.456d08- erence)-334						

The condition numbers in Table 7.5 are incredibly high, however we do see the general trend that the condition number of S_p increases with the length of the assimilation window for any number of observations. We also see that the condition number of S_p increases as the number of observations increase, which is in agreement with the iterations in Table 7.1 and the trend of solution relative errors in Table 7.3. This also agrees with our ndings in Chapter 5.

Assimilation window length	No. of spatial observations							
	40	20	10	8	5	4	2	1
1	1.00	2.83E+06	1.13E+07	1.22E+07	1.52E+07	1.43E+07	1.42E+07	1.57E+07
6	1.00	3.36E+07	1.50E+14	4.20E+16	2.40E+17	5.23E+17	7.14E+17	4.08E+18
12	1.00	8.04E+07	4.33E+14	2.31E+16	2.31E+21	3.25E+21	3.45E+21	1.06E+28
18	1.00	1.28E+09	7.68E+12	2.65E+17	7.92E+20	2.14E+21	5.08E+21	2.76E+26
24	1.00	9.44E+07	2.25E+14	2.22E+15	5.70E+20	1.46E+21	3.00E+21	5.33E+21
30	1.00	6.27E+07	7.19E+11	5.83E+13	8.73E+20	1.52E+21	2.77E+21	1.44E+22
36	1.00	2.86E+07	1.29E+13	9.88E+15	3.80E+21	3.65E+21	1.31E+22	1.99E+22
42	1.00	4.90E+07	1.44E+13	2.20E+16	7.21E+21	1.28E+22	6.27E+21	4.27E+21
48	1.00	2.68E+07	1.36E+12	2.46E+15	2.97E+22	7.96E+20	1.91E+21	7.70E+21

Table 7.6: Condition number values of S_x. $n = 48$ is equivalent to 6 days.

The condition numbers for S_x in Table 7.6 show that if the state is fully observed, the condition number of S_x is consistently 1, which agrees with the lower number of iterations in the same column in Table 7.2 and also the low relative error in Table 7.4. We also see the as the number of observations decreases, the condition numbers of S_x rise very rapidly, reaching a plateau at around 5 observations.

As mentioned previously, the condition number is not the only in uential factor for the poor solution accuracy of the state formulation as seen in Table 7.4, the increasing non-linearity of $J(x)$ may also be a contributor. Evidences of increasing non-linearity of $J(x)$ can be seen in the large number of iterations, poor solution relative errors (to the extent that it looks to have diverged in some cases) and very low condition numbers in comparison to the condition number of the Hessian of $J(p)$. Another possibility is that the iterative minimisation stopping criterion used (as described in Section 3.2.4u. 9.9626 Tf 168.953 t3(condition.a 0 Td [(()]TJ/F22 11.9

The values of the variables X_i are represented by their colour. These variables can be any atmospheric quantity, for example, temperature [62]. The vertical axis represents time, thus the plot shows us the temporal evolution of these atmospheric quantities with respect to their position.

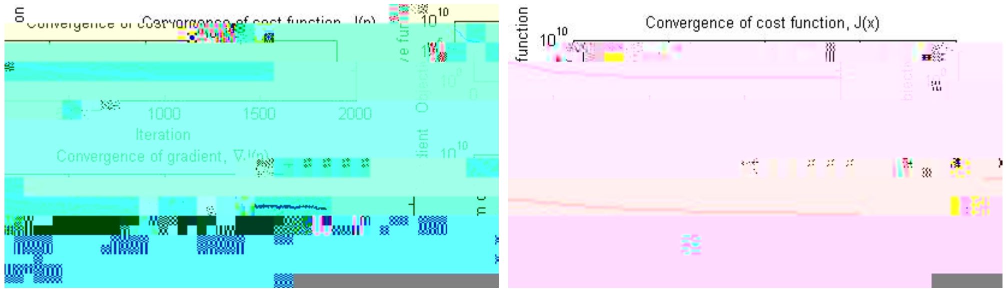

(a) $J(p)$ (top) and $\|\nabla J(p)\|$ (bottom). (b) $J(x)$ (top) and $\|\nabla J(x)\|$ (bottom).

Figure 7.2: Respective objective function and gradient norm values with the number of minimisation iterations.

We see here in Figures 7.2(a) and (b) that the model error formulation requires $O(10^3)$ more iterations than the state formulation to converge to the same tolerance. We now examine the relative errors in the solutions.

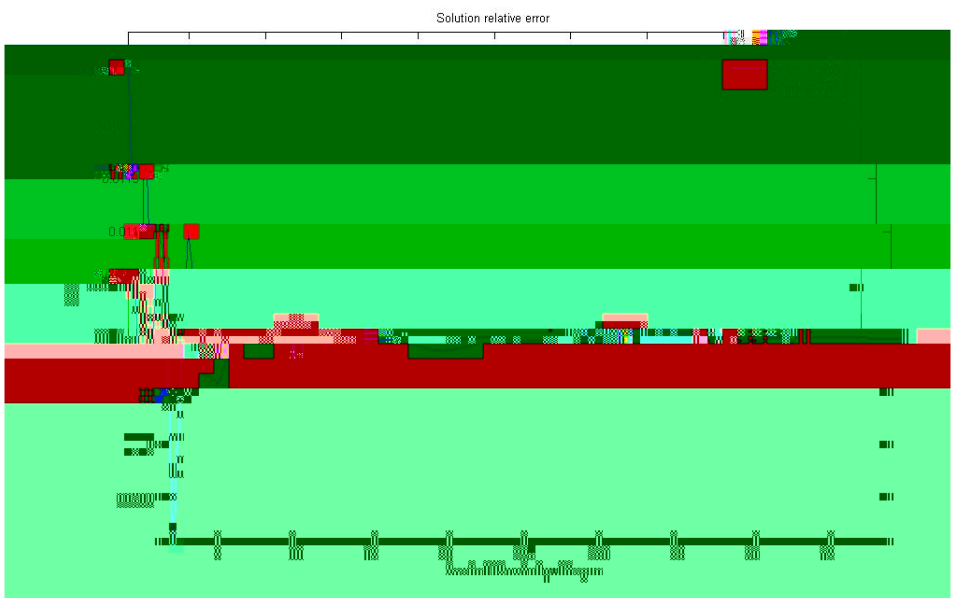

Figure 7.3: Solution relative errors throughout the assimilation window, $J(p)$ (blue line) and $J(x)$ (red line).

Figure 7.3 shows the errors are spread in a similar manner, with the range of errors exhibited by the solution to the $J(p)$ problem being slightly larger than $J(x)$. This is con rmed by the total solution relative error of both the model error and state formulations, which are 0017 and 0012 respectively.

The results in this experiment show that for long assimilation windows with equal $\sigma_b^2 = \sigma_q^2 = \sigma_o^2 = 1$ to ensure that the only source of ill-conditioning will arise from the correlation length-scales being varied.

		$L(C_B)$					
		0.01	0.03	0.05	0.07	0.09	0.11
$L(C_Q)$	0.01	18	31	47	89	155	239
	0.03	25	46	76	79	146	214
	0.05	42	45	57	102	140	201
	0.07	49	56	60	100	170	202
	0.09	77	79	83	123	212	221
	0.11	102	110	100	135	162	277

	$L(C_B)$					
	0.01	0.03	0.05	0.07	0.09	0.11
0.01	61	176	370	685	891	1128
0.03	174	191	420	695	967	1497
0.05	348	508	385	742	1343	1108
0.07						

Table 7.7: Number of iterations for $J(p)$.

are consistently larger than the model error formulation. In a specific example where $L(C_B) = 0.05$ and $L(C_Q) = 0.11$, the solution relative error of the state formulation is almost one order of magnitude higher than the model error formulation. So it is clear that the model error formulation is less sensitive to correlation length-scale and provides consistently more accurate solution in comparison to the state formulation.

		$L(C_B)$					
		0.01	0.03	0.05	0.07	0.09	0.11
$L(C_Q)$	0.01	6.11E+18	5.02E+18	7.16E+18	1.90E+19	3.74E+19	2.45E+20
	0.03	5.70E+18	9.42E+19	3.46E+19	5.70E+20	5.01E+20	6.41E+19
	0.05	3.39E+20	1.12E+19	1.15E+20	1.44E+20	5.55E+19	1.26E+20
	0.07	1.21E+19	2.53E+20	1.48E+20	8.32E+21	9.83E+20	8.40E+20
	0.09	2.73E+21	3.44E+21	2.86E+19	1.57E+20	2.48E+20	2.72E+20
	0.11	9.35E+18	1.56E+20	5.22E+20	3.53E+21	4.42E+20	2.34E+21

Table 7.11: Condition number values for S_p.

		$L(C_B)$					
		0.01	0.03	0.05	0.07	0.09	0.11
$L(C_Q)$	0.01	2.18E+19	1.81E+19	6.50E+19	2.42E+19	7.28E+21	1.18E+19
	0.03	4.18E+20	1.41E+19	7.30E+18	8.48E+20	2.72E+18	1.72E+19
	0.05	8.08E+19	1.17E+19	9.92E+18	6.99E+18	1.95E+19	1.13E+19
	0.07	1.51E+19	5.39E+19	6.06E+19	1.67E+19	3.58E+20	6.93E+19
	0.09	3.08E+19	5.45E+19	1.17E+20	8.44E+20	1.38E+20	1.38E+19
	0.11	1.17E+20	7.82E+19	2.92E+20	1.44E+21	4.03E+22	2.28E+20

Table 7.12: Condition number values for S_x.

The condition numbers in Tables 7.11 and 7.12 for both formulations are very similar which was not expected based on the results obtained in Chapters 5 and 6. However, Tables 7.11 and 7.12 show that as the correlation length-scales of B and Q increase, then so do the condition numbers of S_p and S_x, which is compatible with the iteration results in Tables 7.7 and 7.8. These results do not complement the iteration number figures in Tables 7.7 and 7.8, which indicates that the higher order terms of the Taylor expansion of both objective functions may be large.

To summarise, we see that the results related to the number of iterations in

Tables 7.7 and 7.8 strongly agrees with our ndings in Chapter 5, Section 5.2.1.1 and Section 5.1 and Chapter 6, Section 6.3.4 and Section 6.4.2. The number of iterations of both the model error and state formulations both rise as both correlation length-scales increase, with an increased sensitivity to (C_B) as we expected. The state formulation also exhibits a much more visible increase in iterations in comparison to the model error formulation, which was also to be expected. The relative solution errors in Tables 7.9 and 7.10 were also to be expected, since the experiments in Chapter 5 and Chapter 6 showed that the solution errors of both formulations did not rise with correlation length-scale.

exp3d [()isen4-27isen4-5(sTJ 0 -2 Td3d [i Td3d [Ehapter)-474(5)-474Cii936 -24-27wh

In Experiment 2 we showed that both formulations exhibit an increase in the number of iterations (Tables 7.7 and 7.8) and Hessian condition numbers (Tables 7.11 and 7.12) as the condition number of the background and model error matrix D increases. We increased the condition number of the background and model error matrix by increasing the correlation length-scales of the background and model errors. Additionally, the increased sensitivity of the state formulation over the model error formulation to the background and model error correlation length-scales was also seen in Table 7.7 and Table 7.8.

We now conclude the thesis.

Chapter 8

Conclusions

The weak-constraint 4DVAR problem is a variational data assimilation technique, which unlike the conventional sc4DVAR method, accounts for model error,81cR43].ue, both problems can change dramatically. We found that the formulations were both sensitive to observation density, error variances and the length of the assimilation window. We also found that even when using identical settings for the generated truth and assimilation, both wc4DVAR solutions consistently under-estimated the true model error variance slightly.

We then examined the model error formulation more closely in Chapter 5, by bounding the condition number of the first-order Hessian under simplified assumptions and examining the bound expressions for sensitivities of the solution to specific input parameters. We found that the model error formulation Hessian condition number was sensitive to the background and model error covariance matrix. This implied that the Hessian condition number is sensitive to both the correlation length-scales of the background and model errors, and the ratio of the background and model error variances. We also found that the Hessian condition number of the model error formulation to be sensitive to the observation accuracy, observation density and assimilation window length. We then examined the preconditioned model error formulation showing that the condition number and convergence rates are much improved.

An examination of the condition number of the first-order Hessian of the state formulation followed in Chapter 6. We found that, under simplified assumptions, the state formulation shared certain sensitivities with model error formulation. One of these was the sensitivity to the background and model error error covariance matrix, however this was more pronounced for the state formulation than for the model error formulation. We also found the state formulation to be sensitive to the observation density and assimilation window length, although there were some unique differences. The state formulation Hessian condition number becomes ill-conditioned as the observation density decreases, which also amplifies its sensitivity to the assimilation window length. If the state is fully observed, then the state formulation is no longer sensitive to the assimilation window length. This is an interesting advantage, however, a fully observed state is unrealistic in operational applications.

We finally explored the wider-scope application of the theoretical results on a non-linear, chaotic Lorenz 95 model in Chapter 7. We found that the sensitivities of both formulations also show in specific experiments for the observation density, assimilation window length and correlation length-scales.

The following points were covered in the thesis:

- In Chapter 4 we detailed the practical implementation of the wc4DVAR formulations on the 1-dimensional linear advection model, which highlighted clear differences in the minimisation characteristics of both formulations based on changes in experimental parameters. We also observed in several experiments that a general trait of both wc4DVAR formulations is that the model errors are under-estimated.
- The condition number of the Hessian of the sc4DVAR problem is bounded above by the condition number of the Hessian of the model error formulation, $\mathbf{S}_p$, shown in Appendix A.
- We identified and demonstrated the following sources of ill-conditioning of the Hessian of the model error formulation. We did this both theoretically and complemented it with numerical experiments to show similar effects on the rate of convergence in Chapter 5:
  - The condition number of the background and model error covariance matrix, $\mathbf{D}$.
    - As the ratio of the background and model error variance increases or decreases away from 1, $\mathbf{D}$ becomes ill-conditioned and therefore so does $\mathbf{S}_p$.
    - As the correlation length-scales of the background and model error covariance matrix increases, $\mathbf{S}_p$ becomes more ill-conditioned.
  - Increasing the assimilation window length increases the condition number of $\mathbf{S}_p$ at a potentially quadratic rate.

The ratio of the largest of the background and model error variance to the observation error variance also renders $\mathbf{S}_p$ ill-conditioned if it increases or decreases from 1. This means increasing observation minimisation characteristics of both the model error and state formulations applied to the non-linear chaotic Lorenz 95 model. We showed:

- Increasing the correlation length-scales of the matrices composing D increases the number of iterations required for the model error and state algorithms to converge, where the state formulation exhibits a larger increase in iterations than the model error formulation.
- An increase in the number of observations and assimilation window length increases the number of iterations for the model error algorithm to converge.
- Decreasing the number of observations for any length of assimilation window increases the number of iterations required for the state algorithm to converge.
- For a fully observed state, increasing the assimilation window length does not affect the number of iterates required for the state algorithm to converge.

From the research shown in this thesis we can draw a few general conclusions. The sensitivities shared by both formulations are: background and model error covariance matrix correlation length-scales, error variance ratios, observation density and assimilation window length. These sensitivities are shared but they have different effects on each wc4DVAR formulation, as we have discussed in this chapter. It is interesting and worth noting however that the state formulation is not affected by assimilation window length if the state is fully observed. Although a fully observed state is unrealistic, this suggests that there is a way of enabling the state formulation to be more stable. We also see throughout the thesis that the state formulation exhibits increased sensitivity in comparison to the model error formulation, with regards to the parameters which influence its condition number. We conclude that the model error formulation is not as ‘fragile’ as the state formulation to its own sensitivities and therefore the model error formulation is the more stable of the two wc4DVAR algorithms to use until a suitable preconditioner for the state formulation is found.

We now discuss avenues for further work before bringing the thesis to a close.

8.2 Further Work

The work in this thesis establishes a theoretical basis for the conditioning of the model error and state estimation wc4DVAR problems. However, the theory established in this thesis is limited to the simple assumptions made to derive the theorems. We assumed that observations were taken of the state directly, which allows for a simple observation operator. In reality however, observations may be obtained from satellite radiances for example, which means that the observation operator would be some form of the radiative transfer equation. The radiative transfer equation has the potential of being highly non-linear and quite di cult to deal with, [65].

We could also relax the assumption of uncorrelated observation errors. Observation error spatial correlations are typically ignored in data assimilation while the error variances are over-in ated to compensate for the lack of information on correlations. While this assumption is not realistic, observation correlations are ignored because it makes the implementation of 4DVAR easier in general. Studies into the known sources of observation error have narrowed it down to four sources; measurement error, observation operator errors, quality control errors and representativity errors, [87]. The latter three sources of error are believed to be correlated in space, while it has been suggested that observation errors are potentially temporally correlated, [79]. Incorporating correlated observation errors has only begun to be operationally implemented by the Met O ce, [90], while there are still problems with the conditioning of 4DVAR, [89].

Another assumption we made to obtain the theory was that the background, model and observation errors were not time-correlated. It is common practice in NWP to ignore time correlations because it is simply too computationally expensive to deal with. However, there have been studies to show that, for example, model error can be correlated with time, [26], and also observation errors in remote sensing for example, are correlated in time, [80].

The work in Chapter 7 could have been complemented with using the Gauss-Newton ‘incremental’ wc4DVAR technique. We could also employ the preconditioned model error algorithm using both the incremental technique and the non-linear Polak-Ribiere conjugate gradient technique, to see if the preconditioning has similar effects to those shown in Chapter 5 on the linear advection equation. Comparing the differences in convergence rates and solution errors of the Polak-Ribiere and incremental approach would be interesting. We would expect the incremental approach to at least as good as the iterative minimisation performance of the Polak-Ribiere technique, if not better.

Another practical aspect worth considering would be to investigate the validity of the conditioning theory in this thesis on larger systems such as the ECMWF Object-Orientated Programming System (OOPS), or even the University of California’s operational Regional Ocean Modeling System (ROMS). Testing the theory on bigger systems to investigate the sensitivity of both minimisation algorithms to the input parameters discovered to be sensitive in this thesis would be the next logical step.

In this thesis we preconditioned the model error formulation using the symmetric square root of $\mathbf{D}$, which we showed to improve the conditioning and minimisation properties considerably. We could also consider the preconditioning of the state formulation, which was shown to be very sensitive to the condition number of $\mathbf{D}$. As a first step we could precondition the state formulation using the symmetric square root of $\mathbf{D}$ to understand if it improves its stability. M. Fisher and S. Gurol have established an alternative saddle point formulation of the state formulation, which has the advantage of avoiding the need to invert $\mathbf{D}$, [27], [25]. In [27] the authors identified that the Hessian of the state formulation can be preconditioned using an approximation of the wc4DVAR model propagator $\mathbf{L}$. However they also

Appendix A

General Upper Bound: The Strong-Constraint 4DVAR Hessian Condition Number

We write the sc4DVAR Hessian, $S \in \mathbb{R}^{N \times N}$ as

$$S = B_0^{-1} + \hat{H}^T R^{-1} \hat{H}; \tag{A.1}$$

Proof: We prove this by showing that the largest and smallest eigenvalues of S can be obtained by taking an appropriate Rayleigh Quotient of S_p. To illustrate this we denote the spectrum of S by $[\ _N;\ _1]$, where $_N$ is the smallest eigenvalue and $_1$ is the largest eigenvalue of S. Similarly we let the interval $[\ _{N(n+1)};\ _1]$ denote the spectrum of S_p. Since we know the bounds of the Rayleigh Quotient from Theorem 3.4.7, we aim to show

$$_{N(n+1)} \quad _N \quad _1 \quad _1: \tag{A.4}$$

Note this does not mean that an eigenvalue of S is necessarily an eigenvalue of S_p.

Consider the Rayleigh Quotient of S_p

$$R_{S_p}(w) = w^T(D^{\ 1} + L^{\ T}H^TR^{\ 1}HL^{\ 1})w; \tag{A.5}$$

where $w \ 2\ R^{N(n+1)}$ is such that

$$w = \begin{pmatrix} v_1 \\ 0 \\ \vdots \\ 0 \end{pmatrix}; \tag{A.6}$$

where v_1 is an eigenvector of S corresponding to the largest eigenvalue.

We compute the rst part of the Rayleigh Quotient of S_p,

$$w^TD^{\ 1}w = v_1^TB_0v_1: \tag{A.7}$$

Computing the second part yields

$$HL^{\ 1}w = \hat{H}v_1: \tag{A.8}$$

The transpose of this statement is also true. Therefore the second term yields

$$w^T(L^{\ T}H^TR^{\ 1}HL^{\ 1})w = v_1^T\hat{H}^TR^{\ 1}\hat{H}v_1: \tag{A.9}$$

The Rayleigh Quotient of S_p is then

$$R_{S_p}(w) = v_1^TB_0v_1 + v_1^T\hat{H}^TR^{\ 1}\hat{H}v_1 = R_S(v_1) = \ _1; \tag{A.10}$$

as required. The largest eigenvalue of the Hessian of the strong-constraint problem exists in the eigenvalue interval of the Hessian of the weak-constraint problem (2.32).

The same argument can be made for the smallest eigenvalue of S_N

Bibliography

[1] E. Andersson, M. Fisher, R. Munro, and A. McNally. Diagnosis of background errors for radiances and other observable quantities in a variational data assimilation scheme, and the explanation of a case of poor convergence. Quarterly Journal of the Royal Meteorological Society, 126(565):1455{1472, 2000.

[2] E. Atkins, M. Morzfeld, and A. Chorin. Implicit particle methods and their connection with variational data assimilation. arXiv preprint arXiv:1205.1830, 2012.

[3] O. Axelsson. Iterative solution methods. Cambridge University Press, 1996.

[4] R.N. Bannister. A review of forecast error covariance statistics in atmospheric variational data assimilation. Quarterly Journal of the Royal Meteorological Society, 134(637):1951{1970, 2008.

[5] M. Bell, M. Martin, and N. Nichols. Assimilation of data into an ocean model with systematic errors near the equator. Quarterly Journal of the Royal Meteorological Society, 130(598):873{893, 2004.

[6] A.F. Bennett, B.S. Chua, D. Harrison, and M.J McPhaden. Generalized inversion of tropical atmosphere-ocean data and a coupled model of the tropical paci c. Journal of Climate, 11(7):1768{1792, 1998.

[7] A.F. Bennett, B.S. Chua, D. Harrison, and M.J. McPhaden. Generalized inversion of tropical atmosphere-ocean (tao) data and a coupled model of the

[27] M. Fisher, Y. Tremolet, H. Auvinen, D. Tan, and P. Poli. Weak-constraint and long-window 4d-var. Technical Report 621, European Centre for Medium-Range Weather Forecasts (ECMWF), 2011.

[28] R. Fletcher and C. Reeves. Function minimization by conjugate gradients. The computer journal, 7(2):149{154, 1964.

[29] L. Gandin and R. Hardin. Objective analysis of meteorological elds, volume 242. Israel program for scienti c translations Jerusalem, 1965.

[30] G. Gaspari and S. Cohn. Construction of correlation functions in two and three dimensions. Quarterly Journal of the Royal Meteorological Society, 125(554):723{757, 1999.

[31] P. Gauthier, M. Tanguay, S. Laroche, S. Pellerin, and J. Morneau. Extension

[39] A.K. Gri th and N.K. Nichols. Adjoint methods in data assimilation for estimating model error. Flow, turbulence and combustion, 65(3):469{488, 2000.

[40] D.F. Gri ths and A.R. Mitchell. The nite di erence method in partial di erential equations. John Wiley, 1980.

[41] S.A. Haben. Conditioning and preconditioning of the minimisation problem in variational data assimilation. PhD thesis, University of Reading, 2011.

[42] S.A. Haben, A.S. Lawless, and N.K. Nichols. Conditioning and preconditioning of the variational data assimilation problem. Computers & Fluids, 46(1):252{256, 2011.

[43] S.A. Haben, A.S. Lawless, and N.K. Nichols. Conditioning of incremental

[50] E. Klinker, F. Rabier, G. Kelly, and J.F. Mahfouf. The ecmwf operational implementation of four-dimensional variational assimilation. iii: Experimental

three-dimensional variational data assimilation scheme. Quarterly Journal of the Royal Meteorological Society, 126(570):2991{3012, 2000.

[59] A.C. Lorenc. The potential of the ensemble kalman lter for nwp a comparison with 4d-var. Quarterly Journal of the Royal Meteorological Society, 129(595):3183{3203, 2003.

[60] A.C. Lorenc, N.E. Bowler, A.M. Clayton, S.R. Pring, and D. Fairbairn. Comparison of hybrid-4denvar and hybrid-4dvar data assimilation methods for global nwp. Monthly Weather Review, 140(2014):281{294, 2014.

[61] E.N. Lorenz. Deterministic nonperiodic ow. Journal of the atmospheric sciences, 20(2):130{141, 1963.

[62] E.N. Lorenz. Predictability: A problem partly solved. In Proc. Seminar on predictability, volume 1, 1996.

[63] E.N. Lorenz. Designing chaotic models. Journal of the atmospheric sciences, 62(5), 2005.

[64] J-F. Mahfouf and F. Rabier. The ecmwf operational implementation of four-dimensional variational assimilation. ii: Experimental results with improved physics. Quarterly Journal of the Royal Meteorological Society, 126(564):1171{1190, 2000.

[65] A.P. McNally, P.D. Watts, J.A. Smith, R. Engelen, G.A. Kelly, J.N. Thepaut, and M. Matricardi. The assimilation of airs radiance data at ecmwf. Quarterly Journal of the Royal Meteorological Society, 132(616):935{957, 2006.

[66] A.M. Moore, H.G. Arango, G. Broquet, C. Edwards, M. Veneziani, B. Powell, D. Foley, J.D. Doyle, D. Costa, and P. Robinson. The regional ocean modeling system (roms) 4-dimensional variational data assimilation systems: part ii{performance and application to the california current system. Progress in Oceanography, 91(1):50{73, 2011.

[67] A.M. Moore, H.G. Arango, G. Broquet, C. Edwards, M. Veneziani, B. Powell, D. Foley, J.D. Doyle, D. Costa, and P. Robinson. The regional ocean modeling

system (roms) 4-dimensional variational data assimilation systems: Part iii{observation impact and observation sensitivity in the california current system. Progress in Oceanography, 91(1):74{94, 2011.

[68] A.M. Moore, H.G. Arango, G. Broquet, B.S. Powell, A.T. Weaver, and J. Zavala-Garay. The regional ocean modeling system (roms) 4-dimensional variational data assimilation systems: Part i{system overview and formulation. Progress in Oceanography, 91(1):34{49, 2011.

[69] K.W. Morton, D.F. Mayers, and M. Cullen. Numerical solution of partial di erential equations, volume 2. Cambridge university press Cambridge, 1994.

[70] H. Ngodock and M. Carrier. A 4dvar system for the navy coastal ocean model. part i: System description and assimilation of synthetic observations in monterey bay*. Monthly Weather Review, 142(6):2085{2107, 2014.

[71] H. Ngodock and M. Carrier. A 4dvar system for the navy coastal ocean model. part ii: Strong and weak constraint assimilation experiments with real observations in monterey bay*. Monthly Weather Review, 142(6):2108{2117, 2014.

[72] N.K. Nichols. Treating model error in 3-d and 4-d data assimilation. Data assimilation for the earth system, pages 127{135, 2003.

[73] J. Nocedal and S.J. Wright. Numerical optimization. Springer verlag, 1999.

[74] F. Rabier, H. Jarvinen, E. Klinker, J-F. Mahfouf, and A. Simmons. The ecmwf operational implementation of four-dimensional variational assimilation. i: Experimental results with simpli ed physics. Quarterly Journal of the Royal Meteorological Society, 126(564):1143{1170, 2000.

[75] F. Rawlins, S.P. Ballard, K.J. Bovis, A.M. Clayton, D. Li, G.W. Inverarity, A.C. Lorenc, and T.J. Payne. The met o ce global four-dimensional variational data assimilation scheme. Quarterly Journal of the Royal Meteorological Society, 133(623):347{362, 2007.

[76] Y. Sasaki. A fundamental study of the numerical prediction based on the variational principle. J. Meteor. Soc. Japan, 33(6):262{275, 1955.

[77] Y. Sasaki. An objective analysis based on the variational method. J. Meteor. Soc. Japan, 36(3):77{88, 1958.

[78] Y. Sasaki. Some basic formalisms in numerical variational analysis. Monthly Weather Review, 98(12):875{883, 1970.

high-resolution model. Quarterly Journal of the Royal Meteorological Society, 140(681):1189{1197, 2014.

[88] R.O. Weber and P. Talkner. Some remarks on spatial correlation function models. MONTHLY WEATHER REVIEW-USA, 121:2611{2611, 1993.

[89] P. Weston. Progress towards the implementation of correlated observation errors in 4d-var.